EFFECT OF POLYMER ELECTRODE MORPHOLOGY ON
PERFORMANCE OF A LITHIUM/POLYPYRROLE BATTERY

A Thesis

by

MARJORIE ANNE NICHOLSON

Submitted to the Office of Graduate Studies of
Texas A&M University
in partial fulfillment of the requirements for the degree of

MASTER OF SCIENCE

May 1991

Major Subject: Chemistry

EFFECT OF POLYMER ELECTRODE MORPHOLOGY ON
PERFORMANCE OF A LITHIUM/POLYPYRROLE BATTERY

A Thesis

by

MARJORIE ANNE NICHOLSON

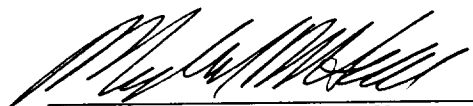Approved as to style and content by

_____
Charles R. Martin
(Chair of Committee)

_____
A. John Appleby
(Member)

_____
Manuel P. Soriaga
(Member)

_____
Michael B. Hall
(Head of Department)

May 1991

ABSTRACT

Effect of Polymer Electrode Morphology on Performance of a

Lithium/Polypyrrole Battery. (May 1991)

Marjorie A. Nicholson, B.A., Texas A&M University

Chair of Advisory Committee: Dr. Charles R. Martin

A variety of conducting polymer batteries have been described in the recent literature. In this work, a Li/Polypyrrole secondary battery is described. The effect of controlling the morphology of the polymer on enhancement of counterion diffusion in the polymer phase is explored. A method of preparing conducting polymers has been developed which yields high surface area per unit volume of electrode material. A porous membrane is used as a template in which to electrochemically polymerize pyrrole, then the membrane is dissolved, leaving the polymer in a fibrillar form. Conventionally, the polymer is electrochemically polymerized as a dense polymer film on a smooth Pt disk electrode. Previous work has shown that when the polymer is electrochemically polymerized in fibrillar form, charge transport rates are faster and charge capacities are greater than for dense, conventionally grown films containing the same amount of polymer.

The purpose of this work is to expand previous work by further investigating the possibilities of the optimization of transport rates in polypyrrole films by controlling the morphology of the films. The utility of fibrillar polypyrrole as a cathode material in a lithium/polymer secondary battery is then assessed. The performance of the fibrillar battery is compared to the performance of an analogous battery which

employed a conventionally grown polypyrrole film. The study includes a comparison of cyclic voltammetry, shape of charge/discharge curves, discharge time and voltage, cycle life, coulombic efficiencies, charge capacities, energy densities, and energy efficiencies.

DEDICATION

This thesis is dedicated to God

and my children, who I also dedicate to Him,

ACKNOWLEDGMENTS

TABLE OF CONTENTS

LIST OF TABLES

LIST OF FIGURES

LIST OF FIGURES (Continued)

LIST OF FIGURES (Continued)

LIST OF SYMBOLS

SYMBOL	Meaning	Units
A	electrode area	cm^2
A_c	calculated electrode area	cm^2
A_g	geometric electrode area	cm^2
A_f	fractional electrode area	cm^2
C	capacitance	microfarads
C_o^*	bulk concentration of oxidized species	moles/l
C_p	practical capacity	microfarads
C_t	theoretical capacity	microfarads
D_o	diffusion coefficent	m^2/sec
e. d.	energy density	watthours/kg
E	potential	volts
E^o	standard electrode potential	volts
E_{ave}	average discharge potential	volts
E_{cell}	overall cell potential	volts
E	energy	watthours
F	Faraday's constant	96,487 coulombs/mole
g	gravitational constant	9.8 m/sec^2
ΔG^o	Gibbs free energy	joules
i	current density	milliamps/cm^2
I	current	milliamps
I_{ave}	average discharge current	milliamps
I_c	capacitive current	microamps
I_p	peak current	current
m	mass	kg
M	molecular weight	g/mole
n	number of moles of electrons	moles
Q	charge	coulombs
Q_f	electropolymerization charge	coulombs
Q_{in}	amount of charge injected	coulombs
Q_{out}	amount of charge withdrawn	coulombs
t	time	seconds
t'	time of discharge	seconds
W	weight	lb_f
ν	scan rate	mV/sec
$h\nu$	photon energy	ergs

CHAPTER I

INTRODUCTION

Electronically conducting polymers are organic compounds which conduct electricity. They have extended π-conjugated backbones of alternating single and double bonds along the polymer chain (1). Many contain a ring structure which may include nitrogen, sulfur, or phosphorous in the ring. An example of such a polymer is polypyrrole (1,2) (Fig. 1).
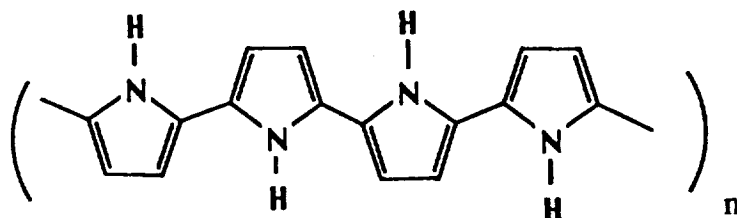
Figure 1. Structure of Polypyrrole

Polypyrrole can be electrochemically synthesized by the oxidation of pyrrole monomer at an electrode surface. A film of polypyrrole is formed (3) which adheres to the electrode surface (Fig. 2). An electron micrograph of the surface of a polypyrrole film is shown in Fig. (3). Anions are incorporated into the film during polymerization and the film is said to be "doped" with anions. Polypyrrole is positively charged when doped, so it is referred to as a "p-doped" electronically conducting

The format of this thesis follows that of the Journal of the Electrochemical Society.
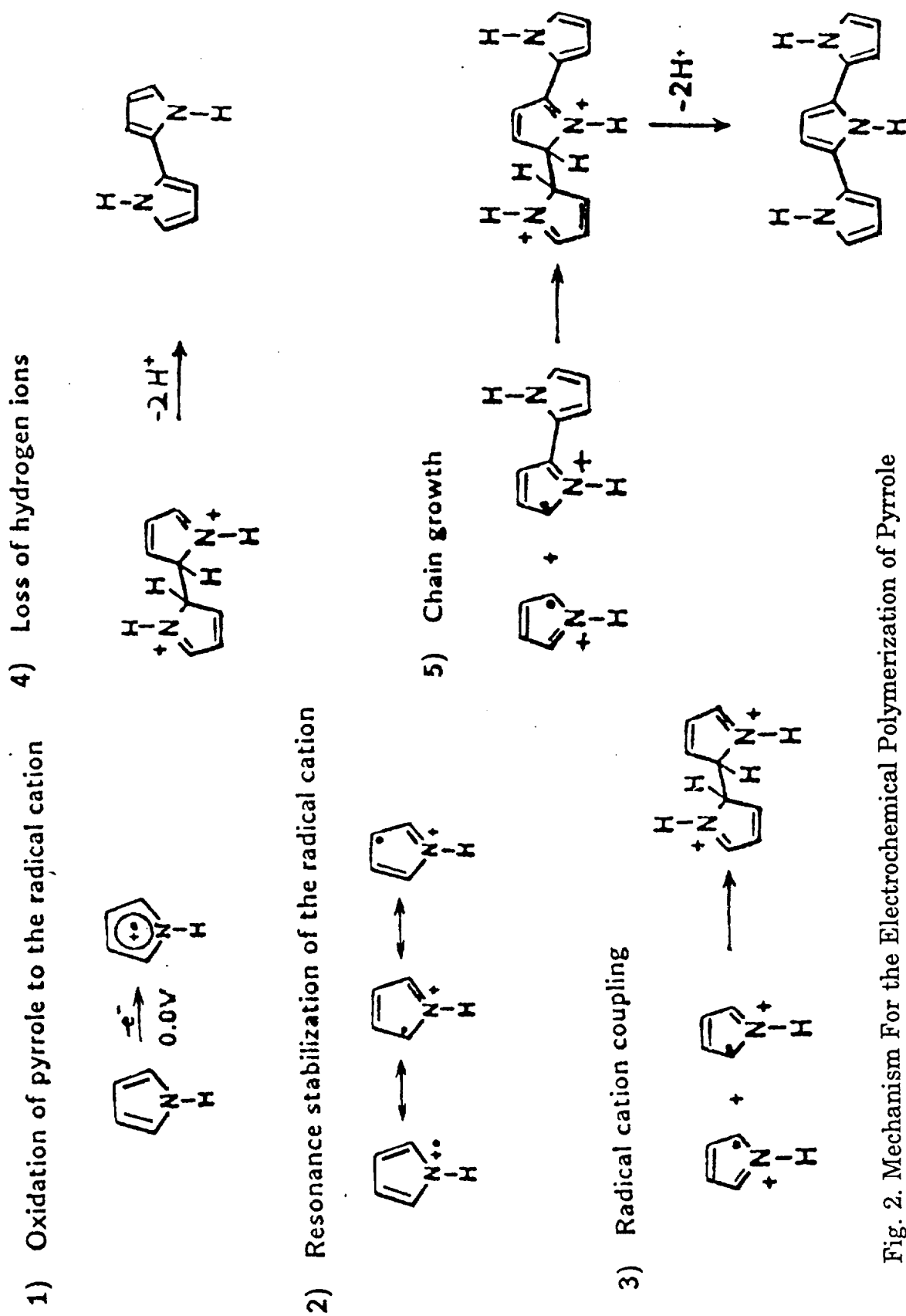
Fig. 2. Mechanism For the Electrochemical Polymerization of Pyrrole

1) Oxidation of pyrrole to the radical cation   4) Loss of hydrogen ions

2) Resonance stabilization of the radical cation

3) Radical cation coupling

5) Chain growth

ORIGINAL PAGE
BLACK AND WHITE PHOTOGRAPH
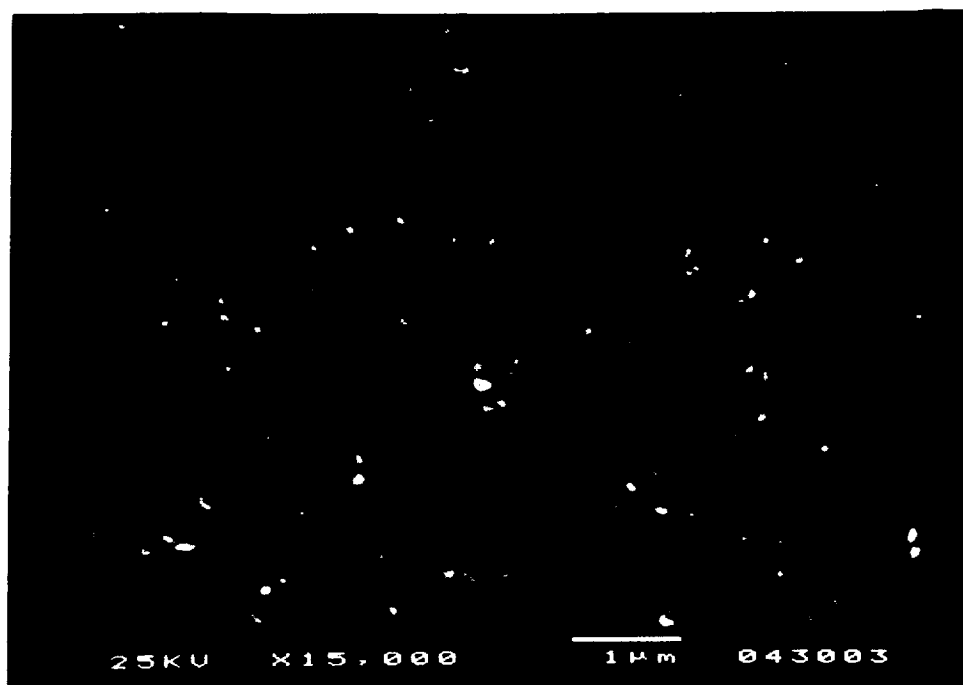
Fig. 3. Electron Micrograph of a Conventional Polypyrrole Film.

polymer. The positive charge is delocalized by the π-conjugated system of the polymer (Fig. 1). When the film is fully doped, polypyrrole has one positive charge, and likewise one anion, for every 3-4 pyrrole monomer units (4).

While polypyrrole (PPy) is synthesized in its oxidized (p-doped) form, it can be reduced to a neutral form. For example, polypyrrole can be reduced by metallic Li; the counterion is expelled from the polymer during reduction.

$$PPy^+ClO_4^- + Li^0 \leftrightarrow PPy^0 + Li^+ + ClO_4^- \qquad [1]$$
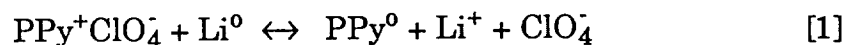
This oxidation/reduction process is reversible. Oxidation can be viewed as charge storage, and reduction can be viewed as release of stored charge. For this reason, and because conducting polymers are lightweight materials, conducting polymers have been explored as cathode materials in secondary lithium batteries (5-28).

A schematic of a hypothetical Li/PPy battery is shown in Fig. 4. Of particular interest in battery applications is the relatively high doping level of the polypyrrole and the possibility of switching it quickly and reversibly from the oxidized form to the reduced form (Eq. [1]). Since the switching is reversible, a battery made with polypyrrole would be rechargeable.

A fast switching reaction rate means that a battery utilizing such an electrode could be discharged at a high rate, or amperage, which in turn means that it could handle a greater load. When oxidizing or reducing polypyrrole, the rate determining step is counterion diffusion in the polymer phase (29-32). When the film is oxidized, counterions are incorporated into the film to maintain charge neutrality in the film. During reduction, anions have to diffuse out of the polymer phase into
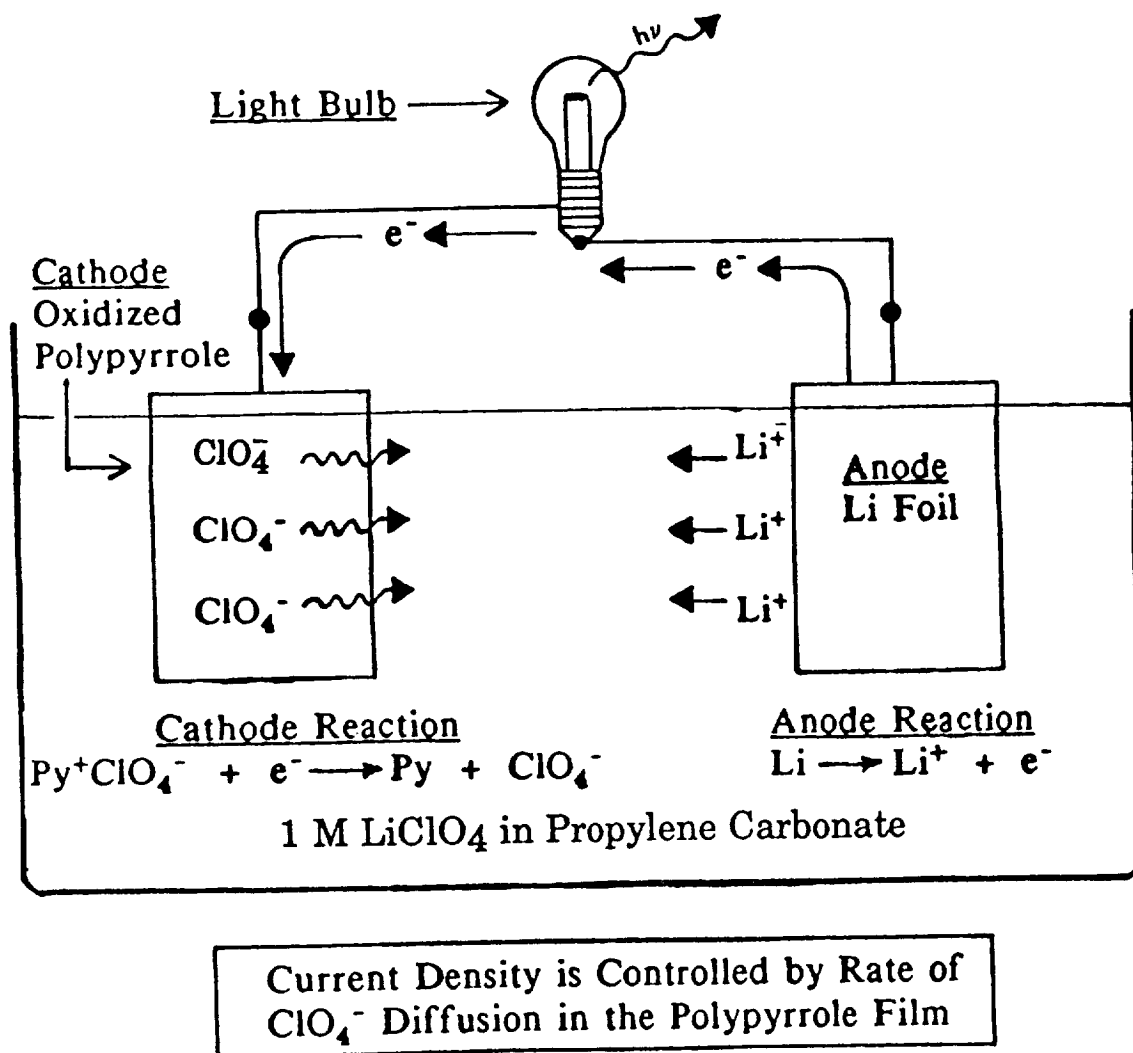
Fig. 4. A Hypothetical Li/Polypyrrole Battery.

the solution phase to maintain the film's charge balance. If the rate of ion transport in the polymer phase could be increased, better battery performance would be obtained. Unfortunately, ion transport in a thick film of conventionally grown polypyrrole is slower than in a thin film (15, 18, 29, 33-35). Therefore, growing a thicker film of polypyrrole does not enhance battery performance (13, 17). Also, charge trapping occurs as oxidized pyrrole sites are isolated by proximate polymer chains in a conventionally grown film. As a result, the polymer cannot become fully doped. However, if the morphology of the film can be changed so that ion transport is facilitated, a higher doping level would result and a battery made with the polymer could be discharged at a higher rate.

Previous research in this laboratory (36) investigated the effect of controlling the morphology of the polymer on enhancement of counterion diffusion in the polymer phase. A method of preparing conducting polymers was developed which yields a much higher surface area per unit volume of polymer than conventionally grown polypyrrole films. A film with a higher surface area results in a greater number of electroactive sites being accessible to counterions. The film is grown in a fibrillar form by using a porous membrane as a template. The membrane is attached to the electrode surface, then the electrode is introduced into a solution containing pyrrole monomer. The pyrrole is polymerized potentiostatically in the pores of the membrane, then the membrane is dissolved away, leaving behind the polypyrrole fibrils standing upright on the electrode surface (Fig. 5). An electron micrograph of 2000 Å diameter fibrils is shown in Fig. 6.

Counterions can diffuse much faster in the solution phase than in the polymer phase (31). Theoretically, the longest distance a counterion
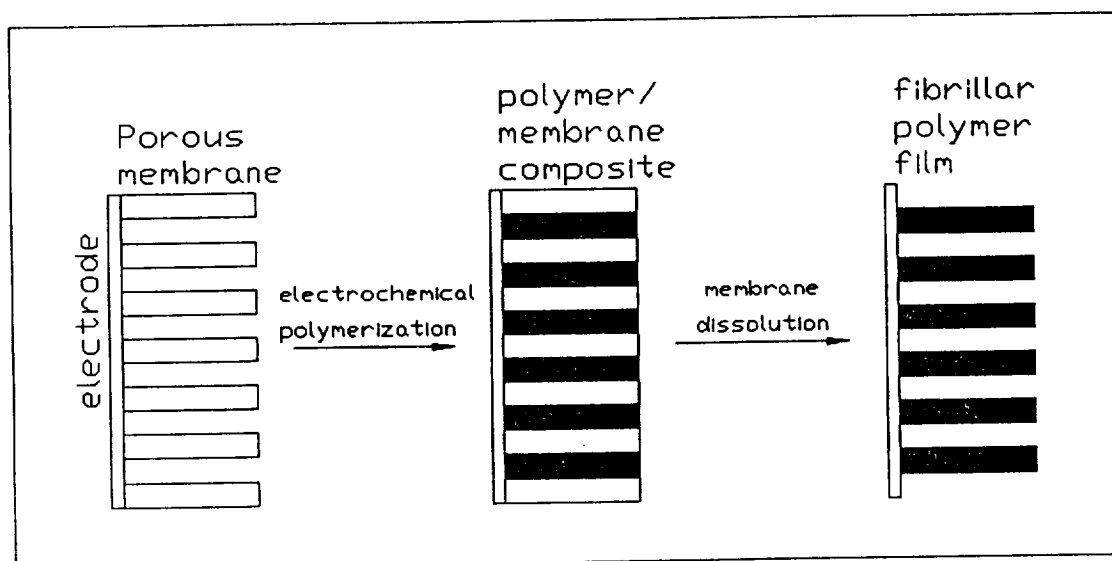
Fig. 5. Schematic Cross-Sectional Diagram of the Procedure for Preparing Fibrillar Conducting Polymer Films.
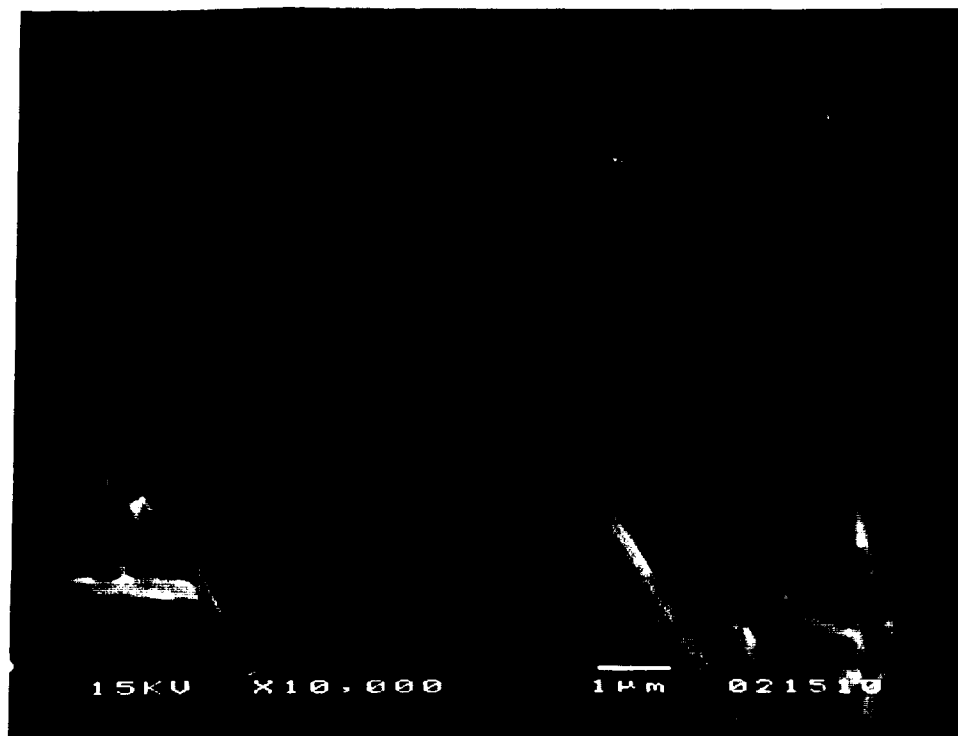
Fig. 6. Electron Micrograph of a Fibrillar Polypyrrole Film.

would have to diffuse in the fibrillar film before reaching the solution phase would be half the diameter of one of the fibrils, as illustrated in Fig. 7. Therefore, a fibrillar film should show a faster switching rate than a conventionally grown dense polymer film with the same electrode area and a comparable amount of polymer. Previous work (37, 38) has shown that when the polymer is electrochemically polymerized in fibrillar form, the fibrils produce a faster charge transfer rate, greater charge capacities, and higher doping level than a conventionally grown film.

Following this work, attempts have been made to improve the performance of these electrodes by making the diameter of the fibrils smaller. A smaller fibril diameter would provide the counterion an even shorter diffusion path from polymer phase to solution phase, and ion transport should be facilitated. Investigation showed that although the performance of the smaller diameter fibrils was better, the current density and charge capacity did not increase proportionately with decreasing fibril diameter, as expected (36). This could be due to the growth of a base layer of polypyrrole between the porous template membrane and the platinum substrate of the electrode. For 0.2 micron fibrils, this base layer was as thick as 0.3-0.5 microns (36). A detailed schematic of an electrode used to make fibrillar films is shown in Fig. 8. The template membrane was stretched across a platinum electrode ('e' of Fig. 8) and held in place by a rubber sheath ('f' of Fig. 8). When the electrode was immersed in solution containing pyrrole monomer, some of the solution leaked into the space between the platinum substrate and the template membrane ('g' of Fig. 8). Upon application of potential, the pyrrole present in the solution between the platinum and the membrane

PPy conventional film

electrode
surface

Counterions must be expelled as
rapidly as possible during discharge
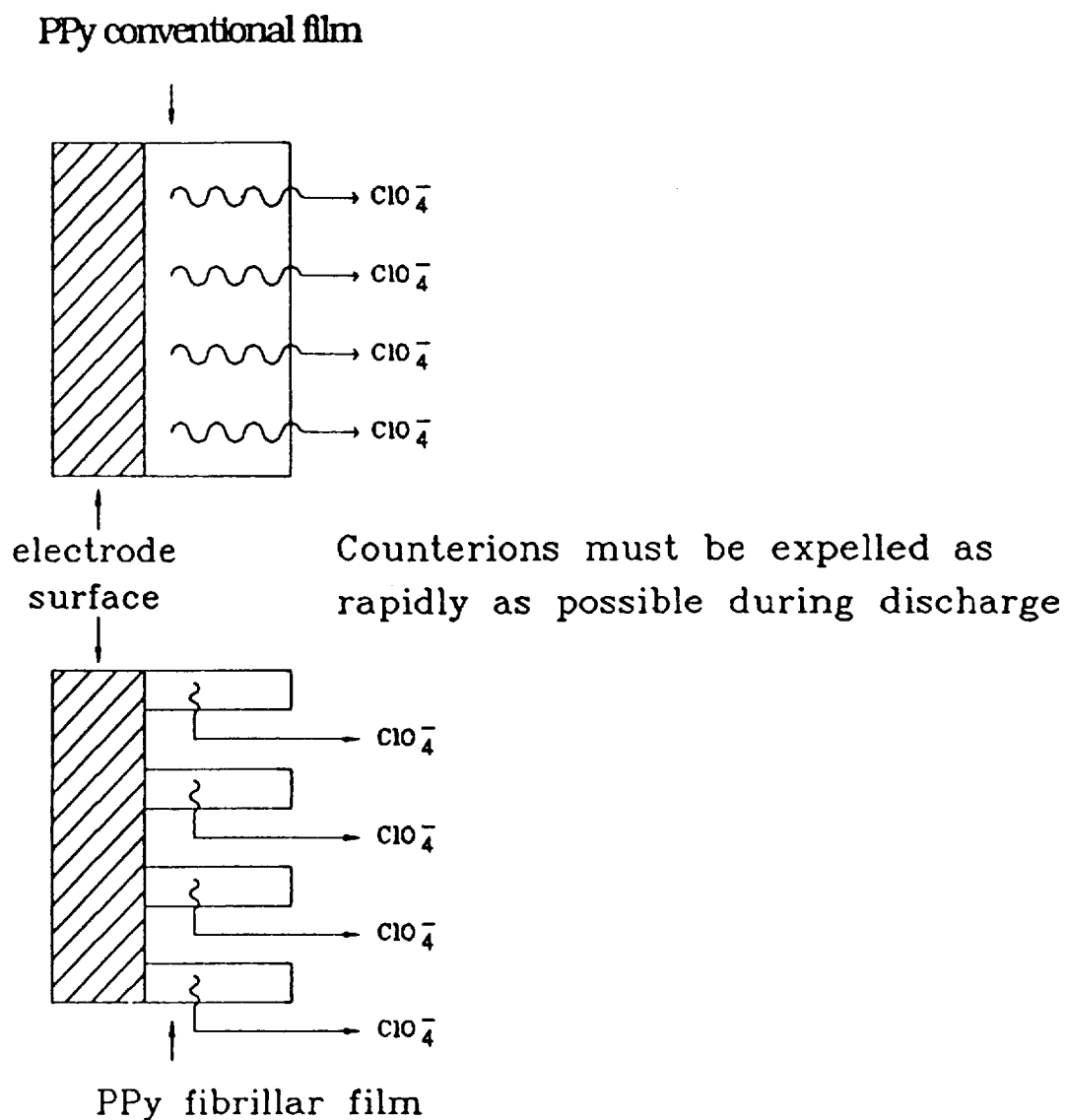
PPy fibrillar film

Fig. 7. Schematic Diagram of Counterion Diffusion in a
Conventional Film vs. Counterion Diffusion in a Fibrillar Film.
Countrions Can Be Expelled More Rapidly in a Fibrillar Film.
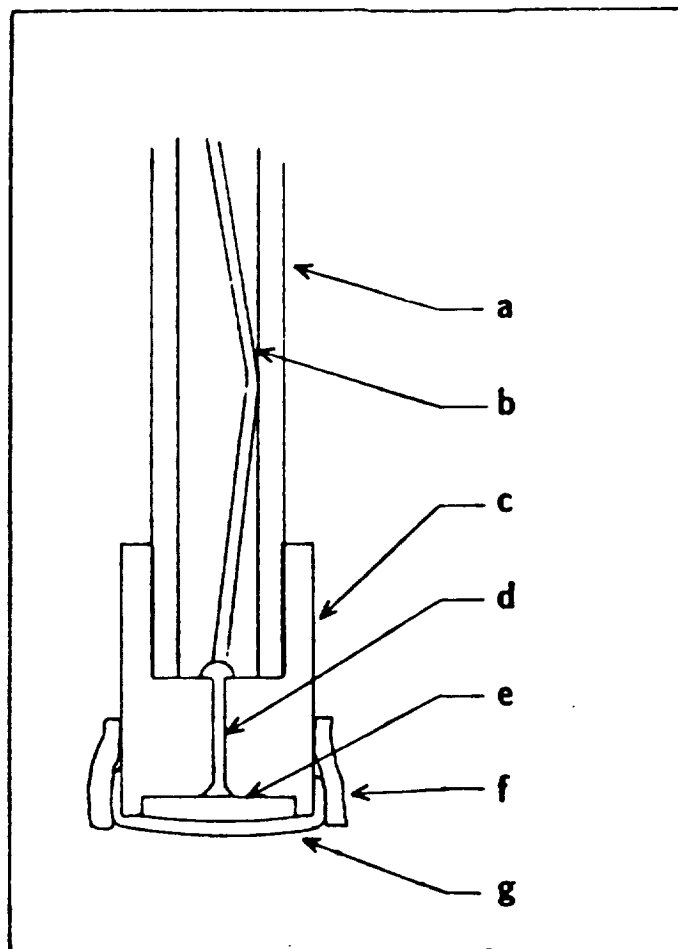
Fig.8. Schematic Diagram of Electrode Employed for Preparation of
Fibrillar Polypyrrole Films (38). a. 7mm Glass Tube, b. Cu Wire,

c. Kel-f® Electrode Body, d. Ag Epoxy Contact, e. Convex Platinum Disk,

f. Rubber Collar, g. Porous Template Membrane.

was polymerized to form a base layer of polypyrrole.

It is logical to assume that a base layer of polypyrrole which is thicker than the fibril diameter itself would serve to negate the advantages of fibrillar morphology described above. Since the base layer of polypyrrole would have to be oxidized and reduced as well as the fibrils, the switching reaction rate of the entire film would be slowed. Eliminating this base layer would allow determination of whether using smaller fibril diameters would provide faster ion transport and greater charge capacity. One of the objectives of this work was to develop a procedure for synthesizing fibrillar polypyrrole that does not have a base layer of conventional polypyrrole.

In this work, a Li/Polypyrrole secondary battery is described. The purpose of this work is to expand previous work by further investigating the possibilities of the optimization of transport rates in polypyrrole films by controlling the morphology of the films and eliminating the formation of a polypyrrole base layer. The utility of fibrillar polypyrrole as a cathode material in a lithium/polymer secondary battery is then assessed. The performance of the fibrillar battery is compared to the performance of an analogous battery which employed a conventionally grown polypyrrole film. The study includes a comparison of cyclic voltammetry, shape of charge/discharge curves, discharge times and voltages, cycle life, coulombic efficiencies, charge capacities, energy densities, and energy efficiencies.

CHAPTER II

EXPERIMENTAL

<u>Materials</u>. The electrolyte used for some of the cyclic voltammetry studies was 0.2 M Et_4BF_4 (Aldrich) in acetonitrile (UV grade, Burdick and Jackson). The tetraethyl ammonium salt (Et_4BF_4) was recrystallized twice from methanol and dried in a vacuum oven 24 hours at 100°C before use. Acetonitrile was used as received and was stored over 4A molecular sieves or CaH_2. Orotemp 24 Au(I)CN gold plating solution was used for fabrication of fibrillar electrodes. Nuclepore® and Poretics® polycarbonate membranes as well as Anopore® Al_2O_3 membranes were used as template materials for the synthesis of the fibrillar polypyrrole.

The electrolyte used for the battery work was 1 M $LiClO_4$ in propylene carbonate (4-methyl-1,3-dioxolan-2-one). Propylene carbonate (Burdick and Jackson) was fractionally distilled under vacuum before use and the second of three fractions was retained for use. The $LiClO_4$ (Fluka) was heated at 100°C in a vacuum oven for 24 hours to eliminate any absorbed water. Pyrrole (99%, Aldrich), used for electropolymerization of the polypyrrole, was distilled under nitrogen prior to use. Platinum foil (Alfa, 0.25 mm thick) imbedded in inert Kel-f® (3/8" diameter, Afton Plastics) was used as a current collector for conventionally grown polypyrrole film electrodes. Lithium foil (Alfa) and Ni gauze (20x20 mesh, 0.014" wire diameter, 99.75 %, Newark Wire Cloth) were used to make the lithium electrode.

<u>Equipment</u>. All work involving lithium batteries was done in a glove box to prevent oxidation of the lithium electrode by atmospheric oxygen.

Polypyrrole is also subject to permanent oxidation by atmospheric oxygen, but is stable at higher levels of O_2 than lithium. Therefore, cyclic voltammetry studies involving a polypyrrole working electrode and a platinum counter electrode were done in a glove bag rather than a glove box. The glove box used for the lithium battery studies was made by Vacuum Atmospheres Corporation and was equipped with a Dri-Train® atmosphere regenerator and a Photohelic® pressure sensor and controller. Glove bags for cyclic voltammetry studies not involving lithium were obtained from Instruments for Industry and Research (I^2R). An EG&G PAR Model 273 Potentiostat/Galvanostat was used for cyclic voltammetry, potential step experiments, and battery charge/discharge studies. A Soltec VP-6424S X-Y recorder was used to record cyclic voltammograms and a Linear strip-chart recorder was used for recording battery charges and discharges. A 3.5 digit Metex M-3650 digital voltmeter was used to check electrode resistances and circuit voltages and currents. Data analysis was conducted using a Macintosh IIci computer with Cricketgraph® and Kaleidagraph® software. Schematics were drawn using an IBM Model 50 PS/2 with Autocad® software and a Macintosh IIci computer with Superpaint ®.

Electrochemical cell design and electrode preparation. Figure 9 shows a schematic of the polypyrrole film electrode, which is the cathode during battery discharge. The polypyrrole electrode will henceforth be referred to as the cathode and the lithium electrode will be referred to as the anode, since the lithium electrode acts as the anode during battery discharge. Two types of polypyrrole films were used in performing these studies. One was a dense mat film electropolymerized on a Pt disk

A
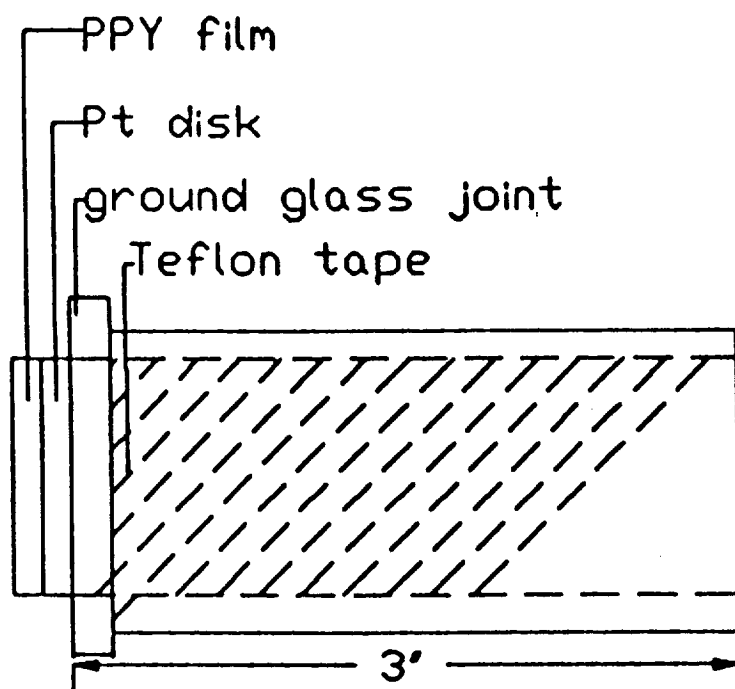
Fig. 9. Schematic for Li/Polypyrrole Conventional Film Cathode.

electrode; such films have been the subject of much investigation (5, 6, 9, 10, 13, 14, 16-18). This type of film will be referred to, henceforth, as a "conventional polypyrrole film."

Conventional polypyrrole films were made by constant-current polymerization of pyrrole at a platinum disk electrode at 1 mA/cm^2. A charge of 376 mC was passed, which resulted in a film that was 2μm thick (36). Figure 9 shows the battery cathode with a conventional polypyrrole film. An electron micrograph of a conventional polypyrrole film is shown in Fig. 3. The film was grown on a platinum disk, which was heat-sealed onto a piece of Kel-f® rod with a hole drilled in the center. Electrical contact was made by silver epoxy and a copper wire through the hole in the Kel-f®. The electrode was held in place by an electrode holder made of teflon rod and housed in glass tubing.

The surface of the electrode was renewed between experiments by polishing with 0.5 micron alumina, rinsing it with Millipore® deionized water, and drying it with a heat gun to reseal it. Teflon tape was used to seal the teflon electrode holder into its glass housing if needed. One end of the glass tubing was flared and had a ground glass joint. This type of joint was chosen because it seals well and allows for facile assembly and disassembly of the cell, which was particularly important when working in the glove box.

The other type of polypyrrole film studied in this work was electropolymerized using a template membrane; this polypyrrole has a fibrillar morphology and will be referred to as a "fibrillar polypyrrole film." Figure 10 is a detailed schematic that illustrates how fibrillar polypyrrole films were made (39). Fibrillar films were prepared by first sputter depositing a thin layer of gold on an Al$_2$O$_3$ template membrane
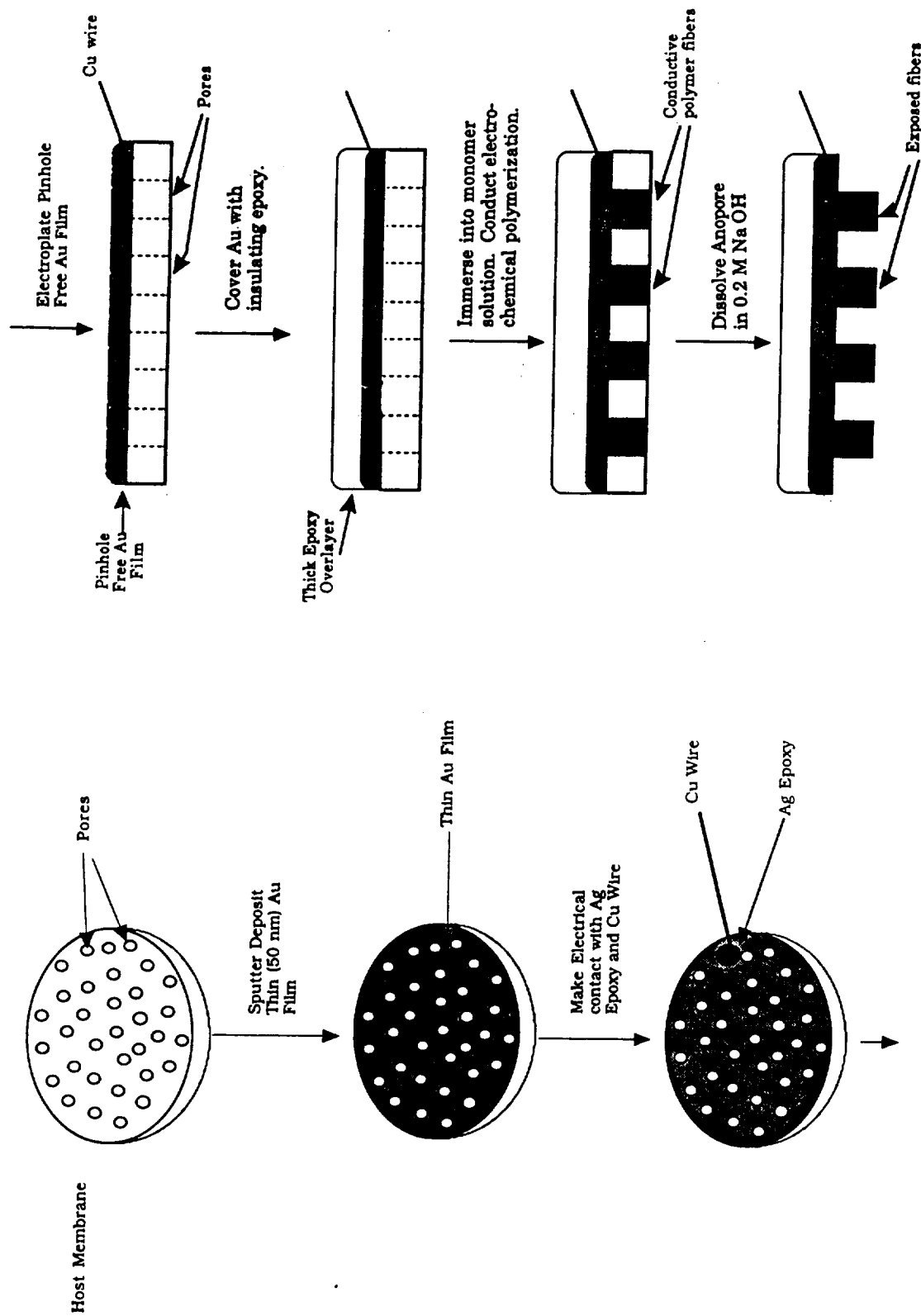
Fig. 10. Schematic of Preparation of Fibrillar Polypyrrole Electrode.

to make it conductive. Electrical contact was then made with silver epoxy and a copper wire. The electrode was immersed in gold plating solution and electroplated until a pinhole-free Au film was obtained on one side of the electrode. The electrode was then coated with Torr-Seal®, an inert epoxy, except for the portion which is to be exposed to solution.

Next, the electrode was immersed into a solution of 1 M $LiClO_4$ and 0.5 M pyrrole in propylene carbonate. Pyrrole is polymerized in the pores of the template membrane at a constant current of 1 mA/cm^2 until 376 mC are passed, which is the same amount of charge passed when growing a 2 μm thick conventional film.

The template membrane was then dissolved, leaving behind the polypyrrole fibrils standing upright (Fig 11). The medium used for dissolution depended on the chemical identity of the membrane. Methylene chloride was used for polycarbonate membranes and 1 M NaOH was used for Al_2O_3 Anopore® membranes. Anopore® membranes have a pore diameter of 2000 Å, while the polycarbonate membranes used had pore diameters ranging from 300 Å to 10,000 Å. The fibril diameter is the same as the pore diameter of the template membrane used to make it. After dissolution of the membrane, the fibrillar film is treated with acid to reprotonate the polypyrrole. For some of the cyclic voltammetry studies, where NH_4BF_4 was used as the electrolyte, HBF_4 was used to reprotonate. For the battery studies, $HClO_4$ was used as the acid because the electrolyte employed was $LiClO_4$. Therefore, it is ensured that there is only one anion present in each system. After rinsing with fresh electrolyte solution, the fibrillar film is ready to be used for cyclic voltammetry and battery charge/discharge experiments.
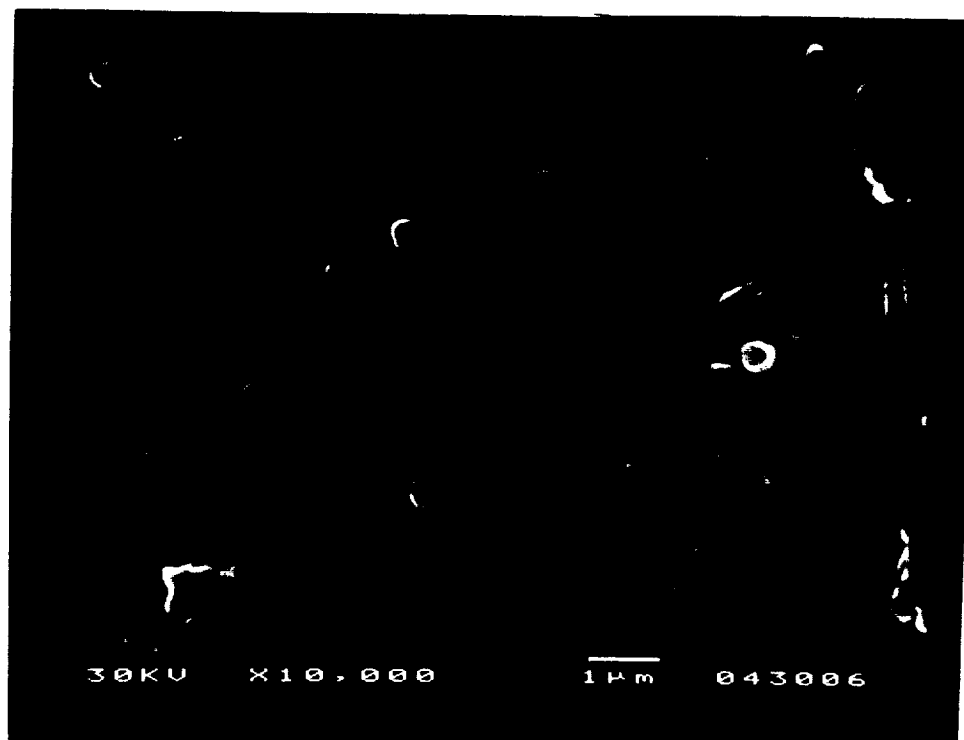
Fig. 11. Electron Micrograph of 0.2 μm Diameter Polypyrrole Fibrils
Prepared Using Anopore® Al$_2$O$_3$ Membrane as the Template Material.

Figure 12 is a schematic of a battery cathode used to make a fibrillar polypyrrole film. A gold-coated Anopore® electrode is attached to one side of a Kel-f® plug with silver epoxy before inserting it into the teflon electrode holder. Electrical contact is made from the other side of the Kel-f plug with silver epoxy and a copper wire. The wire runs out of the cell through a hole drilled in the teflon rod. Since Anopore® membranes are very brittle, they were sometimes attached to a thin ring of glass tubing with five minute epoxy to give them mechanical stability during electrode assembly. The glass tubing and surrounding epoxy were removed before the electrode was used.

Figure 13 is a schematic of the battery cell reservoir. It is made of glass and has a ground glass joint at each end. A glass reservoir is used so that the electrodes and solution can be observed visually. The polypyrrole film could become separated from its current collector or the lithium anode could become passivated during the course of the experiment. Also, degradation of the solvent could occur, evidenced by discoloration of the solution. Being able to monitor visually the experiment in progress prevents erroneous data from being collected and saves valuable time. There is an opening in the top of the solution reservoir to allow thesolution to be introduced into the cell. It also serves as a receptacle for the reference electrode. The reference electrode used for battery studies was a $Ag/AgNO_3$ reference electrode. The $Ag/AgNO_3$ reference was chosen because both the SCE and AgCl references proved unsuitable. The SCE contains an aqueous solution, which, if it leaked into the cell, could passivate the lithium anode. The AgCl reference was ruled out because AgCl is too soluble in propylene carbonate. For some cyclic voltammetric studies carried out in acetonitrile, however, a SCE

Teflon electrode holder
Kel-f plug
copper wire

Ag epoxy
Au, sputtered and plated
Anapore
5 min. epoxy
glass tubing
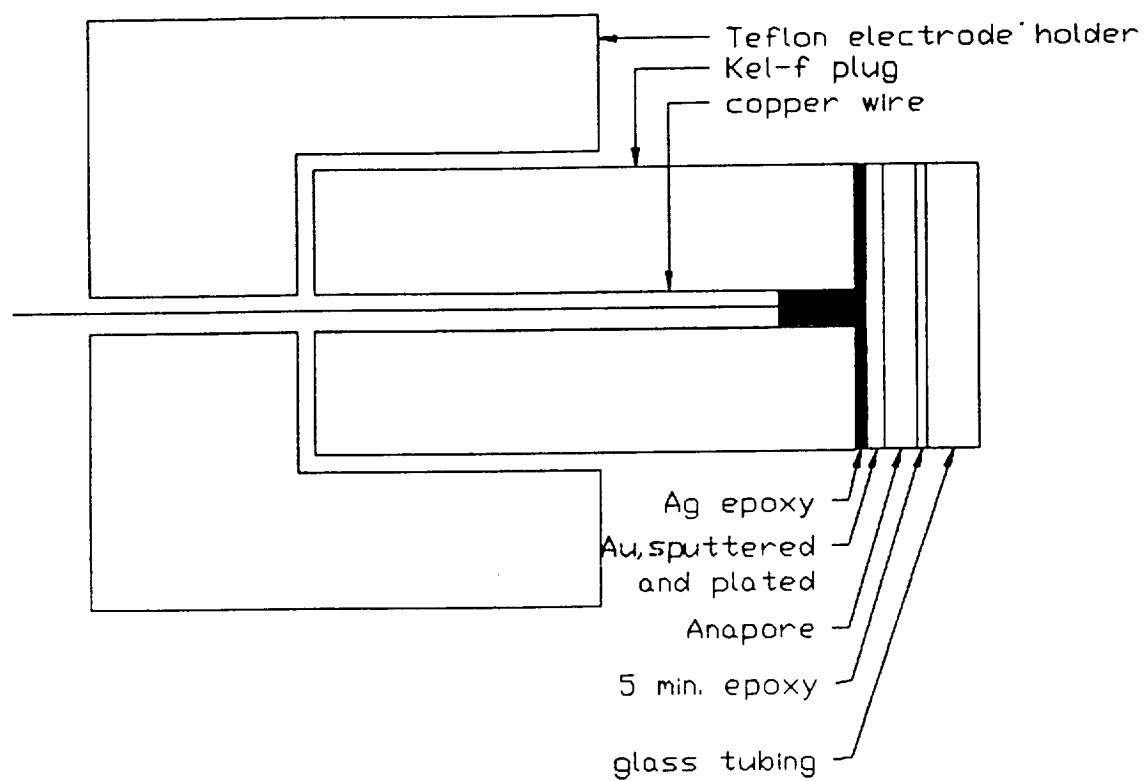
Fig. 12. Schematic of Fibrillar Polypyrrole Battery Cathode.

B

Ag/AgNO3 reference
solution in

1/2"

Luggin capillary

glass tubing

2"
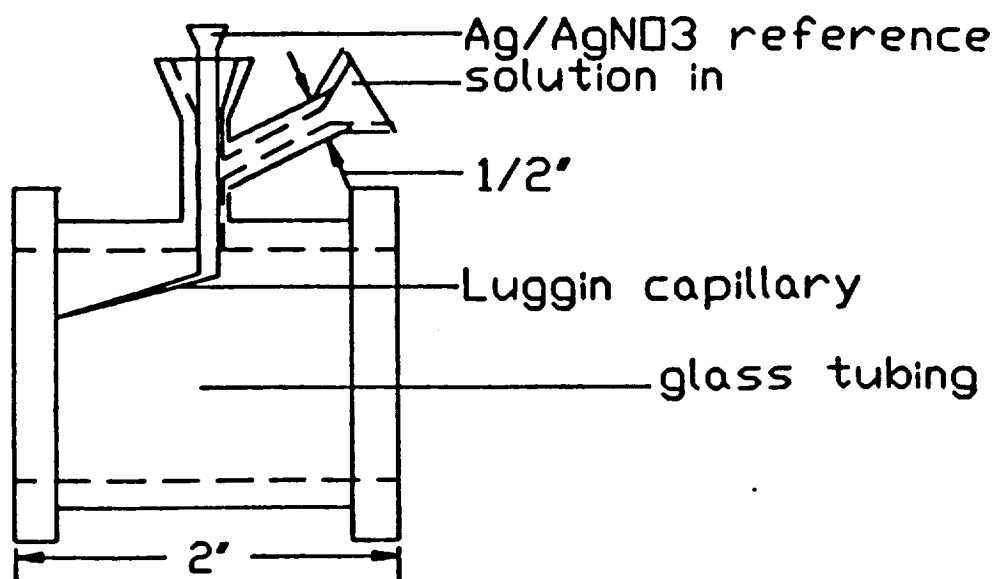
Fig. 13. Schematic of Polypyrrole Battery Reservoir.

reference electrode was used.

Figure 14 is a schematic of the lithium anode. It was constructed by first spot welding a 3/8 inch diameter disc of Ni gauze to a Ni wire. The gauze served as the current collector and the Ni wire served as the electrical contact. The gauze was then imbedded in a Kel-f® plug with the Ni gauze on one side and the Ni wire running out the other side. Lithium foil was pressed onto the Ni gauze and was allowed to cold-weld. The lithium electrode was then placed in a teflon electrode holder equipped with a screw mechanism. This mechanism was used to control the position of the electrode in the electrochemical cell. Before each experiment, the surface of the lithium electrode was renewed by scraping the passivated portion with a scalpel. The screw mechanism was then employed to return the electrode to its original position in the cell. The completely assembled cell is shown in Fig. 15. It is held together with two large metal clamps. An O-ring is used in the joint between the cell reservoir and the anode since the electrode holder for the anode is made out of teflon rather than glass.

As mentioned earlier, cyclic voltammetry studies involving a polypyrrole film-coated working electrode and a platinum counter electrode were done in a glove bag using a 5 dram vial as a cell reservoir. The platinum counter electrode consisted of a 3/8 inch Pt disk spot welded to a Pt wire, which was heat sealed in glass tubing. It was cleaned by soaking it in chromic acid 5-10 minutes on low heat. All solutions were degassed for 20-30 minutes before use in the glove bag or glove box. Also, for the cyclic voltammetric studies using the glove bag, 1% water (0.15 cc in 15 ml) was used in the pyrrole polymerization solution as in previous work done in this laboratory and by Diaz (3, 37). Water was not used for
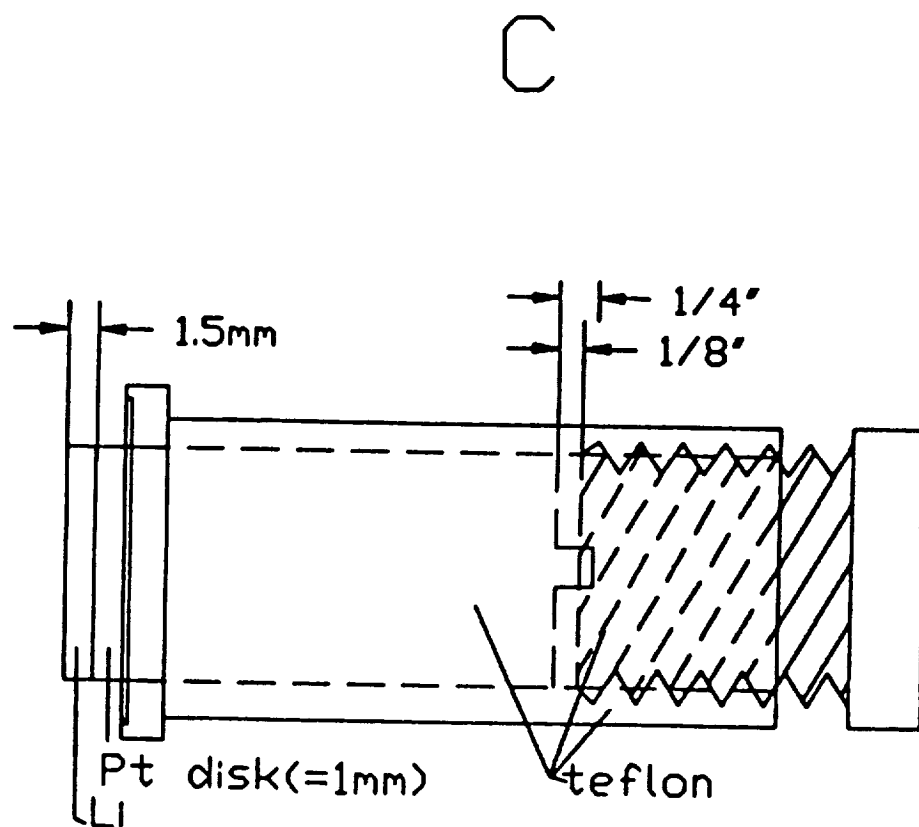
Fig. 14. Schematic of Li/Polypyrrole Battery Anode.
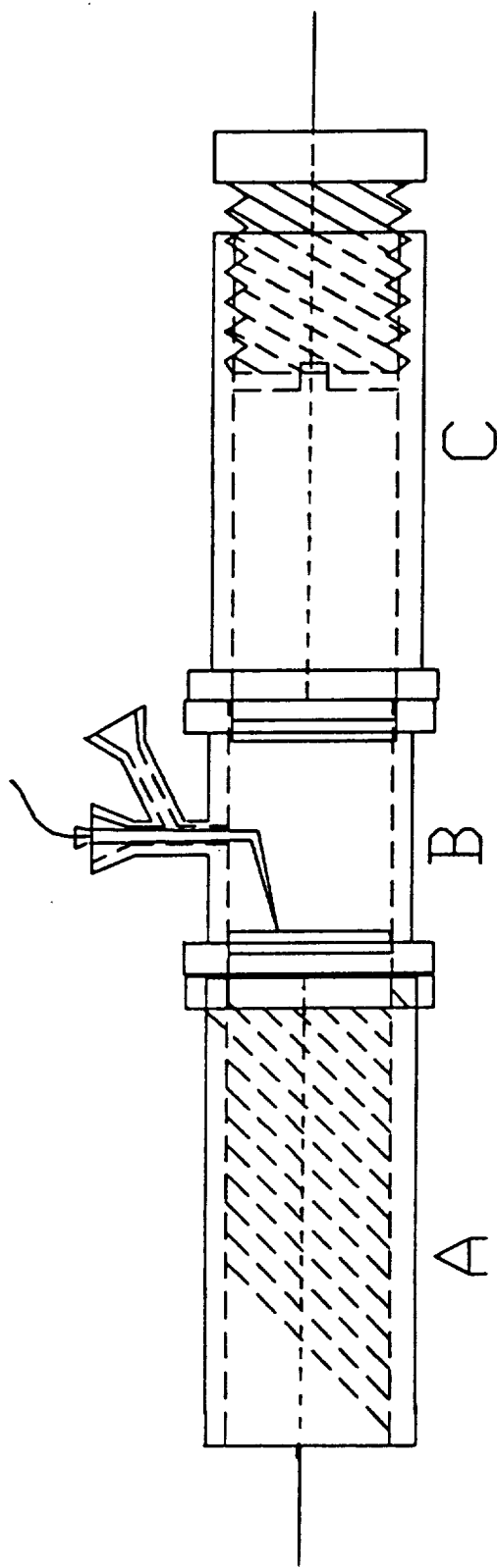
Fig. 15. Schematic of Completely Assembled Li/Polypyrrole Battery.

polymerization in any studies involving lithium.

Procedure for preparing electron microscopy stages. Stages for electron microscopy were made from 3/8 inch long sections of stainless steel rod (3/8 inch diameter). One end was polished with 1 μm alumina so that it could serve as a level base for mounting samples. Samples were mounted using either carbon paint or silver epoxy and sputter deposited with approximately 100 Å of gold. The samples were allowed to air dry 24 hours before electron microscopy was conducted. This method of preparing samples ensures that the samples are sufficiently conductive and are completely dry so that no outgassing occurs in the vacuum chamber of the electron microscope. The surface of some of the electron microscopy stages were ground at a 45° or 90° angle so that the edge of the sample could be viewed and photographed.

Battery charge/discharge experiment. Solutions used in the battery charge/discharge experiment and a materials checklist are presented in Appendix A. The battery charge/discharge experiment was conducted as follows. First, the atmosphere in the glove box was checked. If the oxygen or moisture content was too high, it was purged until the O_2 content was under 10 ppm and the H_2O concentration is less than 20 ppm. This was determined by keeping a vial of $TiCl_4$ and a vial of Et_2Zn in the glove box. $TiCl_4$ will vaporize at 10 ppm of H_2O and Et_2Zn will vaporize at 20 ppm O_2. After the cell was assembled and checked for leaks, the solution in the $Ag/AgNO_3$ reference electrode was checked for clarity. If it was black, there was metallic silver present and the frit could have been clogged. To ascertain whether the electrode was still serviceable, the resistance was checked with a multimeter and a silver

wire in an electrolyte solution to see if the electrode was still conductive. Also, if there was another Ag/AgNO$_3$ reference electrode available, the potential difference between them was checked with the multimeter. If there was a difference of only a few millivolts, the electrode was still considered serviceable. If the electrode was not conductive or had a potential more than a few millivolts different from another Ag/AgNO$_3$ reference, it was replaced.

A background cyclic voltammogram from +0.4 V to -1.25 V vs. Ag/AgNO$_3$ was conducted before growing the polypyrrole film. The cell was then returned to open circuit while the pyrrole monomer solution was added and mixed. After programming the PAR 273 in the galvanostatic mode and resetting the coulometer, the polypyrrole film was grown (‾0.32 mA , 567 sec for conventional films; ‾0.3 mA, 604 sec for fibrillar films). The potential during polymerization was about 0.6 V vs. Ag/AgNO$_3$. The cell was again returned to open circuit and if the film was fibrillar, the template membrane was dissolved. This was accomplished by continuous stirring in 0.2 M NaOH solution for approximately 30 minutes. The film was then gently rinsed with dry propylene carbonate and exposed to 1% HClO$_4$ for approximately five minutes while being stirred continuously. The film was returned to the cell, which contained fresh electrolyte solution. The film was potentiostatically reduced at -1.25 V vs Ag/AgNO$_3$, a cyclic voltammogram was conducted, then the film was reduced again. The galvanostat was then programmed to conduct a constant current charge/ discharge experiment. The battery was charged at -0.032 mA for 600 sec for a conventional film and at -0.03 mA for a fibrillar film. Though the currents used for the two types of films were slightly different, the

current densities were the same. Cycling was continued using more increments of charge until the battery failed. After the completion of the battery charge/discharge experiment, another cyclic voltammetry was conducted to ascertain that the polypyrrole film was irreversibly damaged.

CHAPTER III

THEORETICAL

Mechanism of polypyrrole film growth. In order to understand the
calculation of the amount of polymer deposited on the electrode when a
certain amount of charge is passed, the subjects of polymerization, chain
propagation and electronic conduction along a chain must be addressed.
A repeating unit of polymer with a known number of counterions
involved in the doping reaction is needed in order to calculate amount of
polymer deposited on the electrode. In addition, the doping level is needed
to calculate the energy density of the battery. Polymerization of
polypyrrole can be accomplished either chemically (27) or
electrochemically (3). For the entire body of this work, electrochemical
polymerization was employed.

First, pyrrole monomer is oxidized at the electrode surface by
removal of an electron from the monomer. The radical cation formed
undergoes resonance stabilization (Fig. 2). Chain formation begins
when two radical cations couple and two hydrogen ions are given off,
leaving two neutral pyrrole monomers joined. Chain growth continues
as free radical cations attack sites on the end of existing polypyrrole
chains. As is evident from Fig. 2, two electrons are removed during
polymerization to form a dimer, and two more are removed to form a
trimer. Likewise, two more must be removed to form a tetramer. In
order for the tetramer to be part of a repeating unit on a polymer chain,
another two electrons must be removed.

Previous work by Diaz (3) suggests a 25% doping level for polypyrrole.
One counterion is assumed present for each repeating unit of four

pyrrole monomers. Therefore, there is an additional electron taken away for every four monomer units when the polymer is in its oxidized form, as it is at the time of polymerization. This means that 2.25 electrons are required from each monomer unit for polymerization. Calculation of the amount of polymer deposited on the electrode from amount of charge passed during polymerization is discussed in detail in the following section on energy density. Energy density calculations for the Li/polymer battery are also included.

Energy density. The energy density of a battery, or specific energy as it is sometimes called, is defined (40) as the ratio of the energy obtainable from a cell or battery to its volume (in watt-hours/liter or Joules/liter) or mass (watt-hours/kg or J/kg). Definitions of related terms are given in Appendix B. Energy densities are often used as a measure of battery performance and are used to compare different types of batteries. This section discusses the terms used in battery comparisons, and includes an explanation of how energy density is theoretically and experimentally determined. Other work done in this area is discussed and examples of calculations are given.

The theoretical energy density of a battery is based only on the active materials that participate in the electrochemical reaction and the potential of the cell. Water, electrolyte, and any other material not involved in the electrochemical reaction are not included. Free energy values are used to calculate the theoretical energy density from the relationship

$$- \Delta G^0 = nFE^0 \qquad [2]$$

where n = the number of electrons involved in each of the half-cell reactions that sum to the overall reaction, F = Faraday's constant (96,487 coulombs or 26.8 amp-hours per mole of electrons involved in the half-cell reactions), and E^0 = standard cell potential in volts. Thus, one gram-equivalent weight of material theoretically releases one Faraday of coulombs.

One way to calculate the theoretical energy density of a battery is to assume that one gram of active mass consists of a material whose molecular weight is the sum of the molecular weights of the active mass components. This one gram of mass can be divided by the collective molecular weight, M:

$$\frac{1 \text{ gram of active material}}{M} = \text{\# moles total reactant}$$

$$(\text{\# moles total reactant})(n) = \text{moles of electrons}$$

$$(\text{moles of electrons})(F) = \text{\# of coulombs (or amp-hours)} = \text{capacity}$$

$$(\text{capacity})(E^0) = \text{\# of watt-hours} = \text{energy}$$

$$\frac{\text{energy}}{1 \text{ g of active material}} = \text{energy density}$$

For example, for a Zn/Cl_2 system, assume 1 g of active material. The overall reaction is:

$$Zn + Cl_2 \Rightarrow ZnCl_2$$
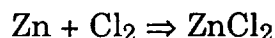
for this system,

$$M = 65.4 \ (Zn) + 70.9 \ (Cl_2) = 136.3 \text{ g/mole}$$

$$n = 2$$

$$F = 26.8 \text{ Ahr/mole of electrons}$$

and $E^0 = 2.12 \text{ V} = 2.12 \text{ J/C}$

Using 1 kilogram as a basis,

$$\frac{1 \text{ kg}}{0.136 \text{ kg/mole}} = 7.34 \text{ mole of of active material}$$

$$(7.34 \text{ mole})(2\frac{\text{moles of electrons}}{\text{mole active material}}) = 14.68 \text{ moles of electrons}$$

$$(14.68 \text{ moles of electrons})(26.8 \frac{\text{Ahr}}{\text{mole of electrons}}) = 394 \text{ Ahr}$$

$$(394 \text{ Ahr})(2.12 \text{ V}) = 835 \text{ Whr}$$

and, finally, divide by the number of grams of material used as a basis, 1 kg in this case, to get the energy density. Therefore, the theoretical energy density of the Zn/Cl_2 battery = 835 Whr/kg.

The units of energy density often cause confusion. One might ask, per kilogram of what? Recall the reaction:

$$Zn + Cl_2 \Rightarrow ZnCl_2$$
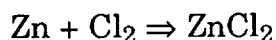
The ΔG^0 value given is per 1 mole of Zn, per one mole of Cl_2, or per one mole of $ZnCl_2$. It is therefore 1,738 Whr per gram of Zn, 1600 Whr per gram of Cl_2, or 835 Wh/kg of "active material," or for both the mass of the Zn and Cl_2 added together, which is the value obtained in the example above. The experimental energy density is lower than the theoretical energy density because in practice one gram-equivalent weight of reactant will not totally react to release a full 26.8 Ahr, and because the entire mass of the battery must be included in calculating the experimental energy density. In fundamental studies of new battery systems, the experimental energy density is often defined using only the active ingredients (14) rather than the entire mass of the battery in order

to simplify calculations and free the experimentalist from engineering restraints. After the basic premise of the battery has been proven, refinement of the system to streamline it using different materials and design can be undertaken. Experimental energy densities in this work are calculated using the formula

$$\text{e. d.} = \frac{iEtA}{m} \qquad [3]$$

where e.d = energy density, i = current density during discharge, E = potential during discharge, t = time of discharge, A = electrode surface area, and m = mass of active components. Since the potential varies during battery discharge, the value Et was obtained from the area under the potential/time curve.

These values are calculated from data recorded during constant current charge/discharge experiments. When discharged at constant current, the potential/time transient looks like the one in Fig. 16. While the theoretical capacity of the battery would be calculated using the following equation:

$$\text{Theoretical capacity} = C_t = \frac{mnF}{M} . \qquad [4]$$

the practical capacity can now be calculated from experimental data using the equation:

$$\text{Practical capacity} = C_p = \frac{it'A}{m} \qquad [5]$$

- i mA/cm^2

Charge

+ i mA/cm^2

Discharge

E

——►TIME

PPy^0 + Li$^+$ + ClO$_4^-$

——►PPy$^+$ + ClO$_4^-$ + Li^0

PPy$^+$ + ClO$_4^-$ + Li^0

——►PPy^0 + Li$^+$ + ClO$_4^-$

i

Q$_{in}$

Q$_{out}$

t
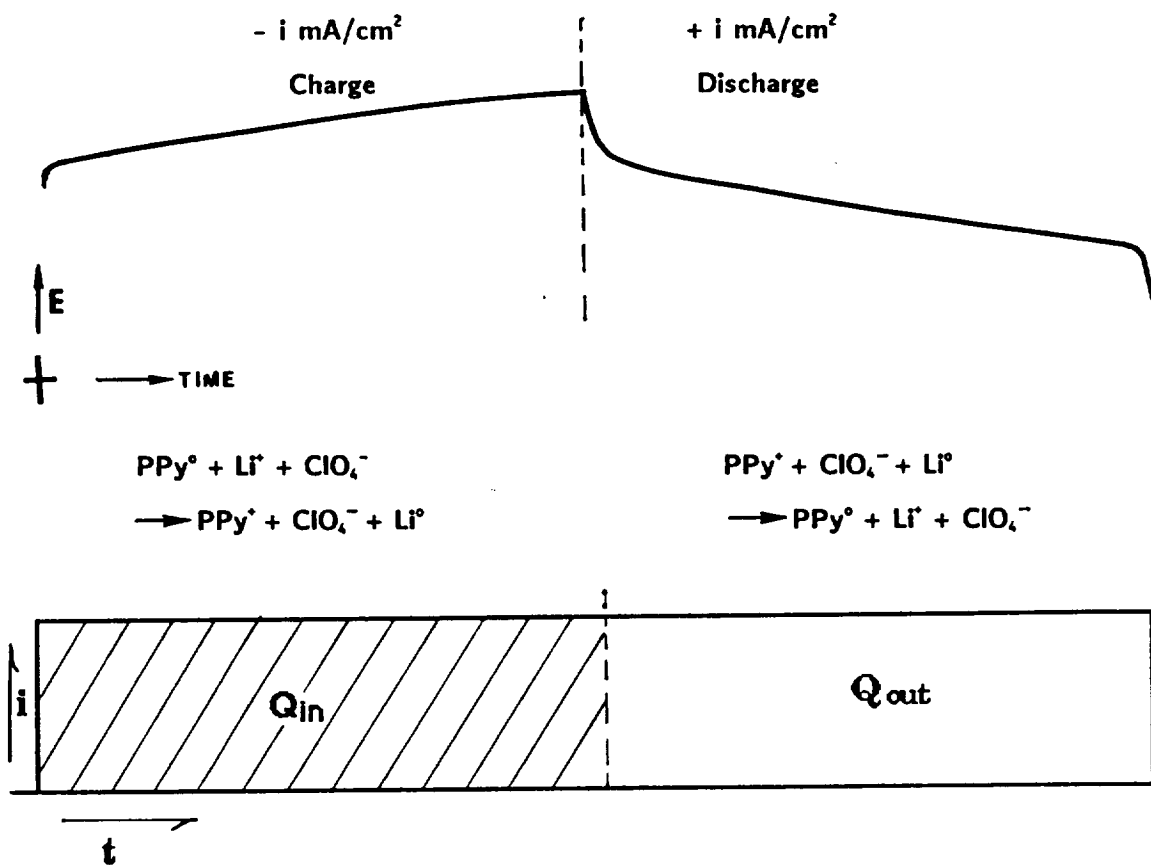
Fig. 16. Charge/Discharge Curve for Li/Polypyrrole Battery.

The time t′ is the discharge time after which the battery can no longer maintain its rated voltage when a constant current is drawn. Getting a average value of potential, E_{ave}, from the plateau of the discharge curve allows calculation of the energy density, as explained below.

For a constant current discharge, the circuit is as shown in Fig. 17. a. Ohm's law for an electronic circuit states that $E = IR$, where E = potential, I = current (not current density), and R = resistance. In this experiment, I, the current, is constant and E and R change. The galvanostat includes a variable resistor and draws a constant current. The potential/time transient is recorded and the practical energy density is calculated from the values of E, t′, I and battery mass in Eq. [3] above .

Another way to determine the energy density experimentally is with a fixed load (resistor). This experimental setup is shown in Fig 17. b. Both the potential/time transient and the current/time transient are recorded, and the areas under both curves are used to determine the total amount of energy, **E**, obtained from the battery from the relationship

$$\mathbf{E} = \int_{t=0}^{t=\infty} EIdt .$$

[6]

This problem can be solved using a simple numerical method such as the trapezoid rule, making a table of IE vs. time to use as input. If the data can be stored in digital form on a computer, a software package such as Kaleidagraph® can be used to determine the area under each curve and then obtain the total energy.

A constant power device can also be used to determine the energy available from a battery. A light bulb or small motor will provide a constant draw of power from the battery. Power = IE; so if the

a.

```
┌─ X-Y Recorder, E vs. t ─┐
├─ + BATTERY - ───────────┤
└─ GALVANOSTAT ───────────┘
```

b.

```
┌─ CHART Recorder, (E vs. t) ─┐
├──── + BATTERY - ────────────┤
└─ RESISTOR ── AMMETER ───────┘
```

c.

```
┌─ + BATTERY - ─┐
├──── MOTOR ────┤
└──── TIMER ────┘
```

d.

```
┌─ AMMETER ─┬─ + BATTERY - ─┐
├──── POTENTIOSTAT ─────────┤
└───────────────────────────┘
```
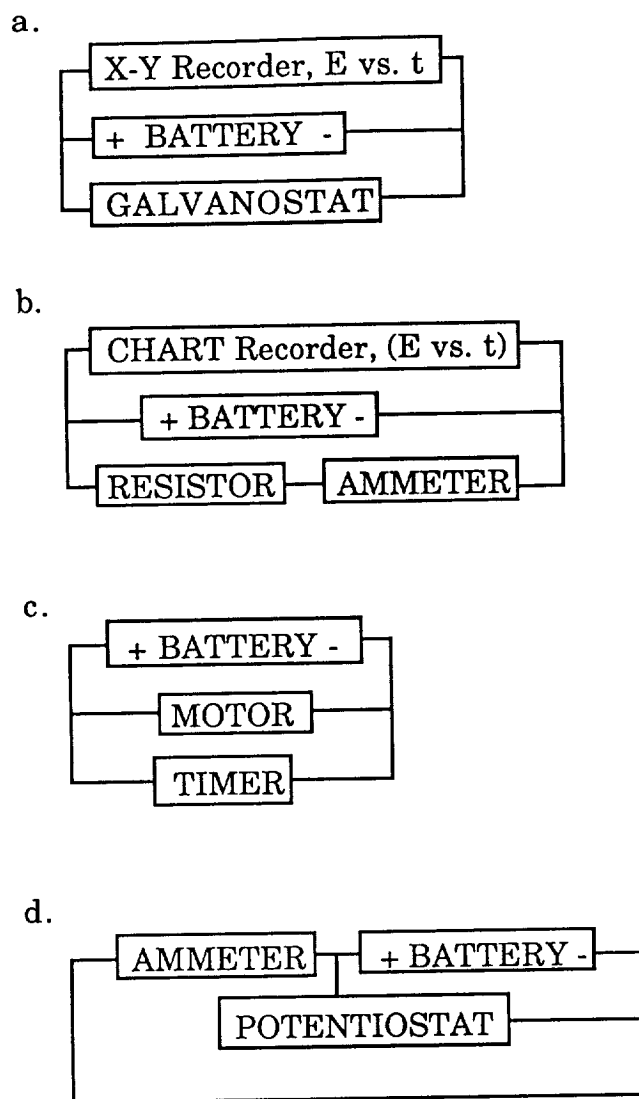
Fig. 17. Circuit Diagrams for Battery Discharge. a. Constant Current Discharge, b. Constant Load Discharge, c. Constant Power Discharge, d. Constant Potential Discharge.

power/time transient is recorded, the area under the power/time curve divided by the total mass of the battery would give the practical energy density of the battery. The circuit diagram for a constant power discharge is shown in Fig. 17. c.

A constant potential discharge is yet another method that can be used to get the energy density of a battery. A potentiostat, which has a variable resistor, draws a constant potential from the battery. The circuit diagram for the constant potential discharge of the battery is shown in Fig. 17. d. The current/time transient resulting from the battery discharge provides information needed in order to calculate the energy density of the battery. An average value of the current, I_{ave}, can be used with the discharge time and value of constant potential to calculate energy, which is equal to IEt. Alternatively, the area under the current /time curve can be used as in Eq. [6] to calculate the energy, $\mathbf{E}$.

A review of recent literature (5-28) reveals that the most common method of determining the energy density of a Li/polymer battery is by constant-current charge and discharge of the battery. In most cases, an average potential, E_{ave}, was multiplied by t′ as in Eq. [3] rather than determining the area under the curve. In some papers by MacDiarmid et al. (19-26) an E vs. Q (charge) curve was constructed by multiplying the time axis of the E/t transient by the constant current used in the experiment. The charge was also correlated to the percent doping of the polymer film.

Methods of determining the denominator of Eq. [3] were varied, as were experimental results. Some work involving a Li/Polyacetylene battery by MacDiarmid et al. (19-26) was reviewed to gain a better understanding of doping level calculations. The discharge equation used

was

$$\left[CH^{+0.06}(ClO_4)^-_{0.06}\right]_x + 0.036xLi \rightarrow \left[CH^{+0.024}(ClO_4)^-_{0.024}\right]_x + 0.036xLiClO_4 \quad [7]$$
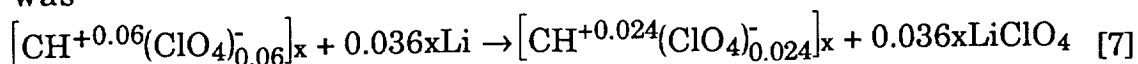
This equation deals with the percent doping of the polymer film being 0.06 before discharge and 0.024 after discharge. Energy densities are calculated by using the mass of film employed and the amount of lithium consumed. In one paper (26) the mass of the polymer used in the cell was considered in the calculation of the energy density. The theoretical energy density for a lithium/ polyacetylene cell was given as 307 Wh/kg and the experimental energy density reported as 176 Whr/kg. An energy density estimate for a packaged battery including the mass of the solvent, electrolyte, and casing was given as either 25 Wh/kg (24, 26), a reduction factor of 7, or 30 Wh/kg, a reduction factor of 6. Attempts to calculate these energy densities from the data given in the papers was unsuccessful. A better definition of the values for E_{ave}, t', and the mass of materials to be considered in the calculations is needed.

Petiot et al. (27) report data in Ahr/kg and call it the "massic capacity." The equation used is:

$$massic\ capacity = \frac{It'}{W}. \quad [8]$$

where W = weight of active components. Chemically synthesized 30 mg pellets of polypyrrole were used. The anode during discharge was a Li/Al alloy or Al foil. Data were obtained by constant current discharge and the massic capacity or capacity reported for the cell was 120-140 Ah/kg.

Shacklette et al. (10) also report capacity rather than energy density and call it gravimetric capacity, in Ah/g. A constant current discharge was employed to collect the data, and the anodes were a Li/Al alloy, a

Li/WO$_2$ alloy, and Li. PPy film was used for the anode. Capacities were based on polymer weights only, including the weight of the BF$_4^-$ anions.

Energy density in the work of Munstedt et al. (5) was calculated using the mass of the polypyrrole plus the dopant anion, BF$_4^-$. Lithium was used as the negative electrode and a value of 297 Wh/kg was reported. The mass of the entire packaged battery was considered for each of three battery types, sandwich #1, sandwich #2, and a spirally-wound cylindrical battery. Sandwich #1 had an energy density of 20 Whr/kg, sandwich #2 had an energy density of 20 Whr/kg, and the cylindrical battery had an energy density of 15 Wh/kg. The battery was cycled using a potential step and a charge/time transient was recorded. The "charge density" in Ah/kg was multiplied by the open circuit potential (vs. Li) to calculate energy density. A reduction factor is the quotient of the experimental energy density calculated using only the mass of active ingredients and the experimental energy density calculated using the weight of the entire packaged battery. The reduction factor for (297 Wh/kg)/(20 Whr/kg) is 14.9, much larger than the empirical reduction factor estimated by MacDiarmid.

In a paper by B. Scrosati et al. (7), a constant current density (33 μA/cm^2) discharge was carried out to determine E$_{ave}$ (3.3 V), which was multiplied by the "specific capacity" in Ahr/g to get an energy density of 100 Wh/kg. The reference electrode and anode were lithium metal. The energy density is quoted for the "Li/polythiophene(ClO$_4^-$) couple only," so only the mass of the active material involved was considered. The authors state that the specific conductivity corresponds to a 10% doping level. The thickness of the film was given, that is, the total charge used to make the film.

In a general paper by Passiniemi and Osterholm (9) entitled "Critical aspects of Organic Polymer Batteries," values for specific charge were given for polyaniline, poly-(p-phenylene), polypyrrole, and polythiophene (PT) were calculated from an assumed polymer density of 0.7 g/cm^3 and a 100 μm thick film. These are not consistent with values found elsewhere which give a density of 1.1-1.6 g/cm^3 for polythiophene and 1.45 - 1.51 g/cm^3 (depending on the dopant anion used) for PPy. The capacity density is given as 103 mAhr/g. This value is multiplied by the open circuit potential and some conversion factors to get the energy density. Apparently the mass used in calculations was based on the assumed polymer densities only.

A paper by Yamamoto et al. (28) gives the surface area of the electrode as well as the mass of the polymer (PPy and PT) on the electrode, a rarity in the papers reviewed. A constant current discharge was done and a potential/time transient was measured. The average discharge potential, E_{ave}, was 1.22 V for the PT cell. The anode used was $Zn/ZnI_2/I_2$. Although no energy density was given, an energy density of 195 Wh/kg could be calculated considering only polymer mass, which compares very favorably with other reported values for polymer batteries.

Trinidad et al. (18) performed a constant current discharge on a PPy/Li battery, and from the potential/time transient, numbers for E_{ave} and t' could be obtained. Using a value of 1.51 g/cm^3 for density of polypyrrole, an energy density of 127 Wh/kg could be calculated. Using the open circuit potential, instead of E_{ave} as some authors do, would result in a value of 174 Whr/kg for the energy density.

Also reviewed were recent papers by Osaka, et al. (11-17). Equation [3] was used;

$$\text{e. d.} = \frac{iEtA}{m}$$

where e.d = energy density, i = current density during discharge, E = average discharge potential, t = time of discharge, A = electrode surface area and m = mass of active components. However, the surface area of the electrode was not given. The mass of the polypyrrole film only was considered, and it was actually weighed, not estimated from the amount of charge applied during polymerization and doping level. Unfortunately, the mass was not given, so attempts at reproducing the calculation of energy density, given as 85.6 Wh/kg, were unsuccessful. In one of the papers (15), a value for energy density can be estimated from the total charge during polymerization, using the density of polypyrrole and considering the mass of the polymer only. This estimated value is 75 Wh/kg.

In many papers, the mass of materials used to calculate the energy density is reported in kg, g, or mg, but is referred to as weight. The units of weight are Newtons, dynes, or pounds force (lbf), and the units of mass are kilograms, grams, or pounds mass (lb_m) (41). The equation that relates weight to mass is

$$W = \frac{(m)(g)}{g_c} \tag{9}$$

where   W = the weight of an object,

           g = the acceleration of gravity,

and g_c = a conversion factor:

$$g_c = 1 \frac{\frac{kg\ m}{sec^2}}{N} = 1 \frac{\frac{g\ cm}{sec^2}}{dyne} = 32.174 \frac{\frac{lb_m\ ft}{sec^2}}{lb_f} \tag{10}$$

From Eq [9] and Eq. [10], one can see that mass and weight are numerically the same unless they are reported in lb_m and lbf, respectively. Even using lb_m and lbf interchangeably could be a mistake, because while g_c is constant, g varies with position. Therefore mass, unlike weight, is constant. An object at sea level would weigh slightly more than it would in Denver, and in Denver it would weigh considerably more than it would in space. Lithium batteries are particularly applicable for space applications because they have lower mass than most batteries, so mass and weight should not be confused with each other in the literature.

This project includes the determination of the theoretical and experimental energy densities of the Li/PPy battery. The experimental energy densities are determined from data collected using the constant-current method of charging and discharging a battery. This method was chosen because it is commonly used in the literature and for purposes of comparison of data it seems the most useful. The experiments were first performed on a commercial Ni/Cd secondary battery. The theoretical energy density of a Ni/Cd Battery can be calculated using the method described earlier and illustrated by the Zn/Cl_2 example. The half reactions and overall reactions are as follows (42):

$$
\begin{array}{lll}
2(NiOOH + H_2O + 1e^- = Ni(OH)_2 + OH^-) & E^0 = & 0.60 \text{ V} \\
+ \quad\quad Cd^0 + 2OH^- = Cd(OH)_2 + 2e^- & E^0 = & -(-0.81)\text{ V} \\
\hline
2NiOOH + 2H_2O + Cd^0 = 2Ni(OH)_2 + Cd(OH)_2 & E^0 = & 1.41 \text{ V}
\end{array}
$$
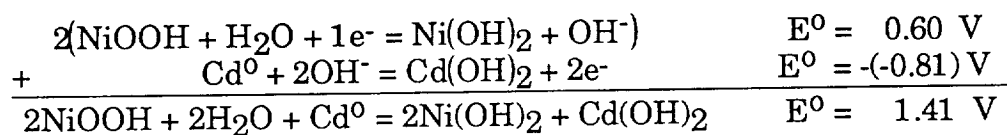
As can be seen in the overall cell reaction above, two moles of NiOOH are needed for every one mole of Cd. Water is not considered in the calculation of the energy density since it is the solvent.

As stated above, to calculate the theoretical energy density of a battery, it is necessary to start with a known amount of active material, called a

basis. Starting with a basis of 1 kg of active material and knowing that the molecular weight of Cd = 112.41 and the molecular weight of NiOOH is 91.7, then it can be calculated that 1 kg of active material = 3.39 moles of active material:

$$2\left(91.7 \frac{g}{\text{mole of Cd}}\right) + 112.41 \frac{g}{\text{mole of NiOOH}} = 295 \frac{g}{\text{mole of active material}}$$

$$295 \frac{g}{\text{mole of active material}}\left(\frac{1\text{kg}}{1000\text{g}}\right) = 0.295 \frac{\text{kg}}{\text{mole of active material}}$$

$$\frac{\text{Basis of 1 kg}}{0.295 \frac{\text{kg}}{\text{mole of active material}}} = 3.39 \text{ moles of active material}$$

Now that the number of moles of active material has been calculated, recall Eq. [2]:

$$-\Delta G^0 = nFE^0$$

where, in this example,

$$n = 3.39 \text{ moles of active material}\left(2 \frac{\text{moles of e}^-}{\text{moles of active material}}\right) = 6.78 \text{ moles of e}^-$$

$$F = 26.8 \frac{A\,h}{\text{mole of electrons}}$$

and $E^0 = 1.41$ V.

The theoretical energy of a Ni/Cd battery is then

$$E = (6.78 \text{ moles of electrons})\left(26.8 \frac{A\,h}{\text{mole of electrons}}\right)(1.41 \text{ V}) = 256.2 \text{ Wh}$$

for 1 kg of active material, therefore the theoretical energy density is 256.2 Wh/kg. When experimental techniques were mastered using the Ni/Cd

battery, a lithium/polypyrrole battery was designed and built, using as guidelines diagrams from references (5) and (28). Both conventional film batteries and fibrillar film batteries were constructed and tested and comparisons were made.

The theoretical energy density of the Li/PPy battery can be calculated as in the previous Zn/Cl$_2$ and Ni/Cd examples. First, the cell potential can be obtained from summing the standard half reactions as before:

$$Li \rightarrow Li + e- \qquad\qquad E^0 = 3.3 \text{ V vs. SCE}$$
$$PPy^+ + e- \rightarrow PPy \qquad\qquad \underline{E^0 = -0.1 \text{ V vs. SCE}}$$
$$E_{cell} = 3.2 \text{ V}$$

The molecular weight of active materials is calculated using the doping level of the polypyrrole. If an optimistic 33% doping level is assumed, then the molecular weight of three units of polypyrrole is used and the molecular weight of one counterion is used. In this work, a conservative 25% doping level was assumed. The molecular weight of one pyrrole monomer is 67 g/mole, but since two hydrogen ions per pyrrole monomer are removed during polymerization, 65 g/mole is used as the molecular weight of a pyrrole unit on a polymer chain. The molecular weight of four pyrrole units on a chain is 4(65 g/mole) = 260 g/mole. The molecular weight of one ClO$_4^-$ ion = 99 g/mole, and the atomic weight of Li = 7 g/mole. Therefore, the molecular weight of active materials = 260 g/mole + 99 g/mole + 7 g/mole = 366 g/mole.

If a basis of 1kg, or 1000 g, is used, then

$$\frac{1000g}{366 \frac{g}{\text{mole of active materials}}} = 2.73 \text{ moles of active materials}$$

and the energy is

$$E = nFE° = (2.73 \text{ moles of electrons})\left(\frac{27 \text{ Ah}}{\text{mole of electrons}}\right)(3.2 \text{ V}) = 236 \text{ Wh}$$

for a basis of 1 kg.

Therefore, e.d. = 236 Wh/kg for a Li/LiClO$_4$/PPy battery. However, the use of a counterion other than ClO$_4^-$ or an assumption of a different doping level would change the calculations and result in a different value.

When calculating the energy density for a battery, the mass of the materials must be measured or calculated. For the the theoretical energy density, a basis of, for instance, 1 kilogram or 1 gram of active material is used. For determination of the experimental energy, the mass of only the active ingredients are used, and for the practical energy density, the mass of all the materials used to make the battery are included in the calculation, even the packaging. In this work, as in most of the similar work reviewed, only the amount of active ingredient was used in the calculations. The procedure used to determine the amount of active ingredient is as follows. As discussed in the previous section on pyrrole polymerization, there are 2e- taken from each monomer unit during polymerization. Assuming a 25% doping level (one counterion for every 4 pyrrole monomer units), there is an additional electron taken away for every 4 monomer units, therefore 2.25 electrons are required from each monomer unit for polymerization.

$$\frac{Q_f \text{ (polymerization charge)}}{F\left(2.25 \dfrac{\text{moles of e}^-}{\text{moles of Py monomer}}\right)} = \text{\# of moles of Py monomer polymerized}$$

For example, if $Q_f = 184$ mC,

$$\frac{0.184 \text{ C}}{\left(96487 \dfrac{\text{C}}{\text{moles of e}^-}\right) 2.25 \dfrac{\text{moles e}^-}{\text{moles Py}}} = 0.847 \ \mu\text{moles}$$

If there are 0.847 μmoles of pyrrole, then there are 0.847 μmoles of $LiClO_4$. The total amount of active material is:

$$0.847 \ \mu\text{moles Py} \left(65.1 \ \frac{\text{g Py}}{10^6 \ \mu\text{mole of Py}}\right) = \ 5.51 \times 10^{-5} \text{ g} = \ 5.51 \times 10^{-8} \text{ kg}$$

$$0.847 \ \mu\text{moles LiClO}_4 \left(\frac{106.5 \text{ g LiClO}_4}{10^6 \ \mu\text{mole LiClO}_4}\right) = 9.03 \times 10^{-5} \text{ g} = 9.03 \times 10^{-8} \text{ kg}$$

$$\text{Total} = 14.54 \times 10^{-8} \text{ kg}$$

Therefore, for a battery with a capacity of 1.93×10^{-5} Wh,

$$\text{e. d.} = \frac{1.93 \times 10^{-5} \text{ Wh}}{14.54 \times 10^{-8} \text{ kg}} = 130.6 \frac{\text{Wh}}{\text{kg}} \ .$$

CHAPTER IV
RESULTS AND DISCUSSION

Capacitance studies and electron microscopy   As mentioned in the introduction, early versions of fibrillar electrodes made in this laboratory showed a base layer of polypyrrole between the template membrane and the current collector. Recall the electrode schematic in Fig. 8, in which the template membrane was attached to the current collector by pressure. In order to eliminate the leakage of polymerization solution between the membrane and the current collector, electrode/membrane adhesion had to be improved. This was accomplished by sputtering or vapor depositing Au directly onto one side of the template membrane. The electrode was then assembled as described in more detail below. Figure 18 is a schematic of a cross section of the electrode used for this work. The membrane is attached to a section of glass tubing to hold it flat and give it mechanical stability, then sputtered with gold. More gold is vapor deposited or electroplated on top. Contact is made with silver epoxy and a copper wire, then Torr Seal®, an inert epoxy, is used to seal the electrode and make it more mechanically stable. Polypyrrole (PPy) was then grown galvanostatically through the pores in the template membrane, and the membrane was dissolved.

In order to ensure that there would be no leakage of solution through the Au layer, experiments were conducted to determined how much Au was needed to deposit a pinhole-free Au film. To determine whether the pores in the template membrane were completely covered, electron micrographs (EMs) were taken of membranes with
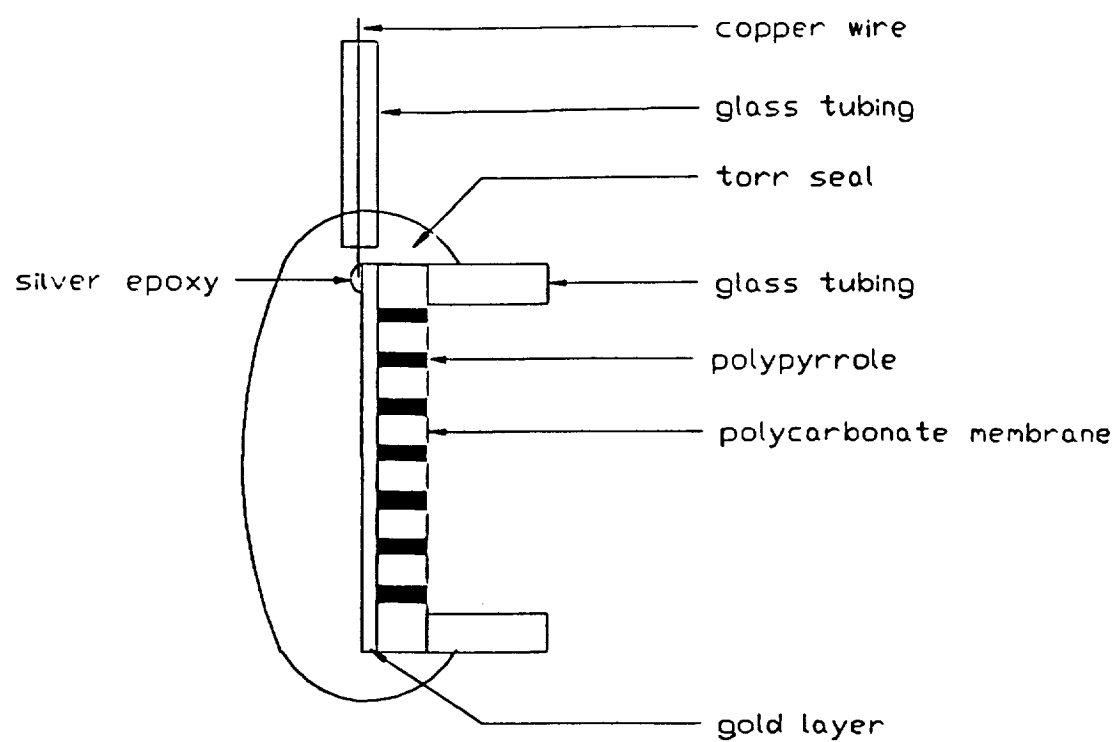
Fig. 18. Cross-section of Fibrillar Polypyrrole Electrode.

varying thicknesses of gold deposited on them. Figures 19-21 show a series of electron micrographs of 300 Å pore diameter polycarbonate membranes with 100 Å, 600 Å, and 900 Å of gold sputtered on them, respectively. Pores are no longer visible in Fig. 21. Also, a spot test with a highly colored (orange) ion, $Ru(bpy)_3^{2+}$, was performed. In this test, a drop of $Ru(bpy)_3^{2+}$ in KCl solution was placed on the Au side of a membrane which had been placed on a piece of white filter paper. The ion did not leak through the membrane shown in Fig. 21. Membranes with pores of 1000 Å diameter and 7000 Å of gold vapor deposited on them also passed the EM and spot tests. When electroplating was used as a method of Au deposition, 30 C/cm^2 were required for membranes with 2000 Å diameter pores to pass the EM and spot tests. The amount of gold necessary to achieve a pinhole-free film on the membrane had been determined for each pore diameter.

Capacitive studies were conducted using various methods of deposition of gold on Poretics® and Nuclepore® membranes. These studies were done to find the method of Au deposition that resulted in the best adhesion between membrane and Au layer. Cyclic voltammetry of an electrolyte solution with no redox couple was conducted so that the electroactive area could be calculated from the capacitive current of the cyclic voltammogram. The equation:

$$I_c = CvA_c \qquad\qquad [11]$$

where Ic is the capacitive current measured from the cyclic voltammogram, C is the standard capacitance of a gold electrode, and v is the scan rate, gives a value for the electroactive area that will be

Fig. 19. Nuclepore® Polycarbonate Membrane with 0.03 μm Pore Diameter and Sputtered with 0.01 μm of Au at 3000 X Magnification.

ORIGINAL PAGE
BLACK AND WHITE PHOTOGRAPH
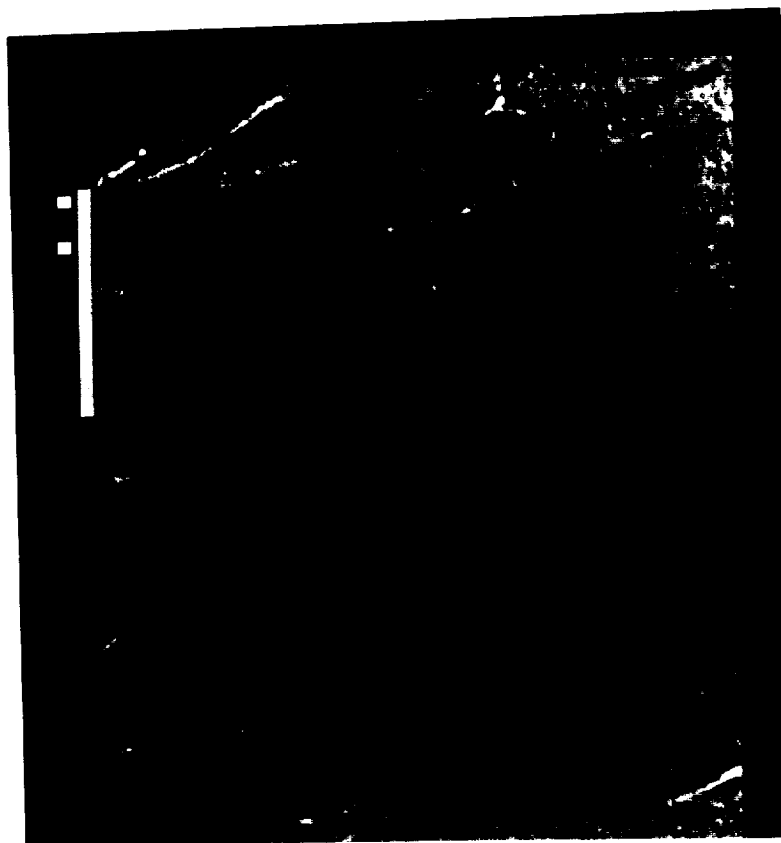
Fig. 20. Nuclepore® Polycarbonate Membrane with 0.03 μm Pore
Diameter and Sputtered with 0.06 μm of Au at 3,000 X Magnification.

Fig. 21. Nuclepore® Polycarbonate Membrane with 0.03 µm Pore Diameter and Sputtered with 0.09 µm of Au at 3,000 X Magnification.

referred to as A_c. The total electrode area including the part covered by the nonporous portion of the template membrane will be referred to as A_g (geometric area). A_f (fractional area) is that part of the geometric area not covered by the nonporous portion of the template membrane. The fractional area can also be defined as the area of the surface of the template membrane which is porous. It should be equal to A_c, the area calculated from the capacitive current of the cyclic voltammogram, if there is no leakage of solution between the Au layer and the template membrane. If a good seal has been made, only the area in the pores of the membrane should contribute to the electroactive area.

The two types of polycarbonate membranes investigated were a 0.1 μm pore diameter membrane made by the Poretics® Corporation and a 0.176 μm pore diameter membrane made by the Nuclepore® Corporation. The two methods employed for depositing gold were sputtering and vapor deposition. Both involve the use of a vacuum chamber and sputtering uses an Argon plasma as the medium in which to carry out the deposition. Sputter deposition is achieved by the bombardment of an Au target with Argon atoms. The gold removed from the target by this bombardment is deposited on the sample. In vapor deposition, gold shavings are heated until they vaporize and gold deposits on the sample as it cools. More gold can be deposited in less time with vapor deposition. Electrodes were made using each of the two methods separately, then some were made with a layer of sputtered gold and a layer of vapor deposited gold on top of the sputtered layer.

Results are tabulated in Table I. In order to determine which of the methods was superior, the data were analyzed in the following manner. If a good seal has been made, then the fractional area and the area

Table I. Capacitive Studies of Au/Membrane Electrodes.

		A_c (cm^2)	A_c/A_f	A_c/A_g
Nuclepore® (0.1 μm pore diameter)	Sputtered only, with 0.1 μm of Au	0.22 ± 0.19	9.94	0.23
	Vapor deposited only, with 0.7 μm Au	0.33 ± 0.19	14.7	0.343
	Sputtered and vapor deposited, with 0.7μm Au	0.38 ± 0.09	16.9	0.395
Poretics® membrane (0.176 μm pore diameter)	Vapor Deposited only	0.53 ± 0.34	1153	0.56
	Sputtered and vapor deposited	0.9	1956	0.95

calculated from the cyclic voltammograms should be the same, and the ratio A_c/A_f should be equal to 1. On the other hand, if a very poor seal has been made, the calculated area should be closer to the geometric area, and the ratio A_c/A_g should be closer to one. As can be seen in Table I, the latter is the case. None of the electrodes have an A_c/A_f ratio of one, and the Poretics® membranes were particularly poorly sealed. It was concluded that the polycarbonate membranes were not sealing well enough, and perhaps an inorganic membrane would make a better metal/membrane seal than an organic membrane. Other work done in the laboratory supported this conclusion. An aluminum oxide membrane made by the Anopore® Corporation was introduced. When the aluminum oxide Anopore® was used, there was no leakage of solution between polypyrrole and no evidence of base layer growth, as shown in Fig. 22. The polypyrrole fibrils are directly attached to gold posts, with no base layer of conventional polypyrrole.

Another issue that must be addressed is pore density. A higher pore density leads to higher fibril density since the fibrils are synthesized within the pores. A higher fibril density would result in increased charge capacity for the same electrode area. One drawback of using Nuclepore® as a template membrane is that the pore density does not increase proportionately with decreasing pore diameter. As can be seen in Table II, the electroactive area of an electrode made with a Nuclepore® membrane with a pore diameter of 0.01 μm would have an electroactive area of only 0.02% of the geometric area. Another company, the Poretics® corporation, can make membranes of much higher pore densities. Figure 23 is an electron micrograph of a Poretics® membrane with a pore density of 10^{10} pores/cm^2, which is two orders of magnitude

30KU   X10,000   1 μm   043007
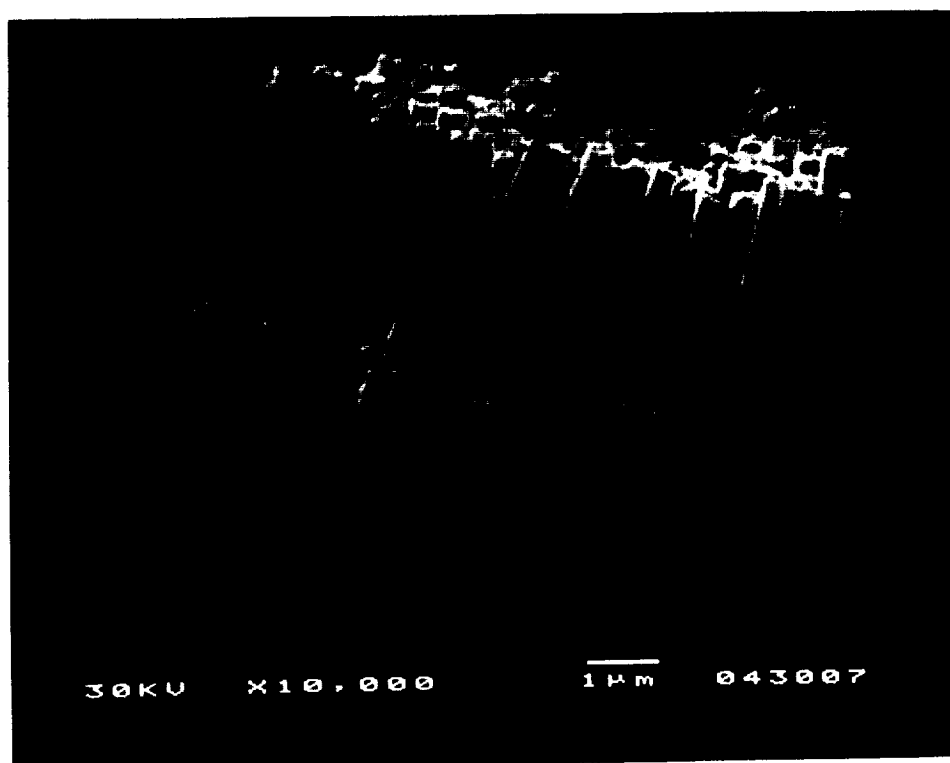
Fig. 22. Cross-section of Fibrillar Polypyrrole on Gold Surface with
Template Membrane Extracted. 1.0 cm = 1.0 μm.

Table II. Nuclepore® Membrane Data.

Pore Diameter (µm)	Pore Density (per cm^2)	Porous Area (%)
12	1.0×10^5	11.3
10	1.0×10^5	7.8
8	1.0×10^5	5.0
5	4.0×10^5	7.9
3	2.0×10^6	14.1
2	2.0×10^6	6.3
1	2.0×10^7	15.7
0.8	3.0×10^7	15.1
0.6	3.0×10^7	8.5
0.4	1.0×10^8	12.6
0.2	3.0×10^8	9.4
0.1	3.0×10^8	2.4
0.08	3.0×10^8	1.5
0.05	3.0×10^8	0.6
0.03	3.0×10^8	0.2
0.015	3.0×10^8	0.05
0.01	3.0×10^8	0.02

25kv 40.7kx .25µ 936
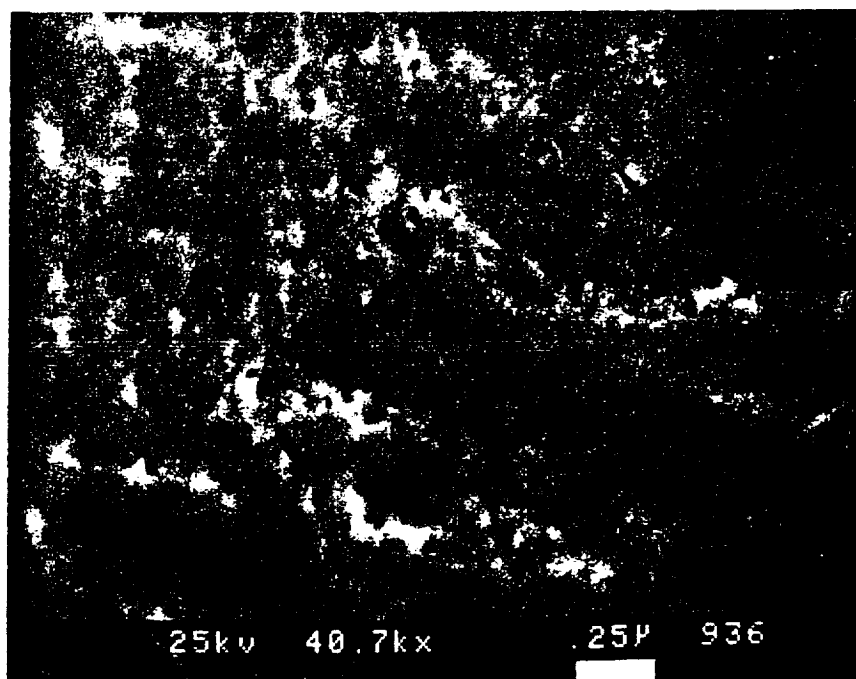
Fig. 23. Electron Micrograph of High Density (@10^{10} pores/cm^2)
Poretics® Membrane. 1cm = 0.25 µm.

higher than the highest pore density that the Nuclepore® corporation offers. However, the aluminum oxide membrane made by the Anopore® Corporation has the highest porosity (Fig. 24). Since the template membrane is about 60%-70% porous, the resulting fibrils cover about 60% of the electrode surface. We are limited to a fibril diameter of 2000 Å with the Anopore® membranes because Anopore® is commercially available only in the 2000 Å size.

Electron micrographs were taken of both conventionally grown films and fibrillar films. Figure 3 shows a representative conventional polypyrrole film and Fig. 11 shows a representative fibrillar film. It was found that for electrodes with the same geometric area, fibril length was approximately 1.6-2.0 times the thickness of a conventionally grown film.

Cyclic voltammetry   A cyclic voltammogram is a plot of potential vs. current, with potential as the independent variable. The potential is varied at a fixed rate, beginning at a certain starting potential, continuing to a certain terminal potential, then scanning back to the starting potential without pause. For the cyclic voltammetry in this work, the potential was held at a value at which the film should exist in its neutral, or reduced, state. This potential is around -1.0 V vs Ag/Ag$^+$ for polypyrrole. When the film was completely reduced, the potential scan was begun. As the potential is scanned positively, a current peak arises corresponding to the oxidation of the polypyrrole film. After the current has reached its maximum, it will decay to a constant value which is greater than the starting potential and remain there until the direction of the potential scan is reversed or another reaction begins to occur. This region is where the polymer is oxidized and conductive, as
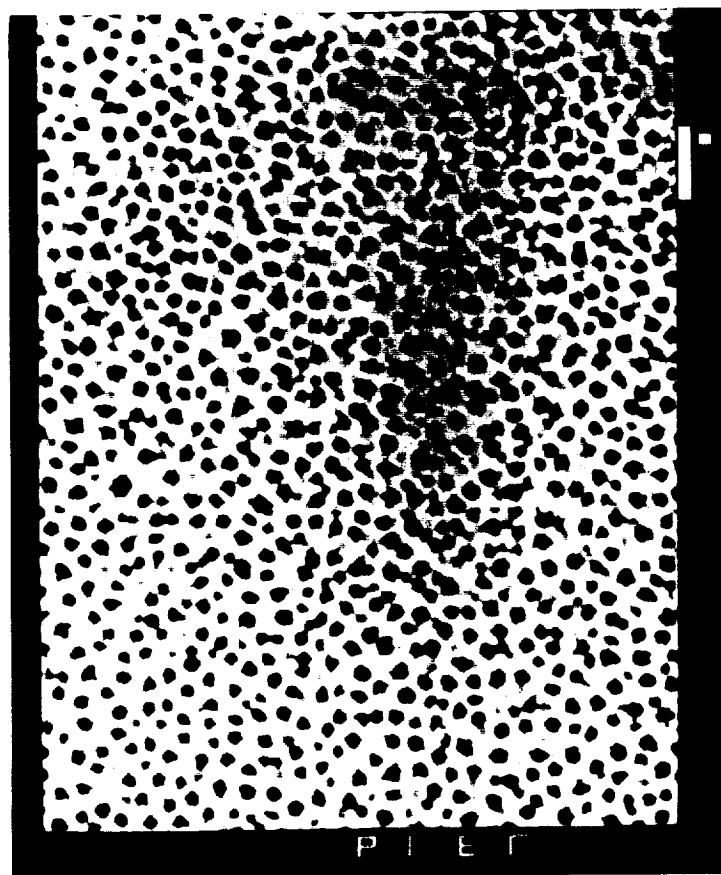
Fig. 24. Scanning Electron Micrograph of the Surface of an Anopore® Filtration Membrane with 0.2 µm Diameter Pores.

evidenced by the capacitive current present. When the potential scan is reversed, a reduction current peak arises, then the current decays to its original value as it was before the scan was begun. In this region there is negligible current and the polymer is in its insulating, or reduced, form again.

Cyclic voltammetry was conducted after the growth of every film to determine whether oxidation and reduction peaks characteristic of polypyrrole were present and to determine the potential at which each of these peaks occur. A representative cyclic voltammogram of a 2 μm thick conventionally grown film in 1 M LiClO$_4$ in propylene carbonate is shown in Fig. 25.

In order to determine rate of ion transport in thick films vs. thin films, a study was made of I$_p$ (anodic peak current) vs. scan rate for various film thicknesses. If diffusion of ions is facile in a thin film, the peak current for oxidation of polypyrrole in the cyclic voltammogram should be directly proportional to scan rate. In a thick film, ion transport is less facile and should be a diffusion-controlled process. One way to determine this is to conduct cyclic voltammetry at different scan rates for different film thicknesses. The peak current (I$_p$) for the anodic peak for each cyclic voltammogram (CV) is measured and plotted as a function of scan rate. For a thin film, the plot should be linear. As film thickness increases and ion transport becomes diffusion-controlled, the plot should begin to fall away from linearity and level off. Instead of being linear with respect to scan rate, the plot should be linear with respect to the square root of scan rate, in accordance with the Sevcik relationship (43):

$$I_p = (2.69 \times 10^5) n^{3/2} A D_0^{1/2} v^{1/2} C_0^* \qquad [12]$$

+ ← E → −

0.02 mA

200 mV
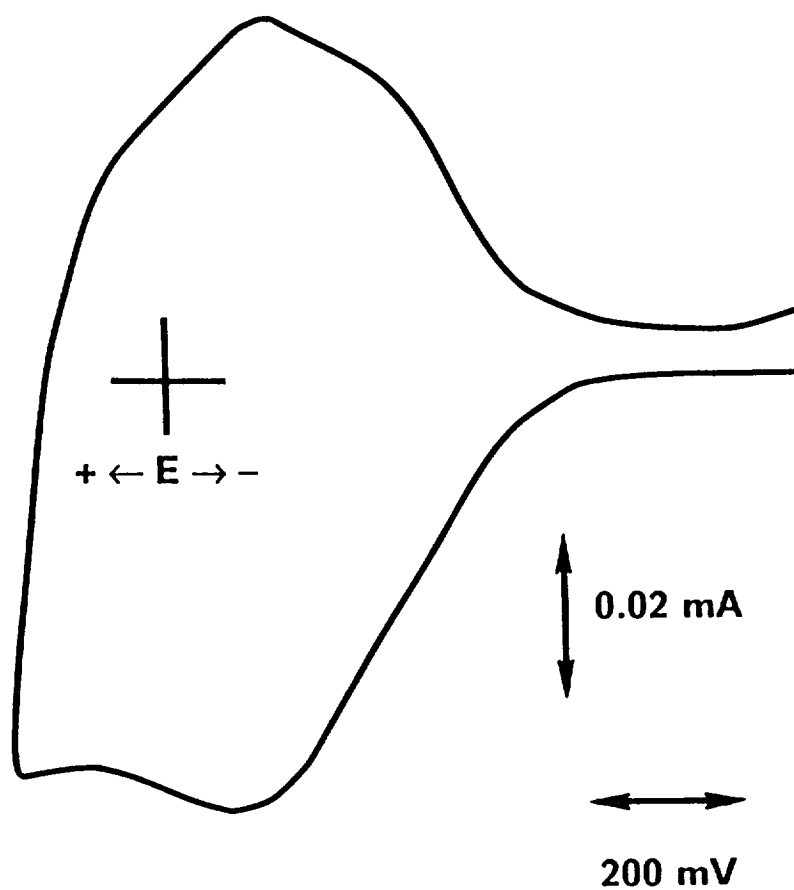
Fig. 25. Cyclic Voltammogram of Li/PPy Battery with 2 μm
Conventional PPy Film. Scan Rate = 1mV/sec.

In fact, this is what was observed when cyclic voltammetry was conducted on films of thicknesses of 0.032 µm, 0.064 µm, 0.128 µm and 0.89 µm. The plots of I_p vs. scan rate were linear for the thinner films, but the plots fell off from linearity as film thickness increased (see Figs. 26-29). Scan rates used were 20 mV/sec, 50 mV/sec, 100 mV/sec, 200 mV/sec, 500 mV/sec, and 1000 mV/sec.

The fibrillar films must be treated with base to dissolve the template membrane. Treating the polypyrrole with strong base (NaOH) has been shown to have a dramatic effect on the cyclic voltammetry of the polymer (44). That is, oxidation and reduction peaks can be shifted negatively as much as one volt. We have found that subsequent treatment of the polymer with strong acid such as 1 % $HClO_4$ restores most of the electrochemical properties, but the oxidation and reduction peaks of the polypyrrole are both shifted about 350-500 mV negatively of their original positions. Note the shift in E_p (peak potential) between a conventional PPy film (Fig. 25) and a fibrillar PPy film (Fig. 30). Using the acid $HClO_4$ ensures that there is only one counterion present in the system, since the electrolyte for battery studies is $LiClO_4$.

<u>Discussion of battery charge/discharge curves</u>. Experiments were conducted with both fibrillar and conventional films to determine the maximum amount of charge that each type of battery could store and discharge. Experiments were designed so that the coulombic efficiencies, energy efficiencies, and energy densities could also be determined. The data analysis was conducted in such a way as to facilitate comparison between the shapes of the charging and discharging curves of both conventional film batteries and fibrillar batteries. Results from these studies are discussed in this section.

Fig. 26. Ip vs. Scan Rate for 0.032 μm Conventional PPy Film.
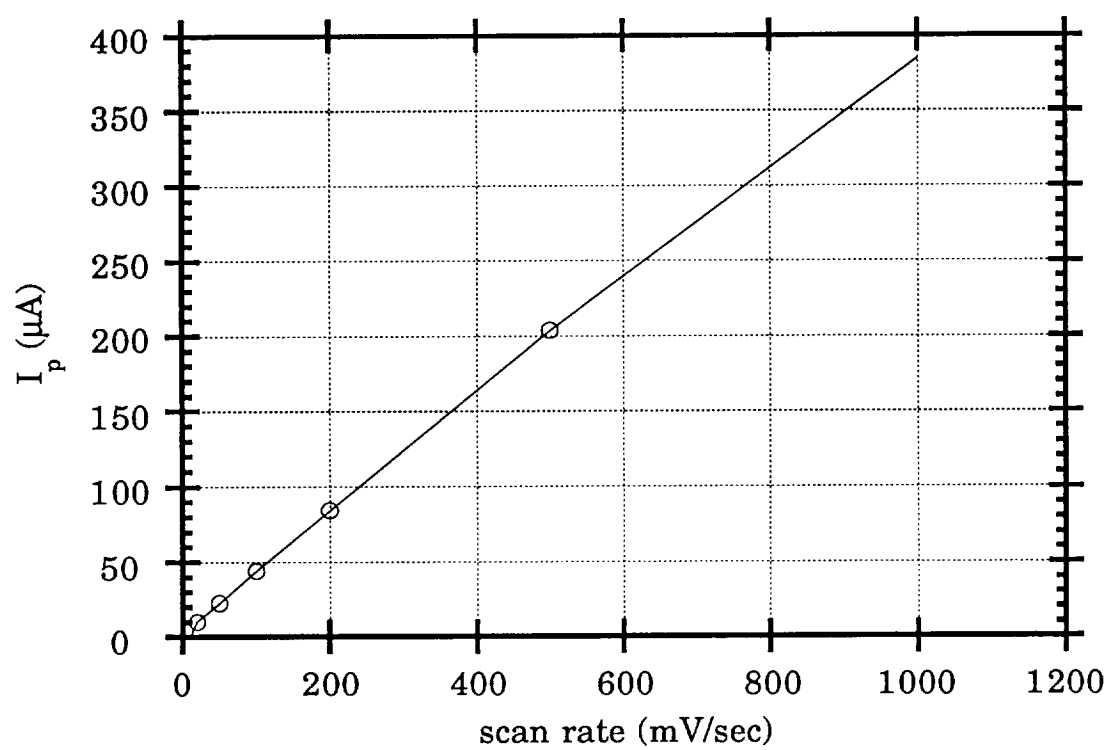
Fig. 27. Ip vs. Scan Rate for 0.064 μm Conventional PPy Film.
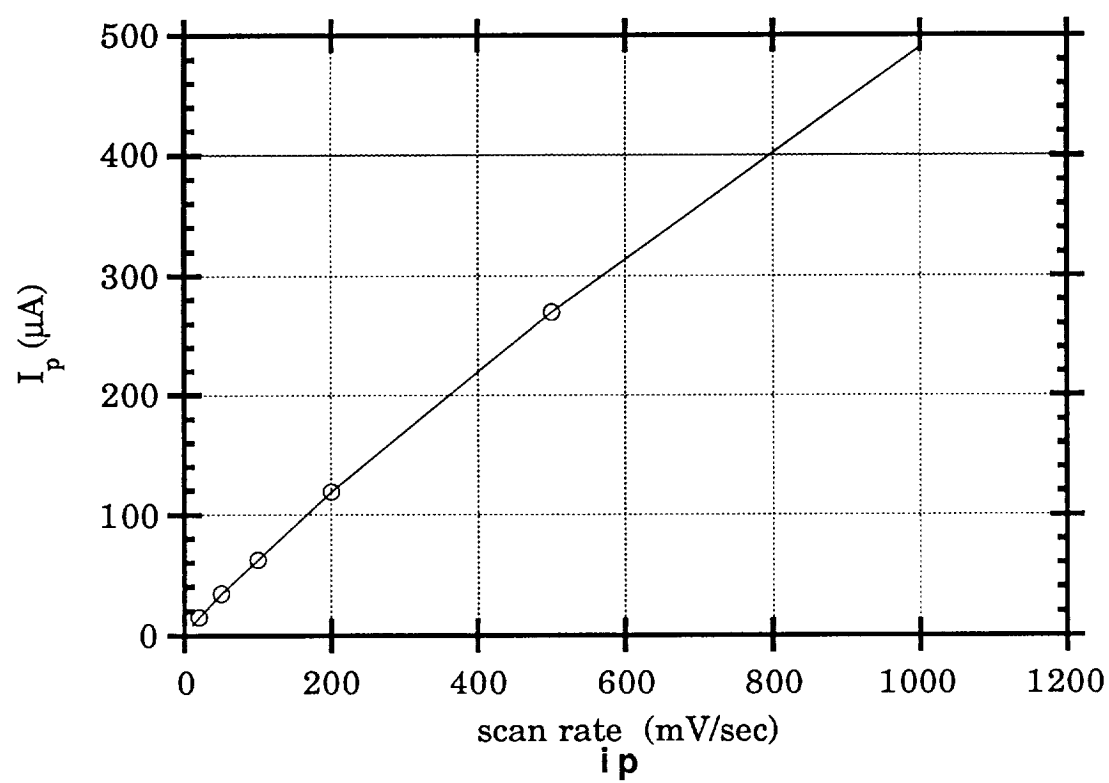
Fig. 28. Ip vs. Scan Rate for 0.128 μm Conventional PPy Film.
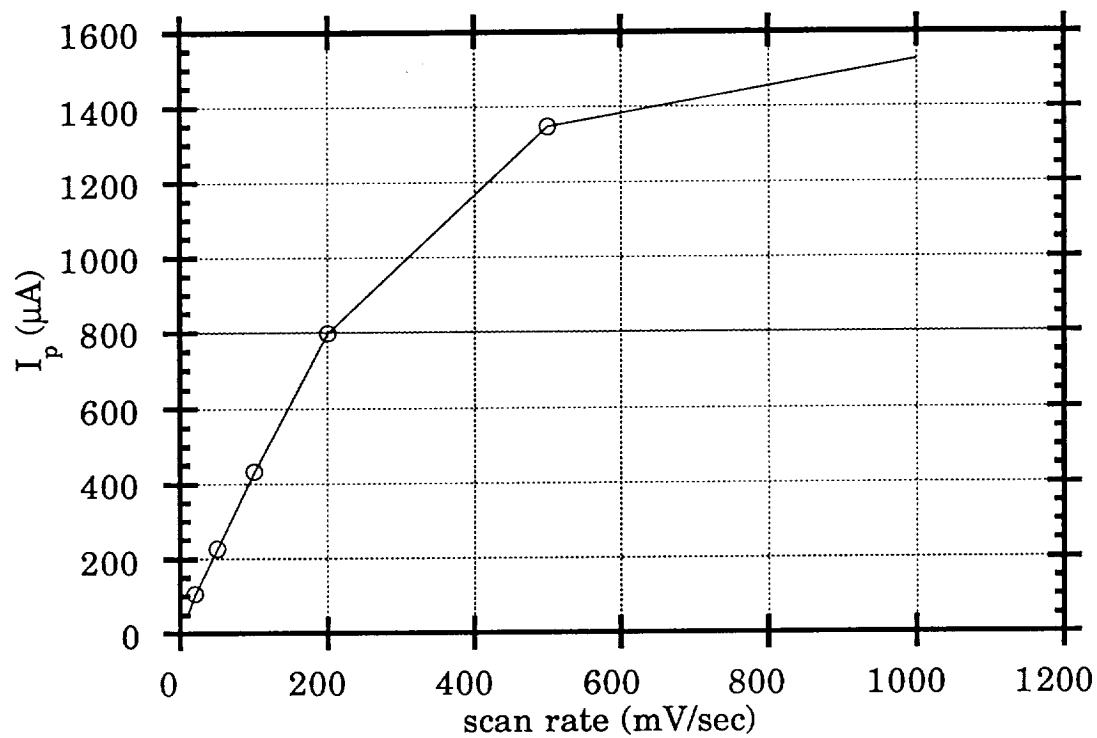
Fig. 29. Ip vs. Scan Rate for 0.89 μm Conventional PPy Film.

+ ← E → −

0.2 mA

200 mV
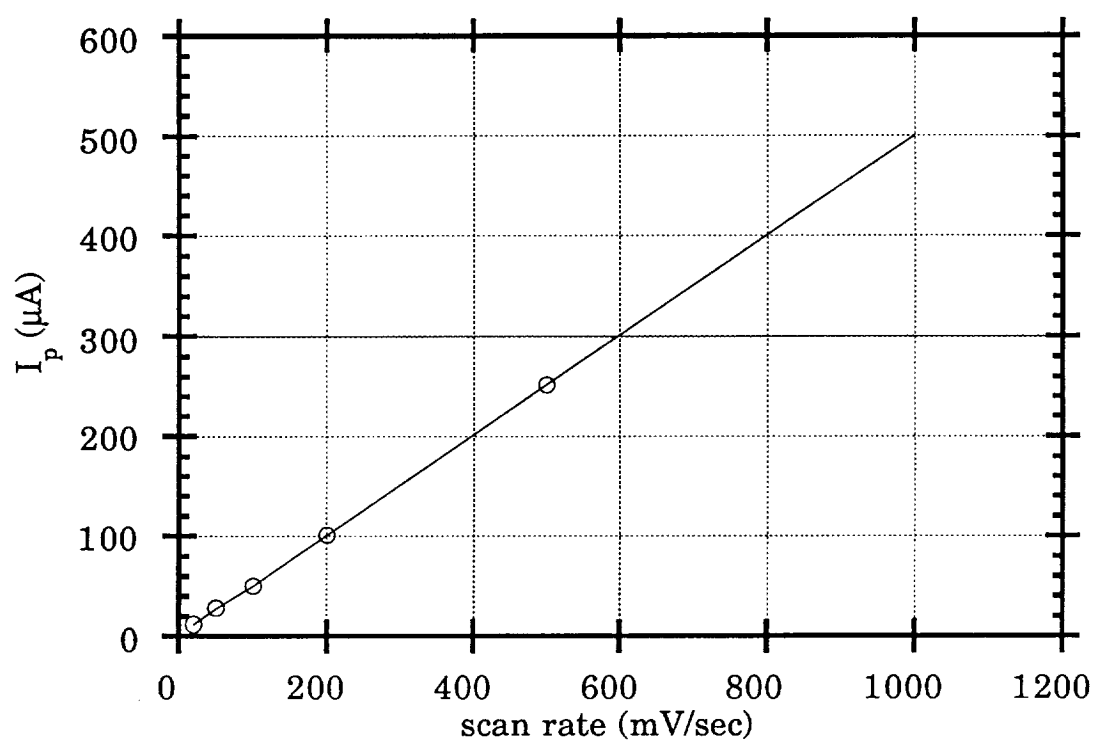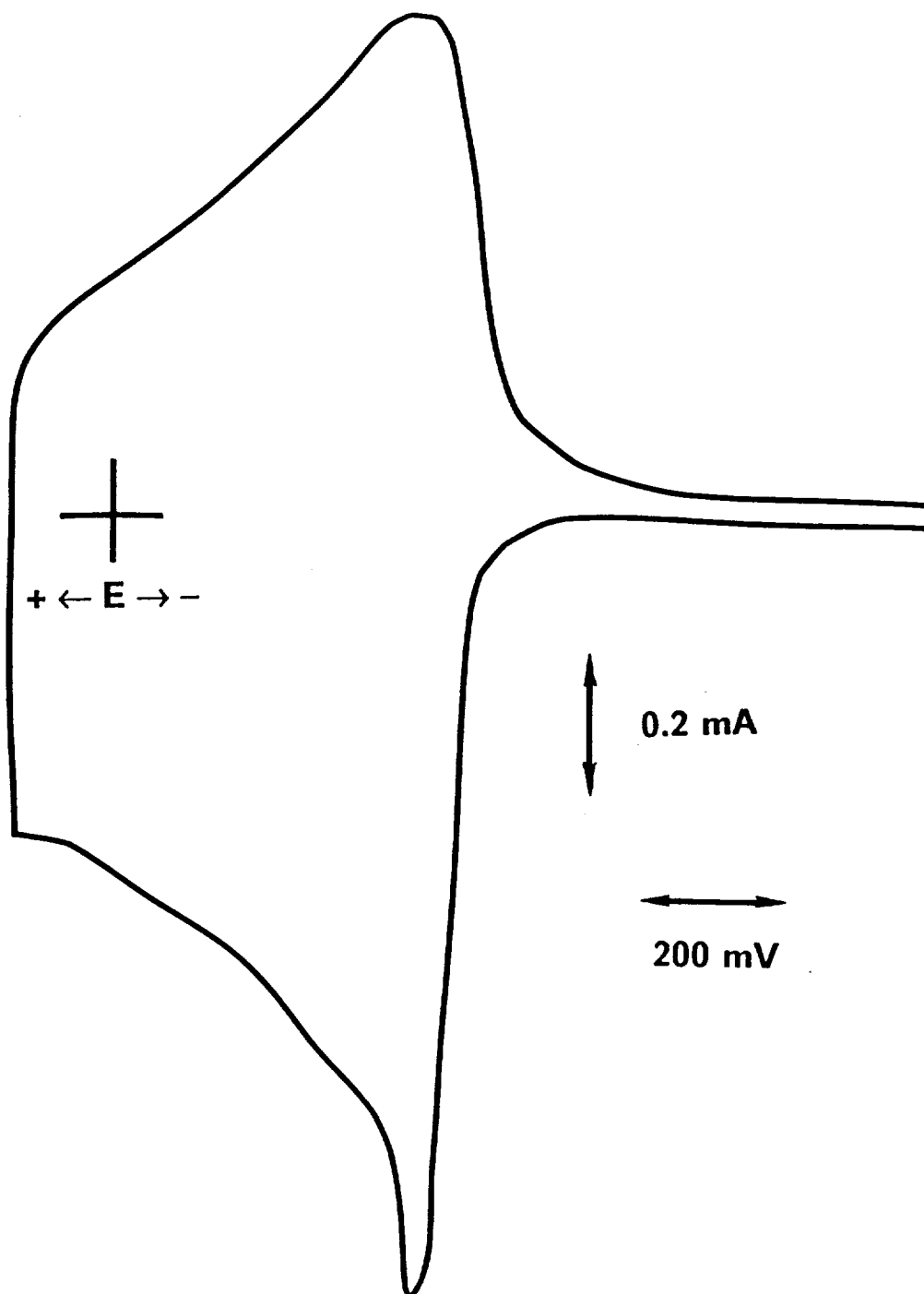
Fig. 30. Cyclic Voltammogram of Li/PPy Battery with 2 μm Fibrillar Equivalent PPy Film. Scan Rate = 10 mV/sec.

A cyclic voltammogram was recorded after the growth of each film, then the film was potentiostatically reduced until no measurable current flowed. The amount of charge under the oxidation portion of the cyclic voltammetry curve was used as a basis from which to start charging the battery. Since that amount of charge, which will hereafter be referred to as 1Q, was passed during oxidation of the polymer film, it was assumed that the battery could store at least that amount of charge.

If the potential on the cyclic voltammogram is scanned more positively after the polymer is oxidized, a potential region is reached at which an irreversible oxidative process occurs. Figure 31 shows a CV which illustrates this region and also the region designated as 1Q. The area under the wave corresponding to the irreversible oxidation process could contain both a reversible contribution and an irreversible contribution. This is evidenced by data presented later in this section that show that more charge than that found under the oxidation wave of the CV can be extracted from the film during battery discharge.

The battery was then charged at a constant current of 0.5 mA/cm^2 until the same amount of charge that was measured under the oxidation portion of the CV had been put back into the film. The battery was then discharged at a constant current of 0.5 mA/cm^2 and the cell potential was measured as a function of time. When the potential dropped to a value of 2.5 V, the discharge of the battery was terminated because the discharge curve dropped off rapidly at this point. The battery was then held at a constant potential until there was negligible current flow. The potential was held in the region in which the polypyrrole film was completely reduced. This potential was determined from the cyclic voltammogram taken at the beginning of the experiment, which showed
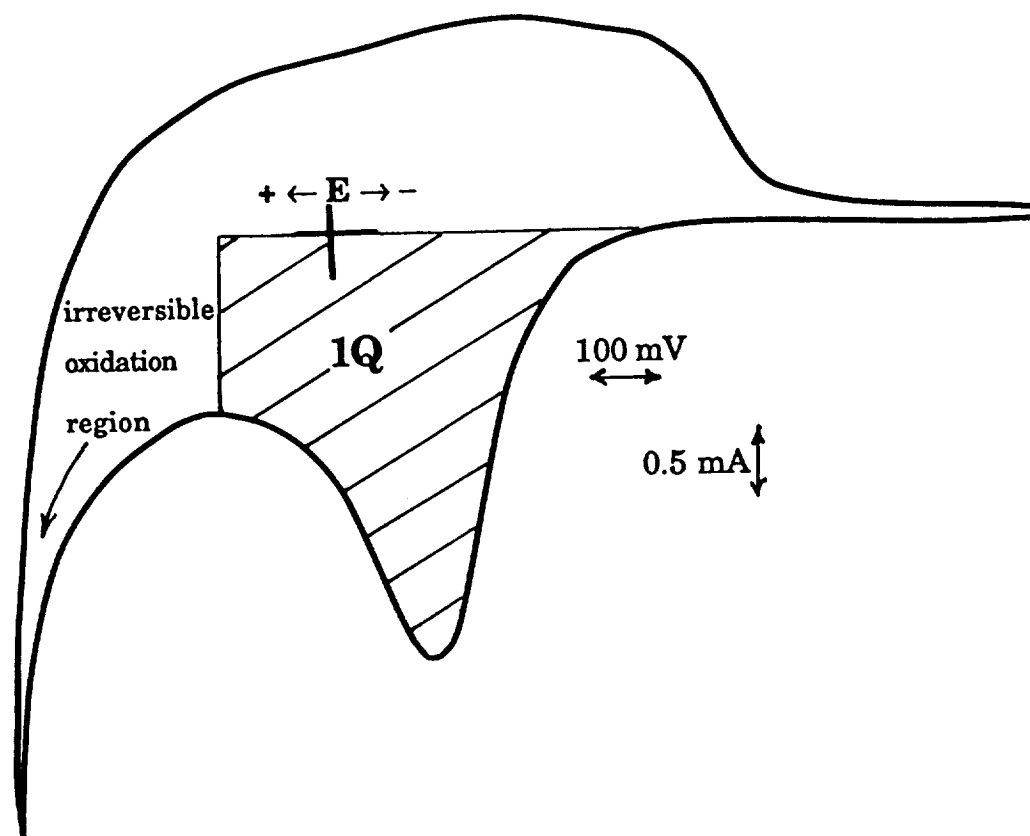
Fig. 31. Cyclic Voltammogram of PPy with Amount of 1Q Charge and Irreversible Oxidation Region Illustrated.

the potentials at which the polypyrrole film was completely oxidized or reduced. When the film was fully reduced, the battery was again charged and discharged using the charge under the oxidation portion of the CV as a basis, and again reduced completely at a constant potential.

Figure 32 is a flow chart that describes the protocol for the experiment. After three cycles using the CV charge, the battery was cycled three times using twice the charge under the CV. Again, between every charge/discharge cycle, the film was potentiostatically reduced. After reduction, the battery was then cycled once again using once the charge under the original CV. The PPy film was reduced again and the battery was cycled three more times using three times the charge under the CV as a basis. This pattern of three cycles, reduction, one cycle using once the charge under the CV, reduction, and three more cycles using a higher increment of charge under the CV was used until the battery failed. Battery failure was defined by a discharge curve that was almost vertical and lasted a considerably shorter time than the first cycle, for which only one times the CV charge was used. These experiments were designed to determine the effect of amount of charge on battery cycle life and to determine the maximum charge each battery could store.

Several series of plots have been made in order to interpret these data. The first series, Figures 33-41, represent each set of three cycles taken with 1Q (one times the charge under the CV), 2Q (twice the charge under the CV), 3Q, and so forth, for both a conventional film and a fibrillar film. The second series of curves, Figures 42 and 43, show the charge/discharge curves of a conventional film and a fibrillar film, respectively, comparing the 1Q the CV charge curves taken between the three cycles each of 2Q, 3Q, & 4Q the CV charge. Figures 44-47 compare

```
┌─────────────────────┐           ┌─────────────────────┐
│ Charge/Discharge    │       ┌──→│ Charge/Discharge    │
│ using 1Q for 3      │       │   │ using 1Q for 1      │
│ cycles              │       │   │ cycle               │
└─────────────────────┘       │   └─────────────────────┘
          │                   │              │
          ▼                   │              ▼
┌─────────────────────┐       │   ┌─────────────────────┐
│ Charge/Discharge    │       │   │ Charge/Discharge    │
│ using 2Q for        │       │   │ using 4Q for 3      │
│ 3 cycles            │       │   │ Cycles              │
└─────────────────────┘       │   └─────────────────────┘
          │                   │              │
          ▼                   │              ▼
┌─────────────────────┐       │   ┌─────────────────────┐
│ Charge/Discharge    │       │   │ Charge/Discharge    │
│ using 1Q for 1      │       │   │ using 1Q for 1      │
│ cycle               │       │   │ cycle               │
└─────────────────────┘       │   └─────────────────────┘
          │                   │              │
          ▼                   │              ▼
┌─────────────────────┐       │   ┌─────────────────────┐
│ Charge/Discharge    │       │   │ Continue  with      │
│ using 3Q for 3      │───────┘   │ more increments     │
│ Cycles              │           │ of charge until     │
└─────────────────────┘           │ battery fails       │
                                  └─────────────────────┘
```
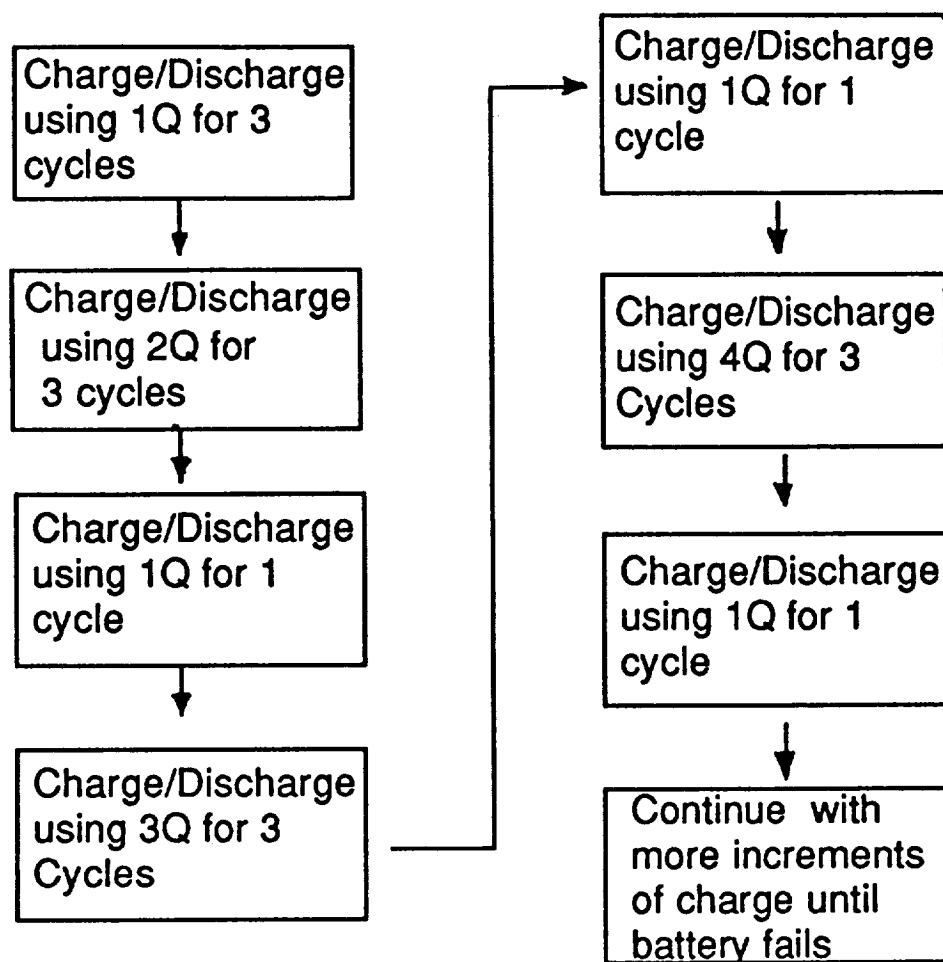
Fig. 32. Protocol for Battery Experiment.

Discharge

Charge

· 1st cycle

+ 2nd cycle

▲ 3d cycle
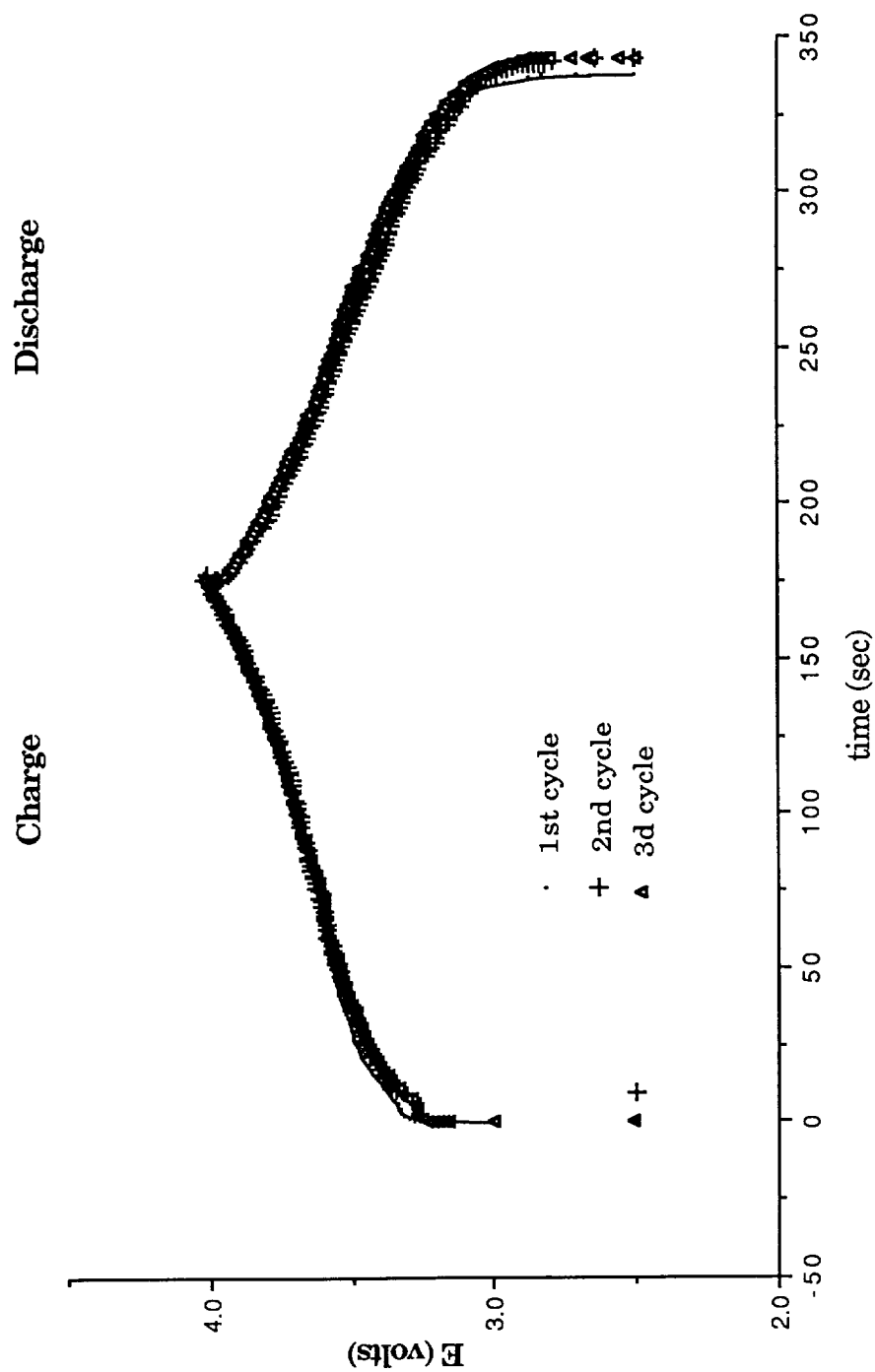
Fig. 33. Charge/Discharge Curves of Li/PPy Conventional Film Battery Using 1 Q CV Charge. First Three Cycles.
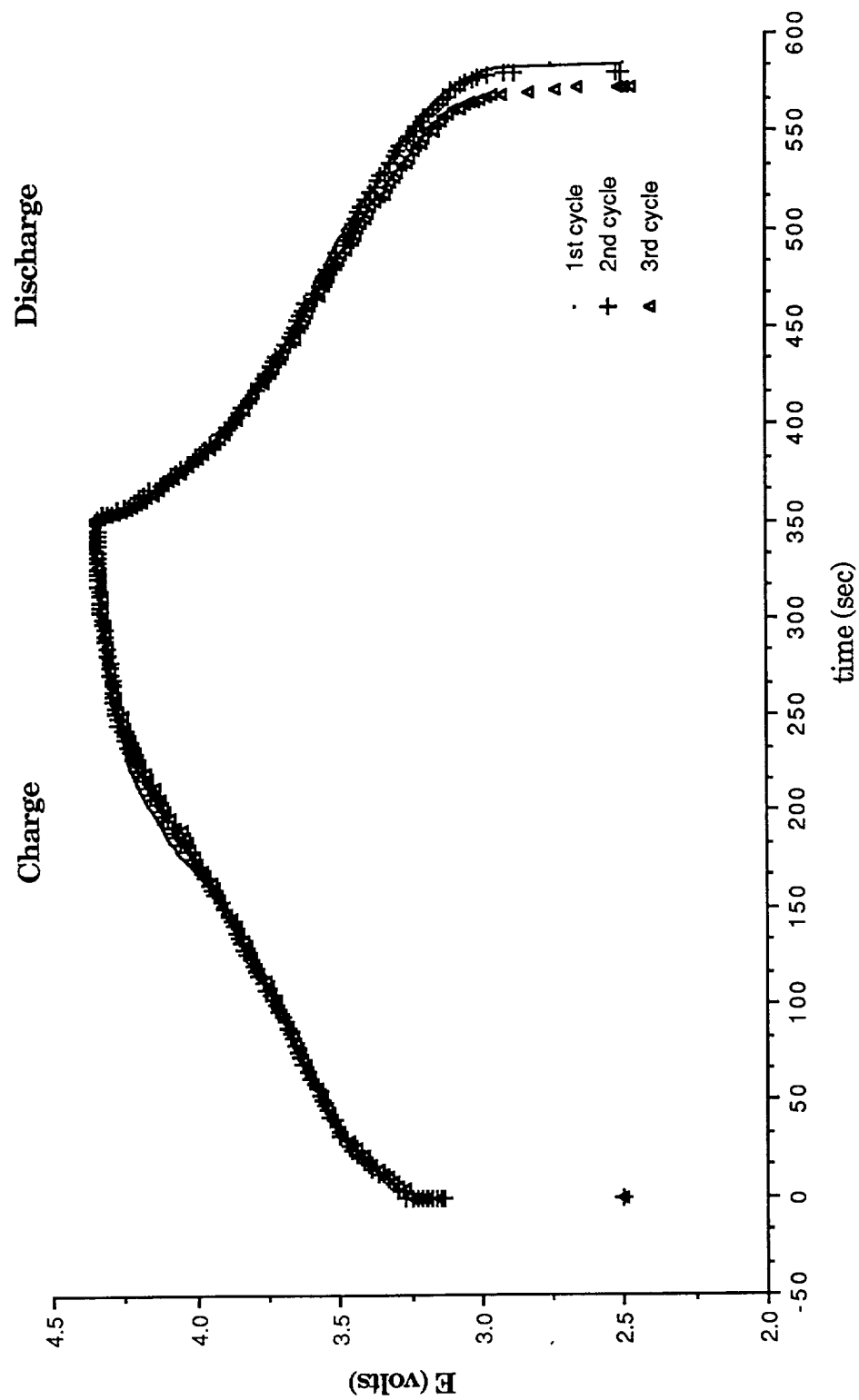
Fig. 34. Charge/Discharge Curves of Li/PPy Conventional Film Battery Using 2Q CV Charge.

Fig. 35. Charge/Discharge Curves of Li/PPy Conventional Film Battery Using 3Q CV Charge.

Fig. 36. Charge/Discharge Curve Of Li/PPy Conventional Film Battery Using 4Q CV Charge.
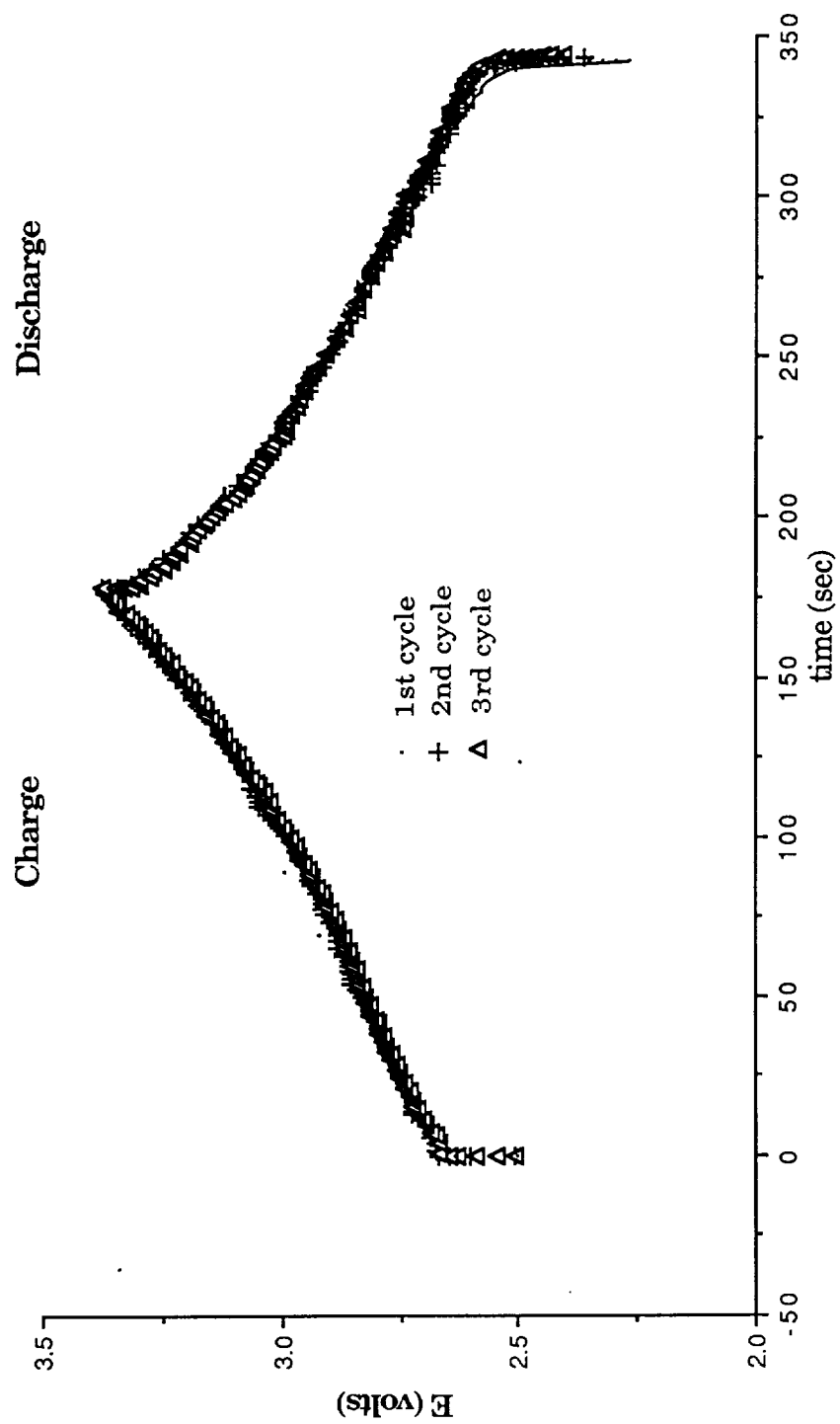
Fig. 37. Charge/Discharge Curves of Li/PPy Fibrillar Film Battery Using 1Q CV Charge. First Three Cycles.
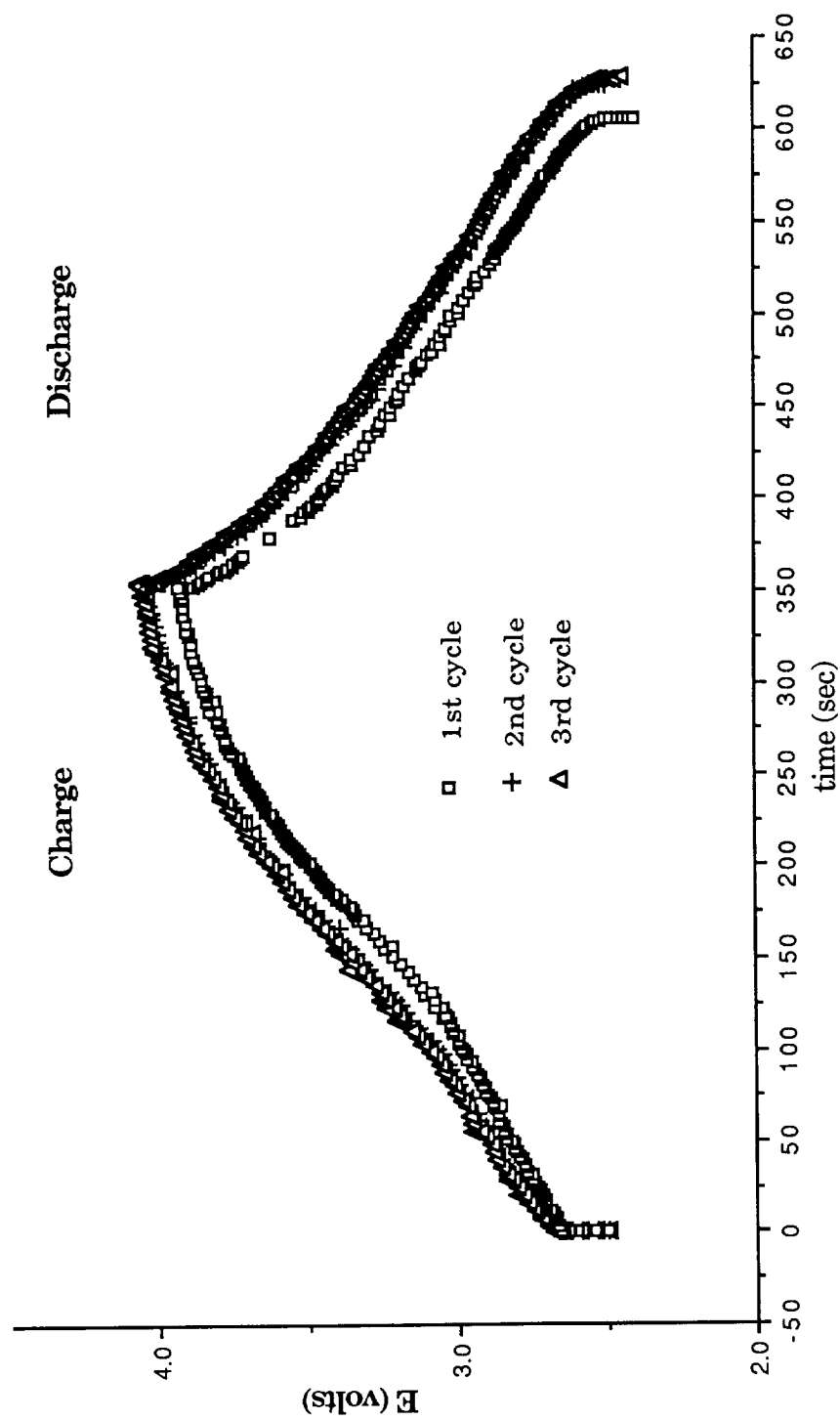
Fig. 38. Charge/Discharge Curves of Li/PPy Fibrillar Film Battery Using 2Q CV Charge.
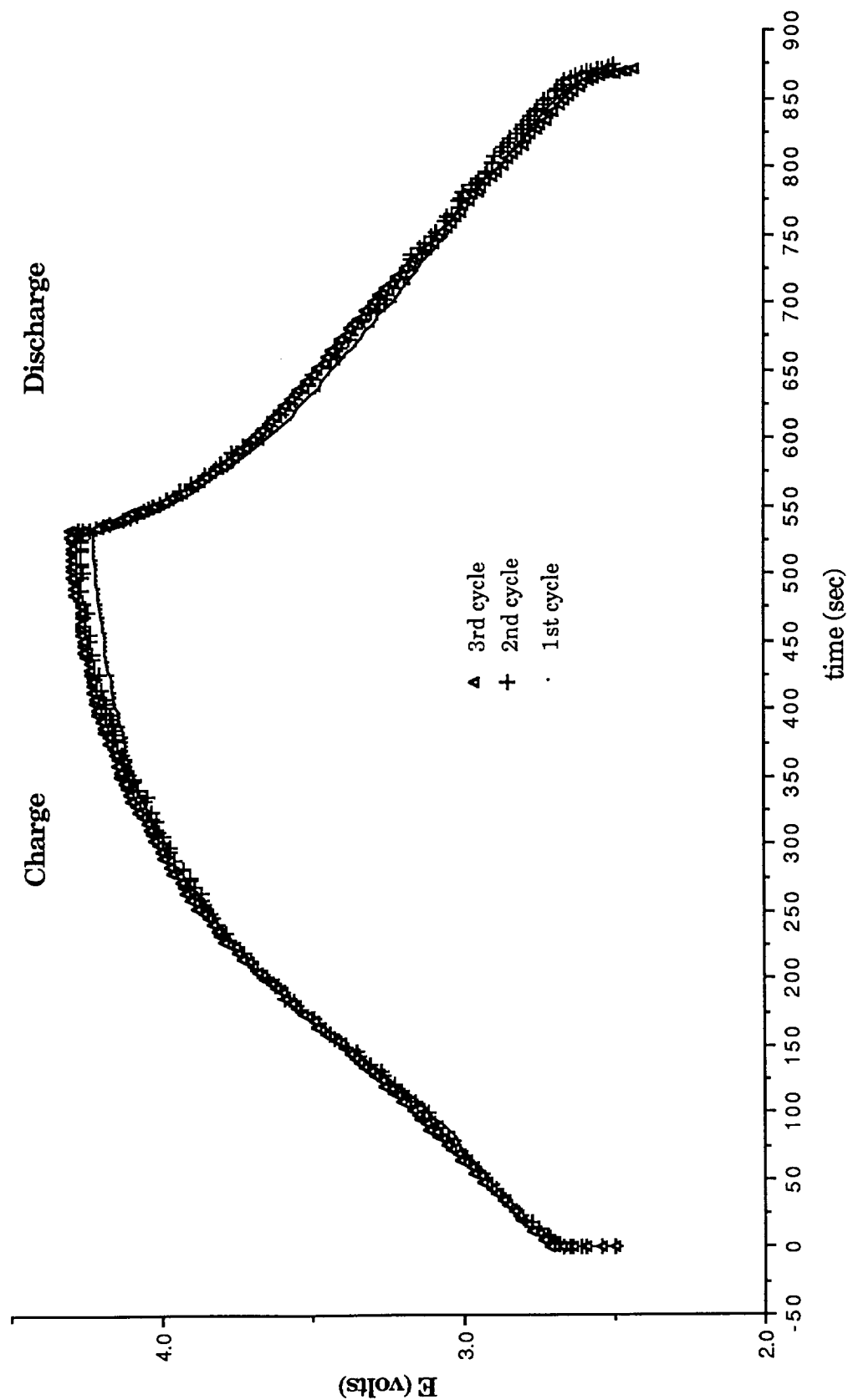
Fig. 39. Charge/Discharge Curves of Li/PPy Fibrillar Film Battery Using 3Q CV Charge.

C-2
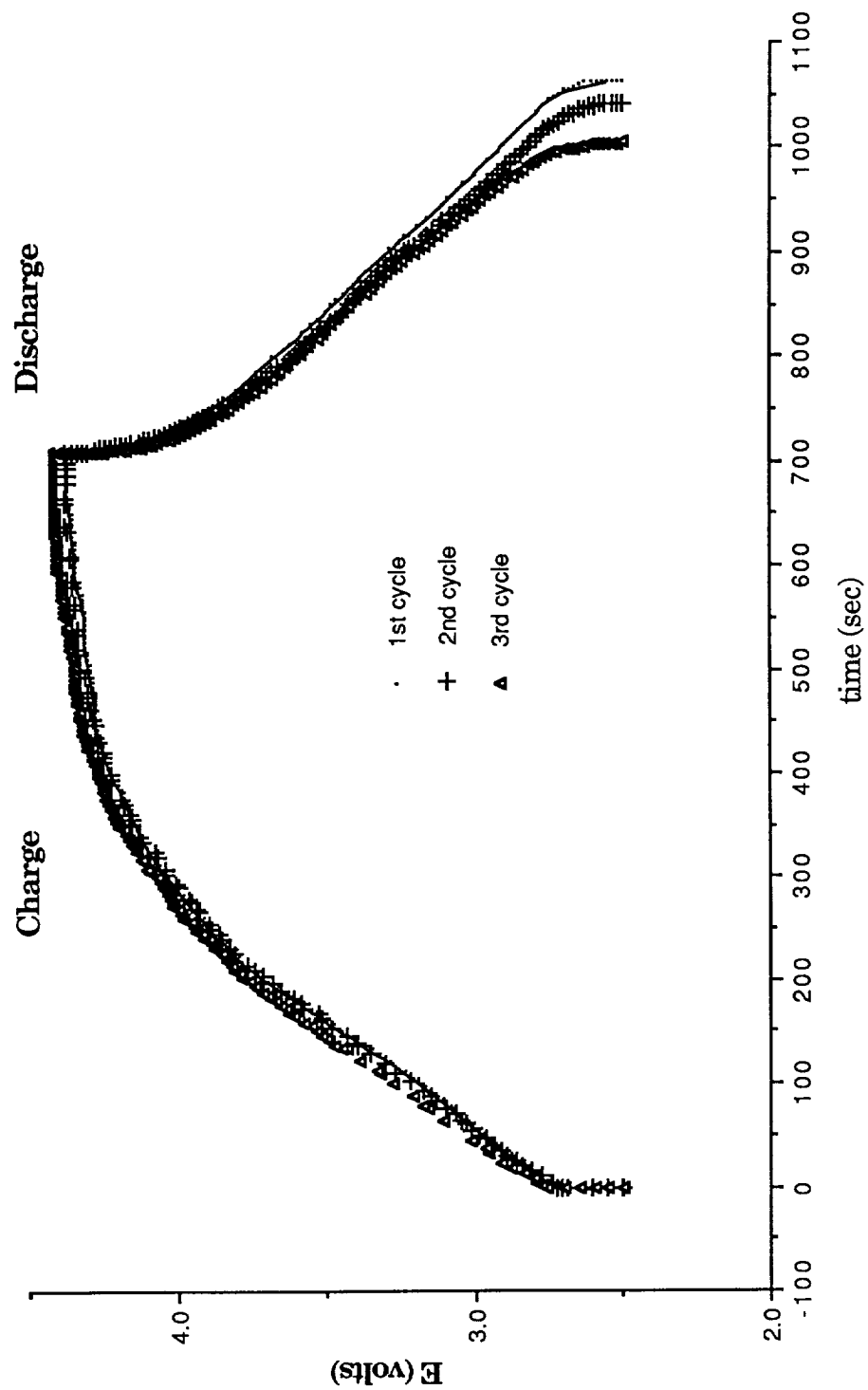
Fig. 40. Charge/Discharge Curves of Li/PPy Fibrillar Film Battery Using 4Q CV Charge.
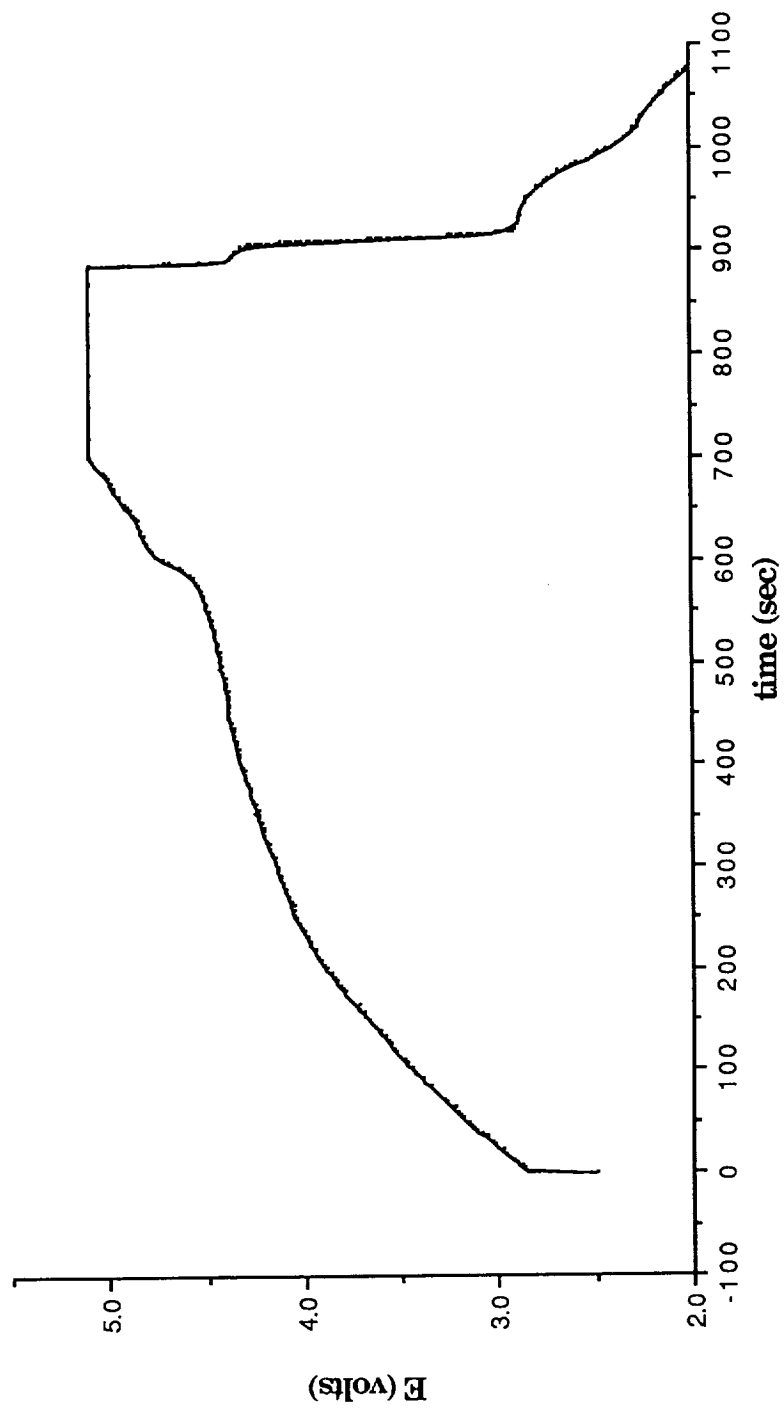
Fig. 41. Charge/Discharge Curve of Li/PPy Fibrillar Film Battery Using 5Q CV Charge.
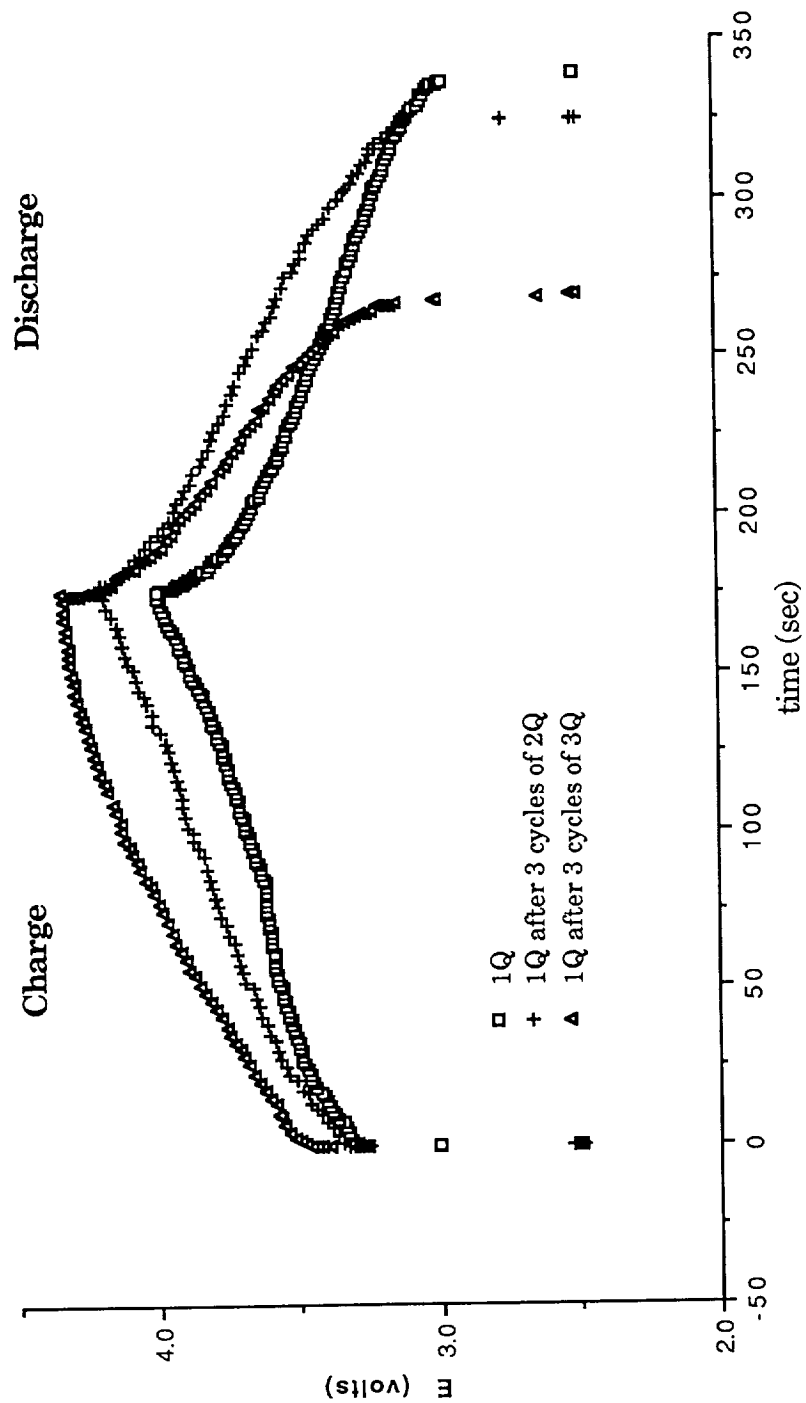
Fig. 42. Charge/Discharge Curves of Li/PPy Conventional Film Battery Using 1Q CV Charge Between 3 Cycles Each of 1Q, 2Q, 3Q, and 4Q CV Charge.
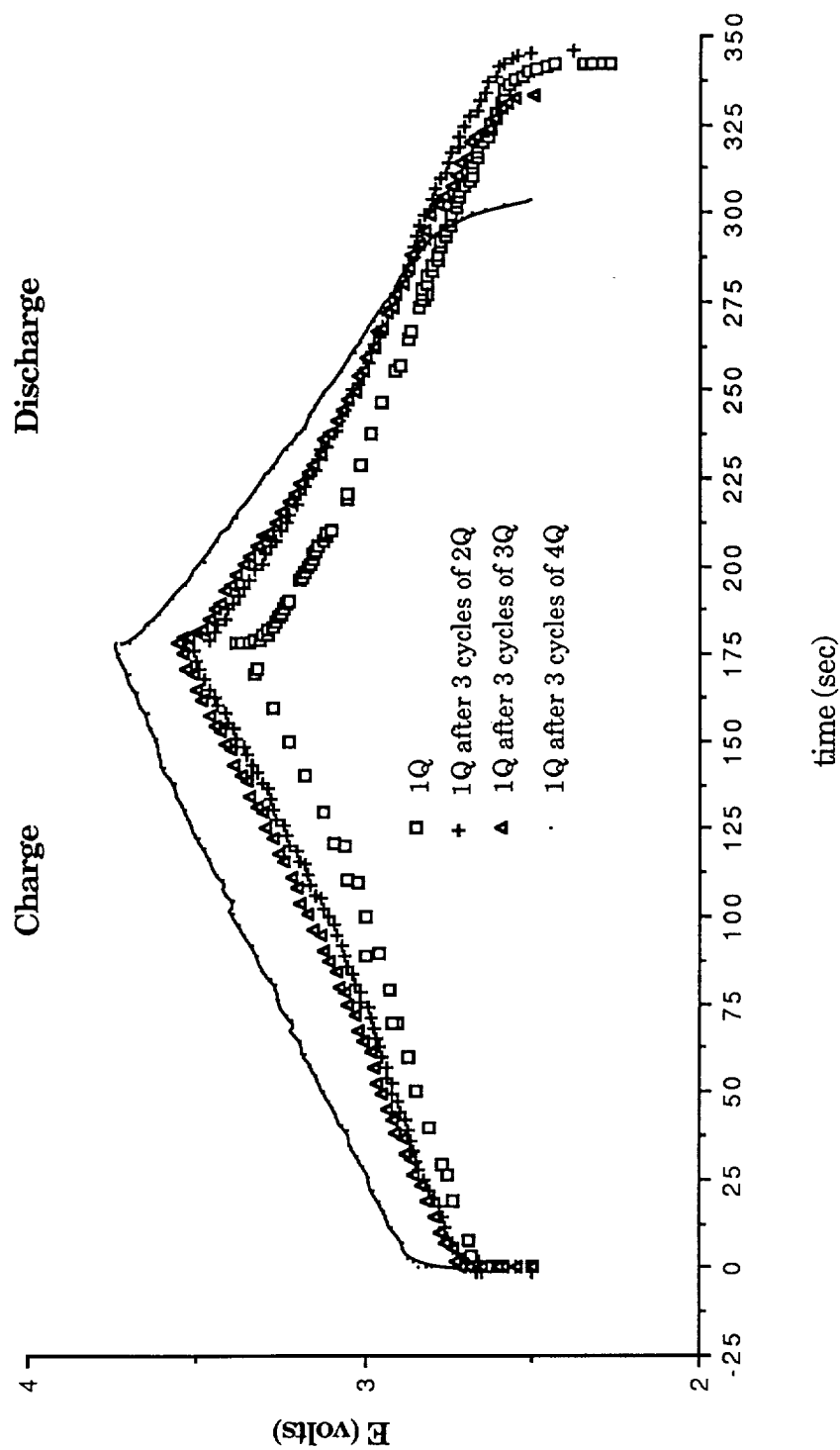
Fig. 43. Charge/Discharge Curves of Li/PPy Fibrillar Film Battery Using 1Q CV Charge Between 3 Cycles Each of 1Q, 2Q, 3Q, and 4Q CV Charge.
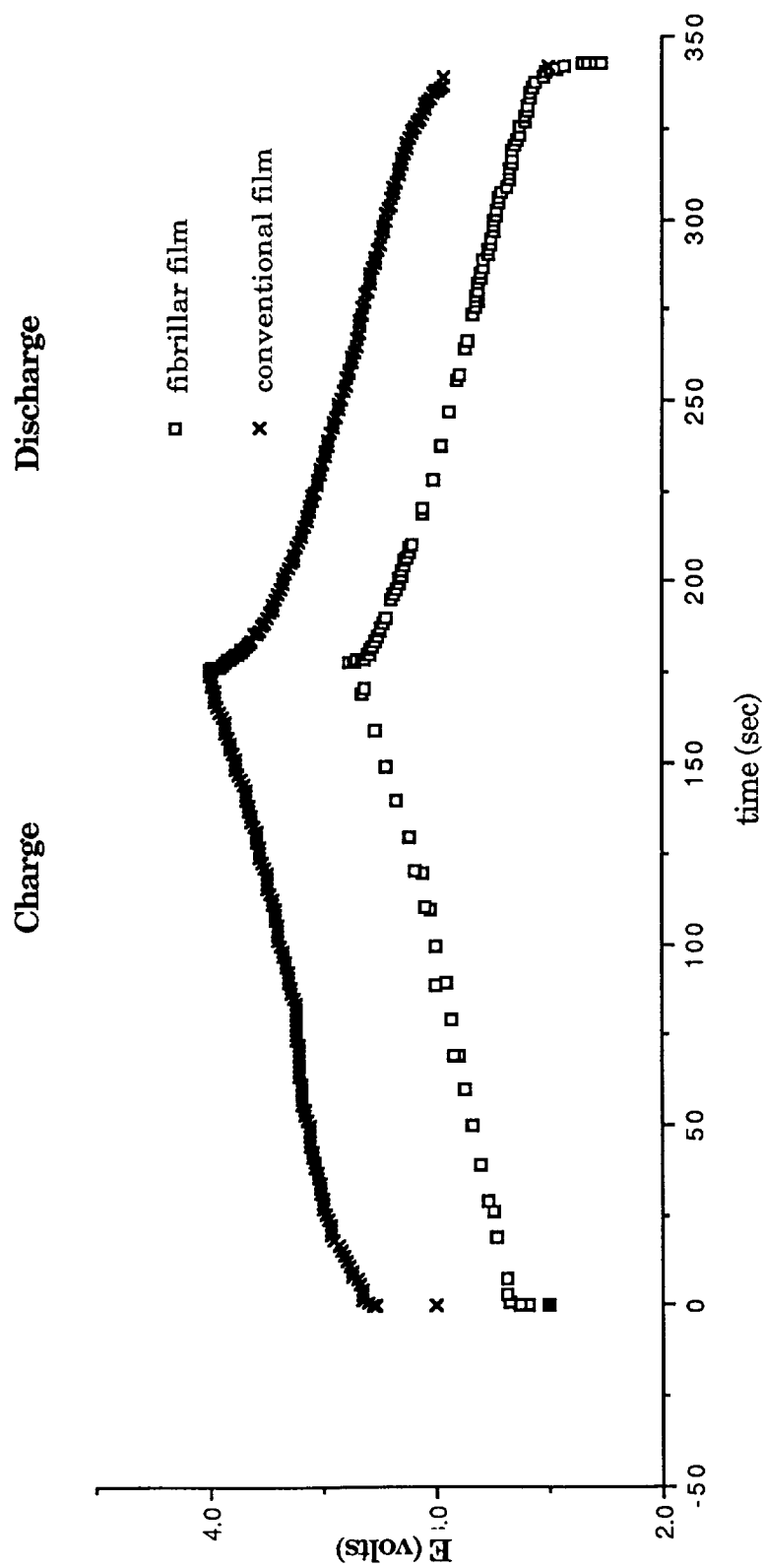
Fig. 44. Charge/Discharge Curves of Li/PPy Conventional Film Battery and Fibrillar Film Battery Using 1Q CV Charge.
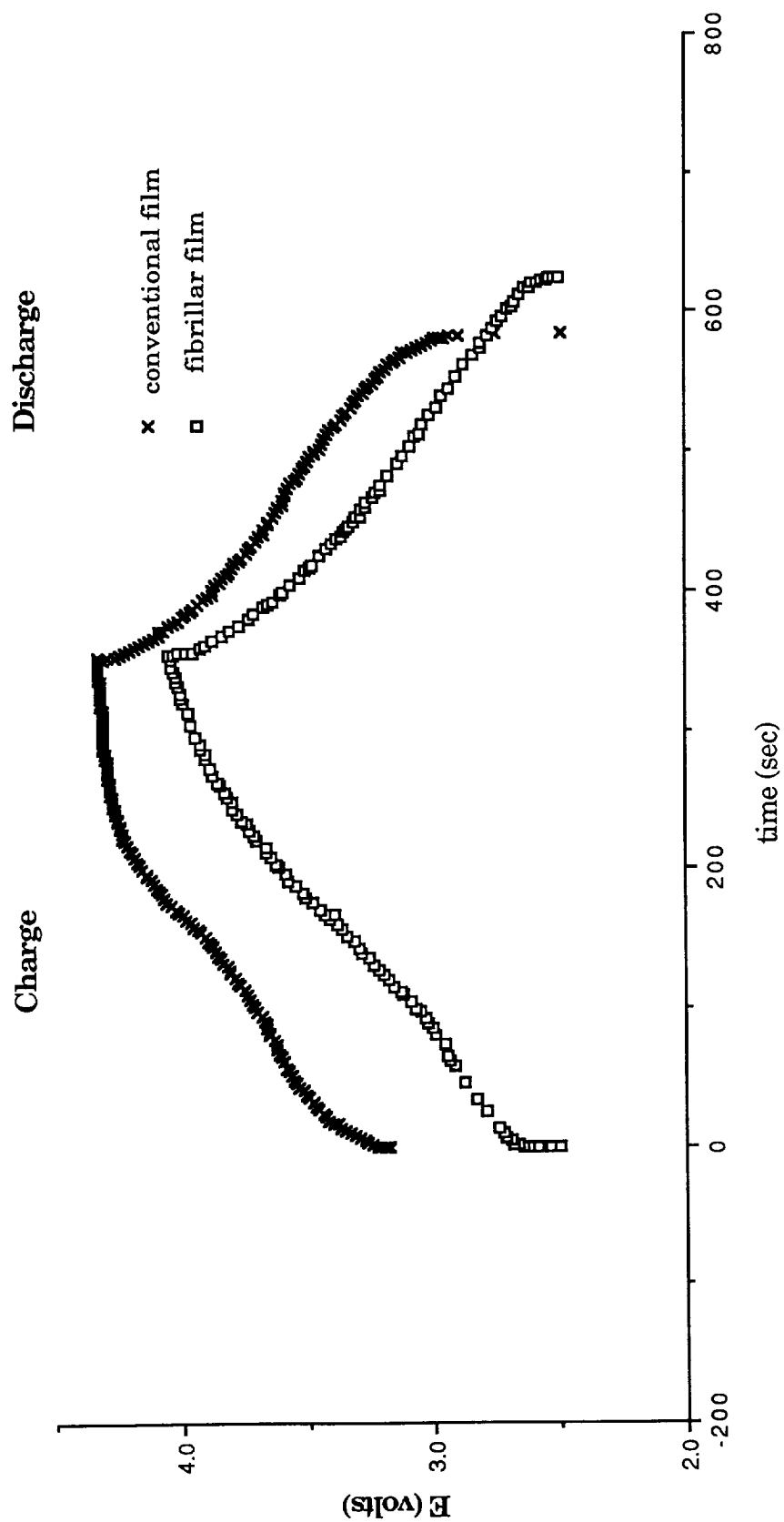
Fig. 45. Charge/Discharge Curves of Li/PPy Conventional Film Battery and Fibrillar Film Battery Using 2Q CV Charge.
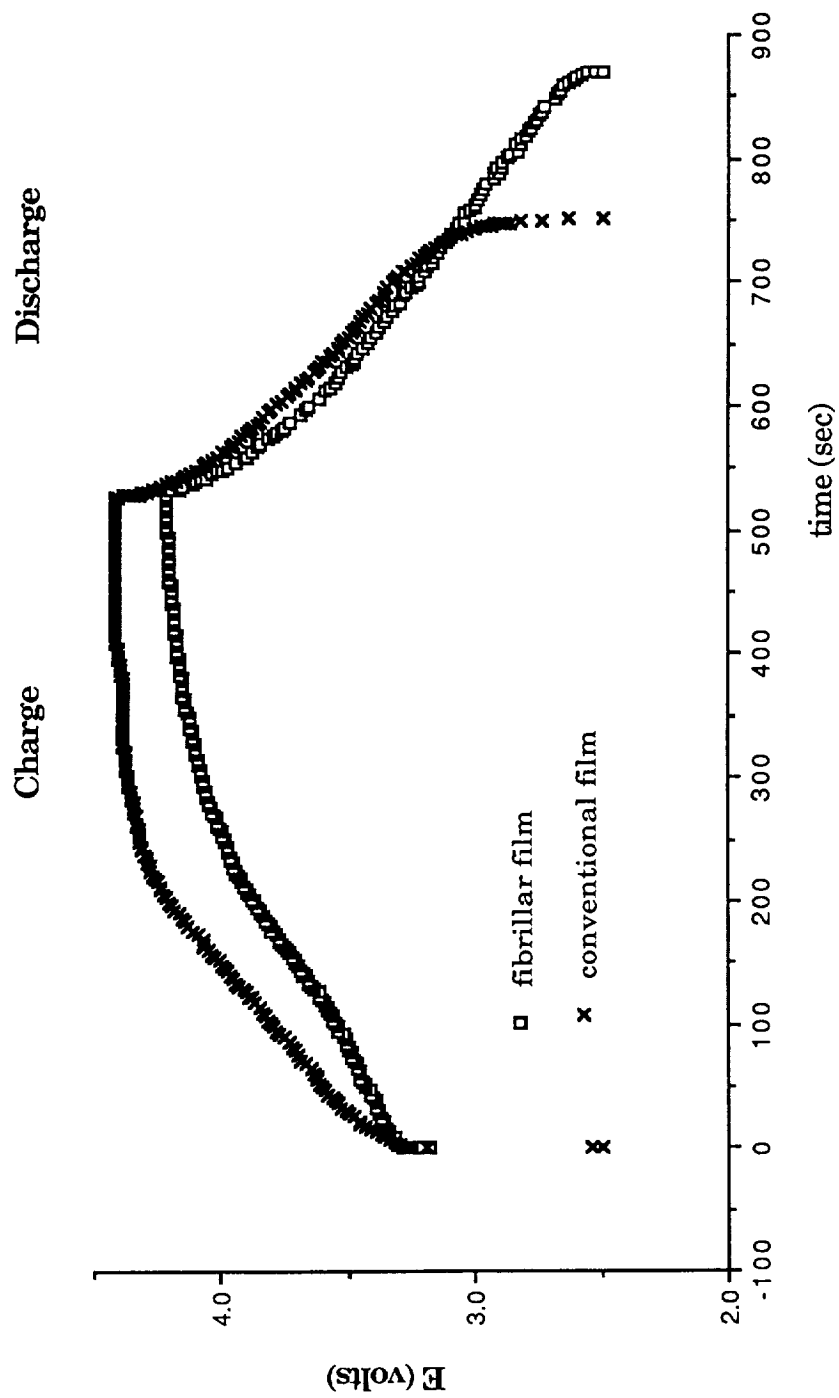
Fig. 46. Charge/Discharge Curves of Li/PPy Conventional Film Battery and
Fibrillar Film Battery Using 3Q CV Charge.
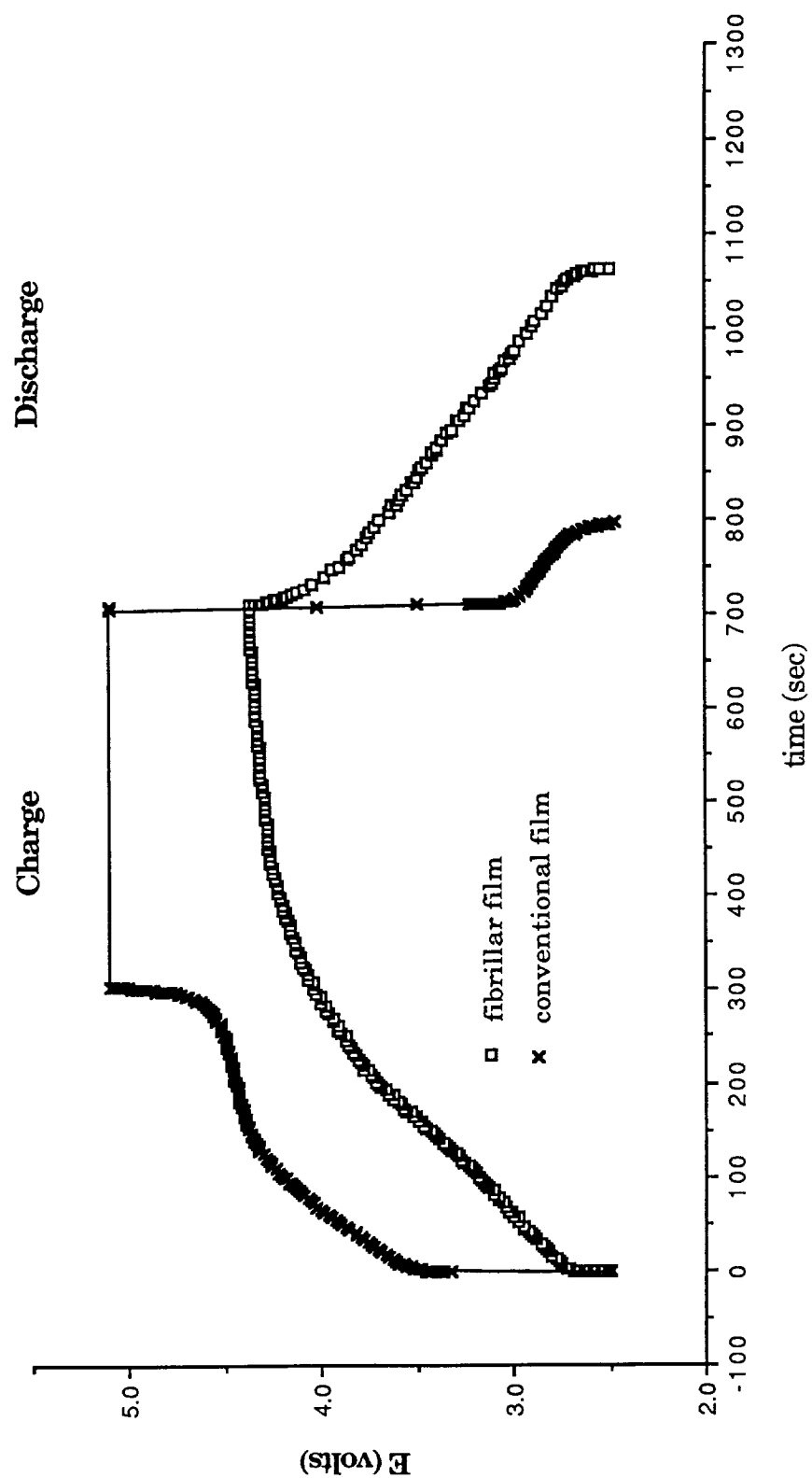
Fig. 47. Charge/Discharge Curves of Li/PPy Conventional Film Battery and Fibrillar Film Battery Using 4Q CV Charge.

various conventional and fibrillar charge/discharge curves into which the same amount of charge was injected. Figures 48 and 49 show charge/discharge curves using 1Q, 2Q, 3Q, 4Q, and 5Q for both a conventional film and a fibrillar film, respectively.

Figure 33 shows the charge/discharge curves from the first three cycles of the conventional film battery using once the charge under the cyclic voltammogram. The curves are very similar in shape and peak current, as well as length of time of discharge. The last two of the three cycles lasted a few seconds longer than the first. This could be because the film may not have been completely reduced after the first charge/discharge cycle, so that the film was still partially charged when the second cycle began.

The next figure, Figure 34, represents three cycles of the same film with twice the amount of CV charge injected. There is a plateau in the charging curve at about the time that 1.5Q CV charge has been injected into the film. This could mean that the battery has reached a maximum charging potential above which it cannot rise until the polymer is completely oxidized. The polymer is considered to be the limiting factor in this experiment because of the amount of lithium used versus the amount of polypyrrole used. There is more lithium metal than polypyrrole present, so the the polypyrrole would become completely oxidized before the lithium electrode would become completely oxidized. The peak potentials rise slightly from first to third cycles, but they are still very similar. The slight rise could be attributed to electrode resistance caused by the film beginning to pull away from the current collector or the beginning of damage to the polymer caused by side reactions not associated with charging. Another sign that polymer
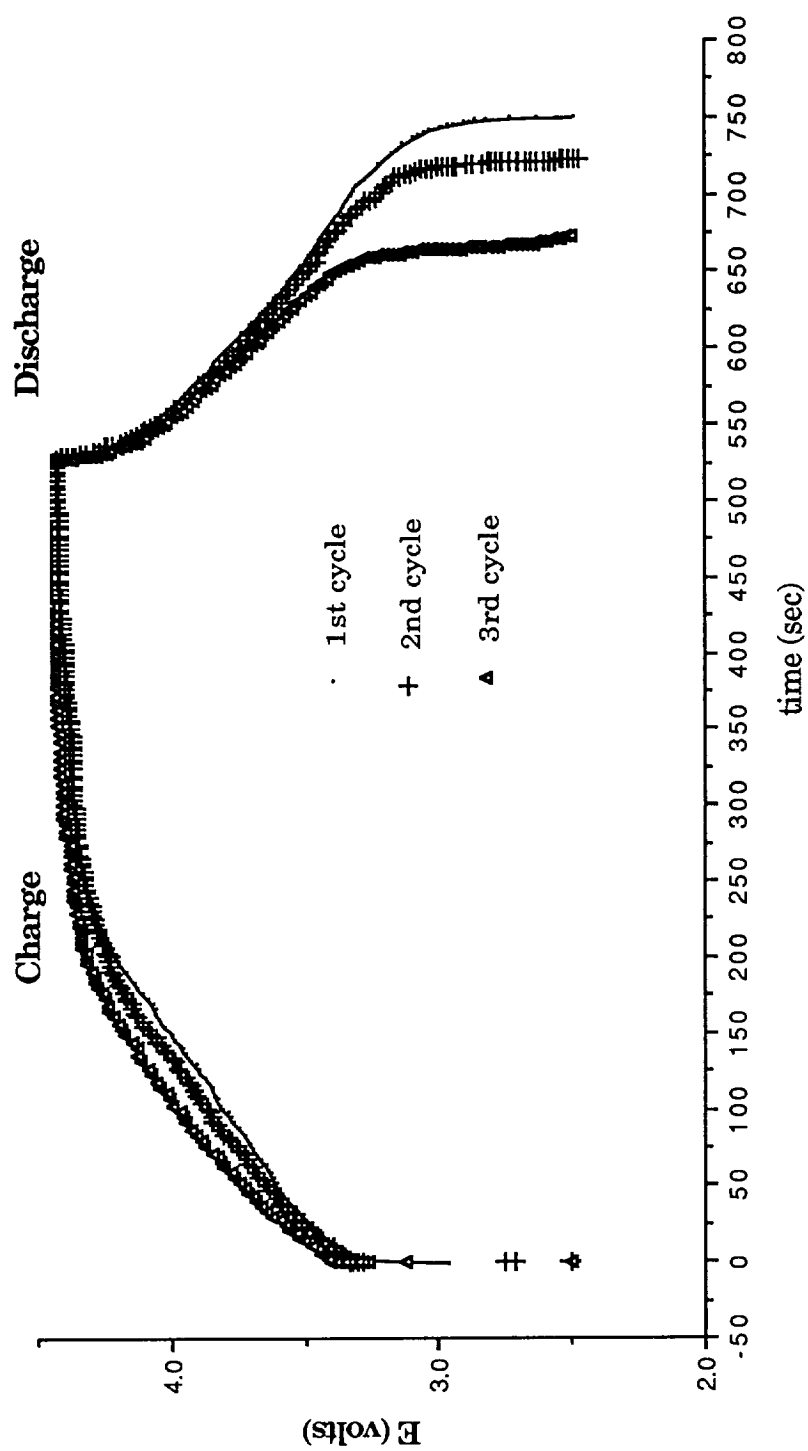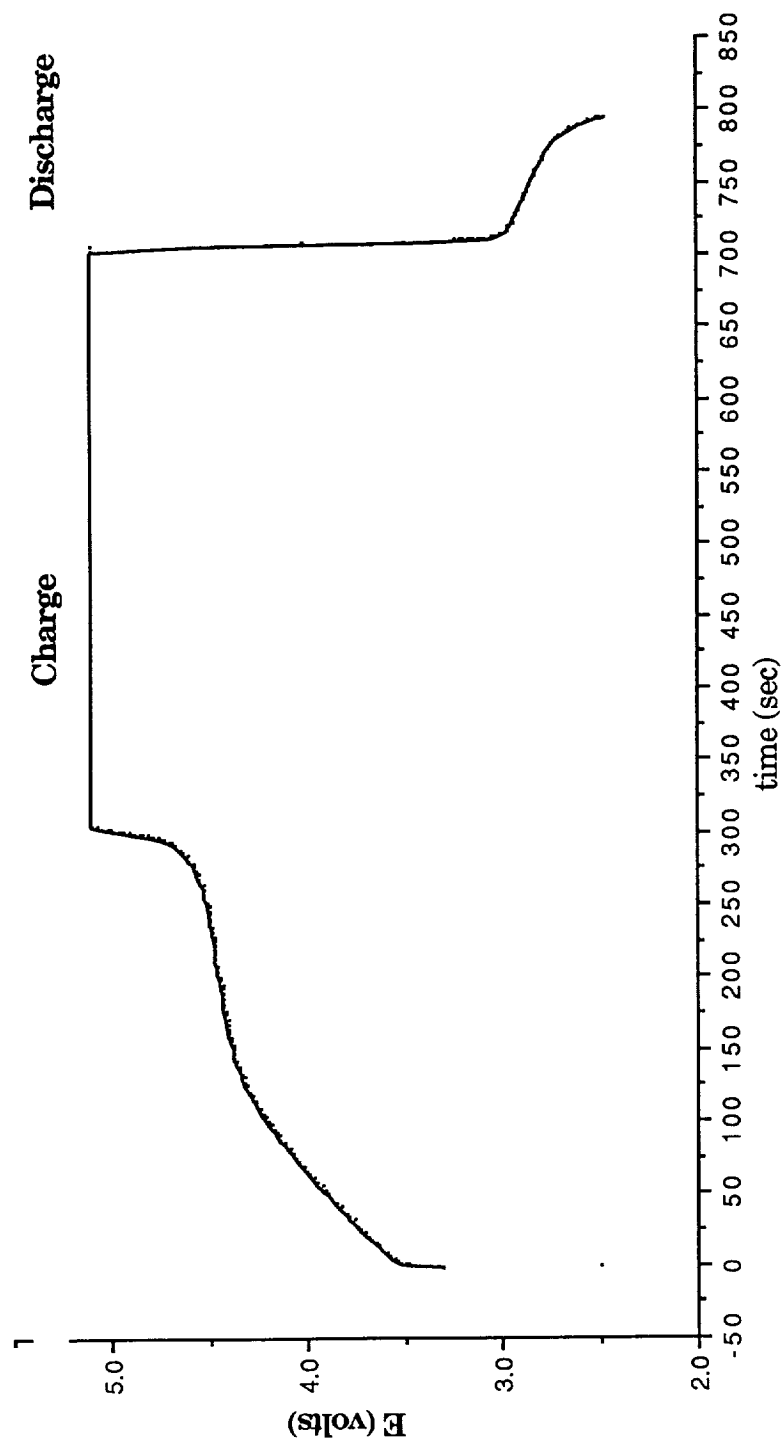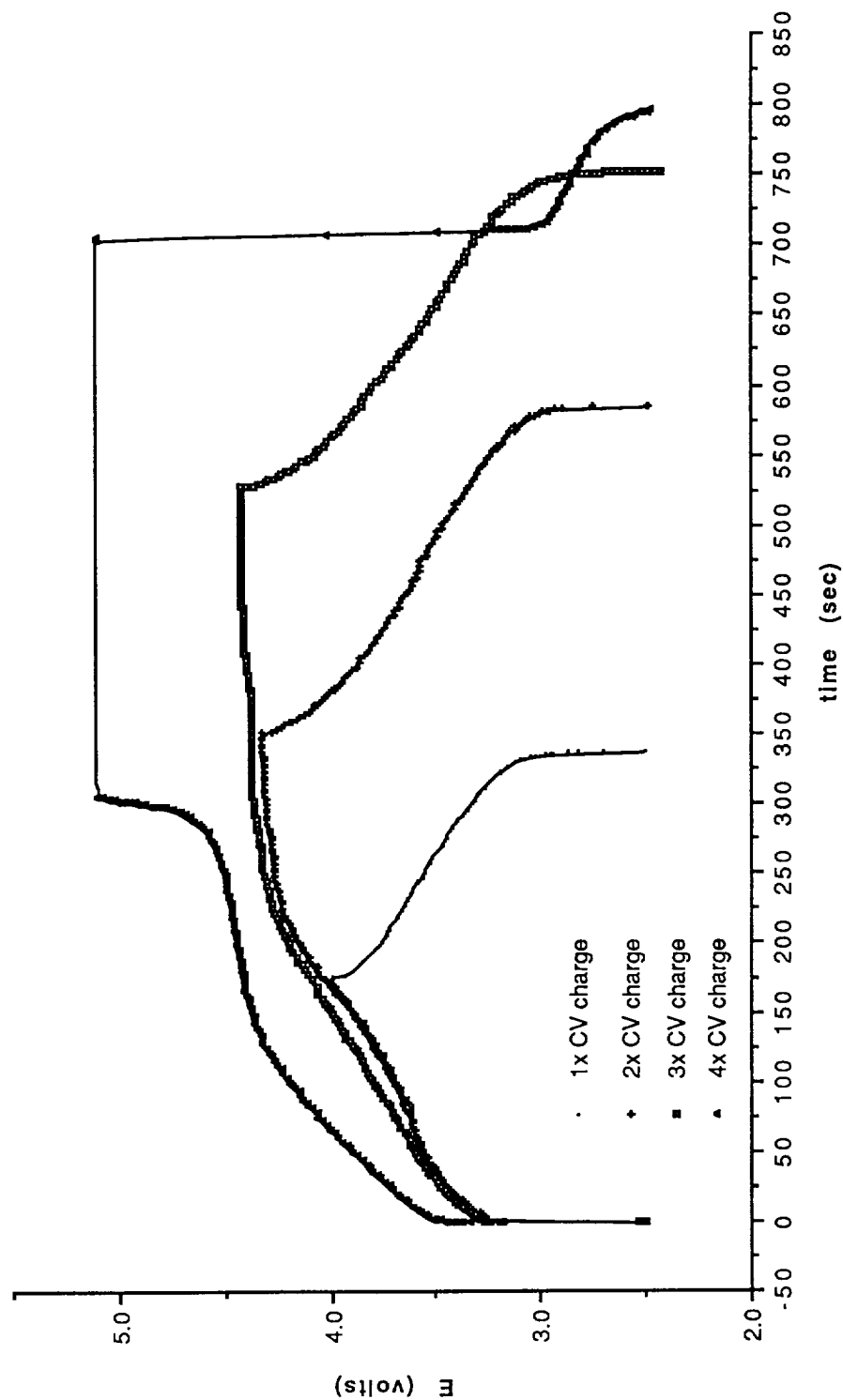
Fig. 48. Charge/Discharge Curves of Li/PPy Conventional Film Battery
Using 1Q, 2Q, 3Q, and 4Q CV Charge.
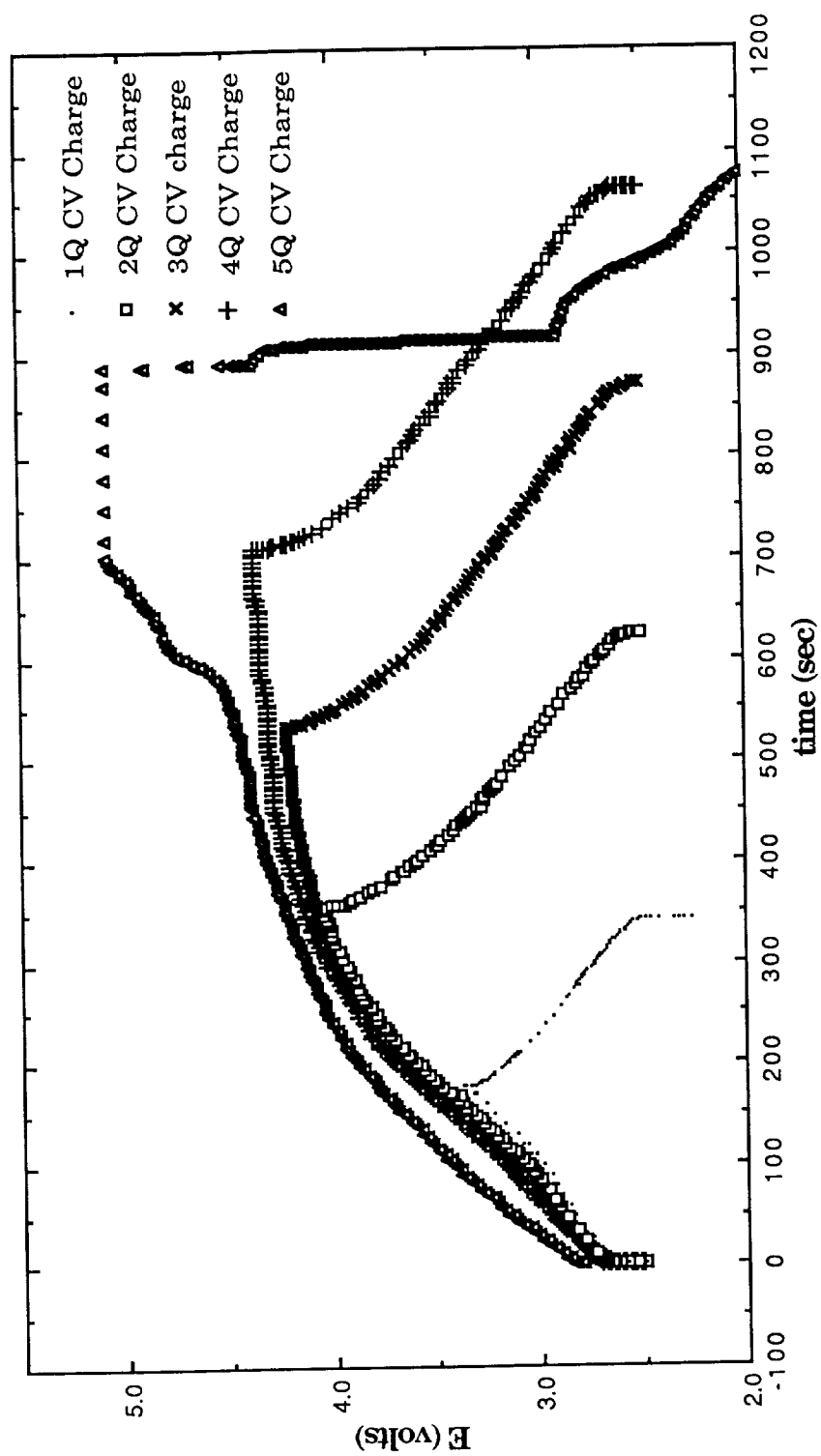
Fig. 49. Charge/Discharge Curves of Li/PPy Fibrillar Film Battery
Using 1Q, 2Q, 3Q, 4Q, & 5Q CV Charge.

damage is beginning to occur is the slight decrease in discharge time for the third cycle.

After cycling the battery once using 1Q CV charge, the battery was charged using 3Q CV charge. Figure 35 shows these three charge/discharge curves. Again the charging curve reaches a plateau when approximately 1.5 Q CV charge has been put into the film. The curve rises more sharply and the peak potential rises with subsequent cycles. The discharge time decreased with subsequent cycles, indicating that the battery was beginning to fail.

The battery was cycled using 4Q CV charge after cycling once at 1Q CV charge (Fig. 36). The charging curve rises slightly more sharply and the potential begins to plateau sooner than in the previous figure, where 3Q CV charge was used. The potential begins to rise again when about 1.5 Q CV charge has been injected into the film, and becomes almost vertical before going off scale at 5.1 volts, beyond which the chart recorder being used could not measure the potential. At the start of discharge, the potential dropped immediately to about 3 volts, which was the potential where the discharge curve in the previous figure began to drop off sharply.

The time of discharge in Fig. 36 was less than 100 seconds, which was less than the discharge time of the third cycle of the series of cycles using 3Q CV charge. Therefore, although more charge was put into the battery, 4Q CV charge rather than 3Q CV charge, less charge has been drawn from the battery at this point than was drawn when 3Q CV charge was used. This fact and the fact that the potential went off scale during charging were used as criteria for battery failure. The polymer has undoubtedly suffered irreversible damage, and delamination from the

substrate has occurred. One explanation for these data could be gas evolution at the polypyrrole electrode during overcharging.

The next series of graphs, Figs. 37-41, is similar to Figs. 33-36 in that they represent the same series of experiments that were conducted with a conventional film battery, but a fibrillar battery was used. A cyclic voltammogram was taken after growing the film and before conducting battery charge/discharge experiments. When the first three curves representing cycling the battery three times using the charge found under the the oxidation portion of the cyclic voltammogram (Fig. 37) are superimposed on each other, they look almost identical, showing that the experiment is highly reproducible.

In Fig. 38, the first cycle has a lower peak voltage and a shorter discharge time than the subsequent two cycles. This could be a reflection of a change in IR drop caused by a slight movement of the reference electrode during the changing of the experiment from the galvanostatic to the potentiostatic mode. This is unlikely, however, because the reference electrode was fixed in position by a rubber stopper inserted into an orifice in the top of the cell. Another possibility is that since the chart speed of the chart recorder was changed between the first and second cycles of this series, the shape of the curve could not be accurately reproduced by the digitization method used to transfer the data from chart paper to computer diskette. The shorter discharge time for the first cycle, as found for Fig. 33 for the conventional film, could be caused by the film not being fully discharged after the first cycle with twice the CV charge injected. If residual charge remained in the film after the battery was discharged, it would follow that the next discharge curve would last longer if the same current density were used, which it was. As for the

peak potential for the first cycle being lower than the second and third cycles, this result is similar to those for the conventional film battery in Figs. 33-34. Increased resistance associated with battery age (cycle life) could be the cause of this phenomena. The shape of the curve for the first cycle is nearly identical to the second and third cycle, however, and the data for the first curve is aberrant when compared to the entire body of data. Therefore, the height of the first curve and its length of discharge should not be weighted heavily when considering the data as a whole.

Figure 39 shows data that are more in line with the rest of the work. Charge/discharge curves are shown for a fibrillar film with 3Q CV charge injected into the battery. The shape of the charging and discharging curves are almost identical, with the peak potential rising slightly for each successive cycle. No substantial polymer damage can be seen, as was apparent by this point in the experiment for the cycling of the conventional film battery. However, in the next figure, Fig. 40, some polymer damage is evident, as time of discharge decreases with cycle number. Also, the charging curve for the third cycle occurred at a slightly higher potential than the charging curves of the first two cycles of the battery, where 4Q CV charge was used to charge the battery. Upon using 5Q CV charge to cycle the battery (Fig. 41), after about 575 seconds or 3.3Q CV charge has been put into the battery, the potential begins to rise sharply. At about 690 seconds, or at about 4Q CV charge, the potential rises off scale at approximately 5.2 V. The discharge curve indicates a two step process, and since the polypyrrole reduction reaction is a one step process, the data indicate that another reaction took place in addition to the oxidation and reduction of polypyrrole, one that did irreparable damage to the polymer film. The discharge time of 100 sec

was only a third of the shortest discharge time for the cycles using only 4Q CV charge. In comparison, the conventional film battery failed after only one cycle using 4Q CV charge.

The next two figures, Figures 42 and 43, compare charge/discharge curves of conventional and fibrillar film batteries using 1Q CV charge between 3 cycles each of 1Q, 2Q, 3Q, etc. the CV charge. This was done in order to get an indicator of resiliency of the battery. Would the battery yield a reproducible cycle using 1Q CV charge between increasing increments of charge? As the figures show, the cycles were not very reproducible, but are representative of the battery life and agree well with the other data shown in Figures 33-41. For both the conventional and fibrillar films, the peak potential rises with cycles that were performed later in the experiment, and the discharge time decreases when the battery nears the point of failure.

The peak potentials, and consequently the average discharge potentials, are higher for the conventional film batteries with less than 3Q of charge injected. This makes calculated energy densities (Wh/kg) higher for the conventional film batteries with less than 3Q of charge injected. Table III compares conventional and fibrillar battery energy densities for each of the curves in the experiment. At the point in the experiment that 3Q CV charge is injected into the battery and thereafter, fibrillar film batteries have higher energy efficiencies. Also, the maximum energy density for a fibrillar film is higher than that for a conventional film.

The discharge times for the fibrillar film batteries are longer than the corresponding discharge times for the conventional film batteries, so calculated capacity densities (Ah/kg) are higher for the fibrillar film

Table III. Energy Densities (Wh/kg).

Cycle	Fibrillar	Conventional
1Q #1	94.5	130.7
1Q #2	94.6	133.1
1Q #3	95.2	134.7
2Q #1	156.6	191.4
2Q #2	170.3	188.7
2Q #3	174.6	181.2
1Q	101.3	124.6
3xQ #1	218.5	184.6
3Q #2	223.2	161.6
3Q #3	221.2	122.5
1Q	93.5	79.2
4Q #1	235.4	61.8
4Q #2	219.5	
4Q #3	197.6	
1Q	79.4	
5Q	64.0	

batteries. Capacity densities are calculated from the charge, in amp-hours, released during battery discharge. Charge = It, so since this is a constant current experiment, a longer discharge time results in a larger capacity density. Also, the shapes of the charge and discharge curves indicate that the energy efficiencies for the fibrillar film batteries should be higher than the energy efficiencies for the conventional film batteries. The energy efficiency is calculated from the ratio of the area under the discharge curve versus the area under the charging curve, so the less symmetrical the charge and discharge curves are, the lower the energy efficiency will be. Energy efficiencies for conventional and fibrillar film batteries are given in Table IV.

Energy efficiencies for the first three cycles are very similar, but thereafter the energy efficiencies are higher for the fibrillar film batteries. The charge and discharge curves in Fig. 42, representing the conventional film battery, begin to plateau near the peak potentials and drop off sharply before beginning a steady decline. The voltage plateau near the end of the charging curve raises the energy put into the battery, and the drop off at the beginning of the discharge curve decreases the area under that curve relative to that of the charging curve, lowering the energy efficiency measured in that cycle. In contrast, the charge/discharge curves for the fibrillar battery shown in Fig. 43 are more symmetrical, with the exception of the curve recorded after 3 cycles of 4Q CV charge had been performed, and the discharge time was much shorter than the charging time. The symmetry of these curves suggests higher energy efficiencies for the fibrillar films.

Coulombic efficiencies for the fibrillar films are higher also. Coulombic efficiency is defined as charge drawn out of the battery divided

Table IV. <u>Energy Efficiencies (%) - Q_{out}/Q_{in}.</u>

<u>Cycle</u>	<u>Fibrillar</u>	<u>Flat</u>
1Q #1	89.9	88.7
1Q #2	90.2	90.3
1Q #3	90.9	91.4
2Q #1	67.0	59.9
2Q #2	70.4	59.0
2Q #3	71.7	56.8
1Q	94.3	81.0
3Q #1	55.9	36.8
3Q #2	56.8	32.0
3Q #3	55.9	23.9
1Q	84.8	48.9
4Q #1	42.8	8.1
4Q #2	39.7	
4Q #3	35.4	
1Q	67.9	
5Q	8.4	

by charge put into the battery. If all the charge which has been put into the battery could be extracted from the battery, the coulombic efficiency would be 100%. Coulombic efficiencies are tabulated in Table V. As with the energy efficiencies, the coulombic efficiencies are similar for the first three cycles but the fibrillar batteries show superior performance thereafter. The discharge times for the fibrillar curves are longer than those for the corresponding conventional film batteries for the cycles recorded later in the battery life (i.e., 2Q, 3Q, and 4Q CV charge). So, although the conventional films have higher energy densities than the fibrillar films because of their higher average discharge voltages, the fibrillar films have higher energy efficiencies because of their symmetry, and higher coulombic efficiencies because of their longer discharge times.

Figures 44-47 illustrate the differences between the charge/discharge curves of the conventional film battery and the fibrillar film battery with the same injected charge. For 1Q CV charge injected, represented in Fig.44, there is no marked difference in time of discharge and curve shape between the conventional and fibrillar batteries. The peak potential and average discharge voltage for the fibrillar film battery are 0.6 V lower than the conventional film battery, making its energy density lower than the conventional film battery. In Fig. 45, charge/discharge curves for 2Q CV charge injected for the conventional and fibrillar films are shown. The peak potential is still higher for the conventional film battery, but this battery fails sooner. The voltage begins to reach a plateau sooner for the charging curve of the conventional film battery. This indicates that it can be saturated with a lesser amount of charge, although it has the same amount of polymer as the fibrillar polypyrrole battery.

Table V. Coulombic Efficiencies (%).

Cycle	Fibrillar	Conventional
1Q #1	90.8	90.6
1Q #2	88.4	91.6
1Q #3	90.4	91.7
2Q #1	69.6	63.9
2Q #2	74.2	64.5
2x #3	76.4	61.9
1Q	92.8	85.6
3Q #1	62.2	44.9
3Q #2	63.0	39.3
3Q #3	63.1	27.0
1Q	86.5	49.9
4Q #1	49.1	12.7
4Q #2	45.7	
4Q #3	40.5	
1Q	67.4	
5Q	16.0	

The steeper drop-off in the discharge curve for the conventional film battery means that IR drop makes a greater percentage contribution to the peak potential of that battery than it does to the peak potential of the fibrillar battery.

Again, since the fibrillar charge and discharge curves are more symmetrical, its energy efficiency will be higher. When 3Q CV charge is injected into each type of battery (Fig. 46), similar effects can be seen. The conventional film battery charging curve reaches a plateau at the same time it did previously, when approximately 1.5 Q CV charge has been used as a basis. The fibrillar film charging curve plateaus when 2Q CV charge has been used, indicating that although it stores more charge before becoming saturated, its full capacity at this current density has been reached. The potential at its peak is still higher for the conventional film battery here, but drops within a few seconds to near the value of the fibrillar battery, and fails over 125 seconds sooner.

In Fig. 47, which shows the conventional film and fibrillar film charge and discharge curves using 4Q CV charge, differences between the two types of batteries are even more pronounced. The potential for the conventional film battery rises immediately upon beginning the charging cycle to 3.6 V, about 0.5 V higher than previously when 3Q CV charge was injected, indicating increased resistance in the battery. As mentioned before, it rises off scale at 1.5Q CV charge and fails in less than 100 seconds upon discharge. The voltage during charging of the fibrillar film battery does not rise off scale when 4Q amount of charge is put into the battery but does begin to plateau at about 2Q CV charge. The discharge time is 362 seconds, more than three times as long as the conventional film battery. However, upon twice more cycling at 4Q CV

charge and once at 1Q CV charge, the fibrillar battery fails during the cycle when 5Q CV charge is used. The potential begins to rise at about 575 seconds into the charging curve and goes off scale at about 4Q CV charge. The discharge curve was recorded for a longer time than the others to illustrate the multi-step process that occurs when the battery is overcharged. The potential rises to several plateaus in the charging curve and drops to several plateaus during discharge. This series of figures (Figs. 44-47) has illustrated that the conventional film batteries charge and discharge at a higher potential than the fibrillar ones, but have shorter discharge times when more than 1Q CV charge is injected and have a shorter cycle life for the experiment conducted.

Figures 48 and 49 compare the charge and discharge curves for the first cycle of every charge increment put into each type of batteries. Figure 48 shows cycles of 1Q, 2Q, 3Q, and 4Q CV charge for the conventional film battery and Fig. 49 pictures cycles of 1Q, 2Q, 3Q, 4Q, and 5Q CV charge for the fibrillar film battery. The charging curve for 4Q CV charge in Fig. 48, for the conventional film, departs from the rest of the charging curves at the beginning of the cycle, indicating that the resistance in the battery has increased. Also, it can be seen that although 1.5 times the amount of charge has been put into the film, the discharge time for 3Q CV charge curve is slightly less (223.8 sec) than the discharge time for the 2Q CV charge (229.5 sec). When 4Q amount of CV charge is put into the film, the discharge time (92 sec) is considerably less than even the discharge time when 1Q amount of charge under the CV is used (162.5 sec).

In Fig. 49, which shows data for the fibrillar film, the potential of the charging curve for 5Q CV charge used remains similar to the

previously recorded curves in the experiment until the potential rises off the plateau, which shows lesser internal resistance in the battery and little polymer electrode damage up to that point. More evidence that the polymer remains undamaged until that point can be found when comparing discharge times. Each time the battery is cycled using a greater increment of charge, more charge is obtained from the battery, until battery failure occurred. The discharge times are 158.5 seconds for the 1Q cycle, 252 seconds for the 2Q cycle, 338 seconds for the 3Q cycle, 354 seconds for the 4Q cycle, and 105 seconds for the 5Q cycle. The data in Fig. 49, when compared with the conventional film data in Fig. 48, show that the conventional film battery has increased internal resistance at an earlier point in the experiment, at the beginning of the first 4Q cycle rather than near the end of the first 5Q cycle. Also, the lesser relative discharge times for the conventional films are well illustrated in these two figures.

CHAPTER V

CONCLUSIONS

Li/polypyrrole batteries have been made and studied using electron microscopy, cyclic voltammetry, and constant current charge and discharge. Electron microscopy showed that one side of a porous Al_2O_3 membrane can be covered with a pinhole-free Au film and the base layer of PPy present in previous work can be eliminated. Cyclic voltammetry showed that as conventional film thickness increases, charge transport in the film becomes diffusion-controlled. The peak current, I_p, is directly proportional to scan rate for thin films, but as film thickness increases, I_p becomes directly proportional to the square root of scan rate as is expected for diffusion-controlled processes.

Battery charge/discharge studies showed that a battery made with fibrillar polypyrrole film can store more charge than one made with a conventionally grown polypyrrole film. For greater increments of charge injected into the battery, fibrillar film batteries exhibit higher charge capacities, energy densities and coulombic efficiencies. However, for lesser increments of charge, battery performance was very similar for the two types of batteries. A higher degree of charge /discharge curve symmetry resulted in higher energy efficiencies for the fibrillar film batteries.

Future work in this area should include investigation into improving treatment of the fibrillar polypyrrole films so that the negative shift in E_p seen in the cyclic voltammetry (Figs. 25 and 30) can be eliminated. Elimination of this negative shift would result in a rise in the cell potential during discharge. This would in turn result in higher

energy densities for the fibrillar film batteries. Alternatively, a polymer with a higher oxidation potential (e.g., polythiophene) could be used. A study of fibrillar film batteries with different amounts of polymer discharged at different current densities would also be useful in order to find the optimum value of energy density for the battery. Also, a constant load or constant potential discharge of the battery rather than a constant current discharge might give a better overall view of the battery's utility.

REFERENCES

1. M. Kanatzidis, *C&E News*, 36, December (1990).

2. J. R. Reynolds, *CHEMTECH*, 440, July (1988).

3. A. Diaz, *Chemica Scripta*, **17**, 145 (1981).

4. G. B. Street, R. H. Geiss, S. E. Lindsay, A. Nazzal, and P. Pfluger,in *Proceedings of the Conference on Electronic Excitation, and Interaction Processes in Organic Molecular Aggregates*, P. Reineker, H. Haken, and H. C. Wolf, eds., Springer,New York, 242 (1983).

5. H. Munstedt, G. Kohler, H. Mohwald, D. Naegle, R. Bitthin, G. Ely, and E. Meissner, *Synthetic Metals*, **18**, 259 (1987).

6. S. Panero, P.Prosperi, and B. Scrosati, *Electrochimica Acta*, **32**, 1465 (1987).

7. S. Panero, P.Prosperi, B. Klaptse, and B. Scrosati, *Electrochimica Acta*, **31**, 1597 (1986).

8. P. Buttol, M. Mastragostino, S. Panero, and B. Scrosati, *Electrochimica Acta*, **31**, 783 (1986).

9. P. Passiniemi and J.-E. Osterholm, *Synthetic Metals*, **18**, 637 (1987).

10. L. W. Shacklette, M. Maxfield, S. Gould, J. S. Wolf, T. R. Jow, and R. H. Baughman, *Synthetic Metals*, **18**, 611 (1987).

11. T. Osaka, K. Naoi, M. Maeda, and S. Nakamura, *J. Electrochem. Soc.*, **136**, 1385 (1989).

12. K. Naoi and T. Osaka, *J. Electrochem. Soc.*, **134**, 2479 (1987).

13. T Osaka, K. Naoi, and S. Ogano, *J. Electrochem. Soc.*, **134**, 2096 (1987).

14. T. Osaka, K. Naoi, H. Sakai, and S. Ogano, *J. Electrochem. Soc.*, **134**, 285 (1987).

15. K. Naoi, A. Ishijima, and T. Osaka, *J. Electroanalytical Chem.*, **217**, 203 (1987).

16. K. Naoi, T Hirabayashi, I. Tsubota, and T. Osaka, *Bull. Chem. Soc. Jpn.*, **60**, 1213 (1987).

17. T Osaka, K. Naoi, S. Ogano, and S. Nakamura, *Chemistry Letters*, 1687 (1986).

18. F. Trinidad, J. Alonso-Lopez, and M. Nebot, *J. App. Electrochem.*, **17**, 215 (1987).

19. A. G. MacDiarmid, L. S. Kang, W. S. Huang, and B. D. Humphrey, *Synthetic Metals*, **18**, 393 (1987).

20. R. B. Kaner and A. G. MacDiarmid, *Synthetic Metals*, **14**, 3 (1986).

21. M. Maxfield, S. L. Mu, and A. G. MacDiarmid, *J. Electrochem. Soc.*, **134**, 838 (1985).

22. W. Wanqun, R. J. Mammone, and A. G. MacDiarmid, *Synthetic Metals*, **10**, 235 (1985).

23. J. Caja, R. B. Kaner, A. G. MacDiarmid, *J. Electrochem Soc.*, **131**, 2744 (1984).

24. K. Kaneto, M. Maxfield, D. P. Nairns, A. G. MacDiarmid,.and A. J. Heeger, *J. Am. Chem. Soc, Faraday Trans. 1*, **78**, 3417 (1982).

25. P. J. Nigrey, A. G. MacDiarmid, and A. J. Heeger, *Mol. Cryst. Liq. Cryst*, **83**, 309 (1982).

26. P. J. Nigrey, David MacInnes, Jr., D. P. Nairns, A. G. MacDiarmid, and A. J. Heeger, *J. Electrochem. Soc.*, **128**, 1652 (1981).

27. N. Mermilliod, J. Tanguy, and F. Petiot, *J. Electrochem. Soc.*, **133**, 1073 (1986).

28. T. Yamamoto, M. Zama, and A. Yamamoto, *Chemistry Letters (Chemical Soc. Japan)*, 563 (1985).

29. A. F. Diaz, J. I. Castillo, J. A. Logan, and W. Lee, *J. Electroanal. Chem.*,**129**, 115 (1981).

30. B. J. Feldman, R. Burgmayer, and R. W. Murray, *J Am. Chem. Soc.*, **107**, 872 (1985).

31. M. Gazzard, in "Handbook of Conducting Polymers", vol. 1 , T. A. Skotheim, ed., New York: Marcel Dekker, 673 (1986).

32. J. W. Thackeray, H. S. White, and M. S. Wrighton, *J. Phys. Chem.*, **89**, 5133 (1985).

33. A. F. Diaz and J. I. Castillo, *J. C. S. Chem Comm*, 397 (1980).

34. G. B. Street, in "Handbook of Conducting Polymers," vol. 1 , T. A. Skotheim, ed., New York: Marcel Dekker, 265 (1986).

35. D. A. Buttry, Invited Lecture, , 193rd ACS National Meeting, Denver, CO, April 5 (1987).

36. R. M. Penner, Ph. D. Dissertation, Texas A&M University (1987).

37. R. M. Penner, L. Van Dyke and C. Martin, *J. Phys. Chem.*, **92**, 5274 (1988).

38. L. Van Dyke and C. Martin, *Langmuir*, **6**, 1118 (1990).

39. L. Van Dyke and C. Martin, *Synthetic Metals*, **36**, 275 (1990).

40. "Handbook of Batteries and Fuel Cells," ed. by D. Linden, McGraw-Hill, Inc., New York, A3-A10 (1984).

41. R. M. Felder and R. W. Rousseau,in "Elementary Principles of Chemical Processes," Wiley & Sons, New York, 385 (1978).

42. Derek Pletcher, "Industrial Electrochemistry," Chapman and Hall, New York, 242 (1982).

43. A. J. Bard, and L. R. Faulkner, in "Electrochemical Methods, Fundamentals and Applications," Wiley & Sons, New York, 218 (1980).

44. W. Wernet and G. Wegner, *Makromol. Chem.*, **188**, 1465 (1987).

APPENDIX A

EXPERIMENTAL CHECKLIST

The solutions used for the battery experiments include 1 M $LiClO_4$ in PC (propylene carbonate) in the reaction chamber and 0.2 M $AgNO_3$ in 1M $LiClO_4$ (PC) for the Ag/Ag^+ reference electrode. The solution used for all other experiments was 0.2 M Et_4NBF_4 in acetonitrile. Necessary calculations for preparing these solutions are included in this appendix.

Molecular weight :

$LiClO4$ 106.46 g/mole

$AgNO_3$ 169.89 g/mole

Et_4NBF_4 217.06 g/mole $= 8(12.011) + 20(1) + 14.007 + 10.81 + 4(18.999)$

(element)   C   H   N   B   F

$LiClO_4$ 1.0 M in 250 ml: (106.46 g/mole)(1.0 mole/l)(0.25 l) = 26.6 grams

$AgNO_3$ 0.2 M in 100 ml: (169.89 g/mole)(0.2 mole/l)(0.10 l) = 3.4 grams

Et_4NBF_4 0.2 M in 250 ml: (217.06 g/mole)(0.2 mole/l)(0.25 l) = 10.85 grams

Et_4NBF_4 0.2 M in 100 ml: (217.06 g/mole)(0.2 mole/l)(0.10 l) = 4.34 grams

Before beginning any experiment, it is important to gather all essential materials so that the experiment will not be delayed at a crucial point. Below is a checklist of materials needed for the Li/PPy battery charge/discharge experiment.

     Beaker for waste

     Disposable pipettes and bulb

     25 ml or 10 ml graduated cylinder

     Electrodes: working - platinum disk for conventionally grown

                polypyrrole film

- Au-plated Anopore® for fibrillar films

counter - Li foil with imbedded Ni gauze for battery charge/discharge, platinum disk for growing film

reference - Ag/AgNO$_3$ (0.2 M) in 1 M LiClO$_4$/PC

Battery cell reservoir

Pyrrole in vial

Syringe for pyrrole

Dry PC or MeCN (acetonitrile) for rinsing

Par 273 or 173/175 with leads

X-Y recorder and strip chart recorder

Magnetic stirrer and stirring magnet

Degassed electrolyte solution and extraction solutions (NaOH and HBF$_4$ or HClO$_4$, depending on the work done)

Vials in which to conduct membrane dissolution

APPENDIX B

DEFINITIONS OF TERMS

<u>Ampere - hour Capacity</u> - the quantity of electricity measured in ampere-hours (Ah) which may be delivered by a cell or battery under specified conditions (also coulombic efficiency).

<u>Available Capacity</u> - the total capacity, in Ah, that will be obtained from a cell or battery, at a defined discharge rate or other specified discharge or operating conditions.

<u>Capacity</u> - the total number of ampere-hours or coulombs that can be drawn from a fully charged cell or battery under specified conditions of discharge.

<u>Capacity Density</u> - capacity per unit volume or mass, reported in units of Ah/cm, Ah/l, or Ah/kg.

<u>Cutoff Voltage</u> - The cell or battery potential at which the discharge (or charge) is terminated, generally a function of discharge rate. Also referred to as the end voltage.

<u>Discharge Rate</u> - usually for a constant current discharge, the rate in amperes at which current is drawn from the cell. For a constant potential discharge, it is an average value.

<u>Energy Density</u> - the ratio of the energy available from a battery or cell to its volume (in Wh/l or J/m^3 = 1 $kg/msec^2$) or mass (in Wh/kg or J/kg). One kilowatt hour = 3.6 x 106 joules. One joule = one watt-second = 1 kgm^2/sec^2.

<u>Power</u> - current multiplied by potential, or IE, measured in watts. A watt = (1A)(1V) = (1 C/second)(1 joule/C) = 1 joule/second.

<u>Power Density</u> - the ratio of the power available from a battery to its mass(W/kg) or volume (W/l).

<u>Rated Capacity</u> - the number of Ampere - hours a cell or battery can deliver under specific conditions (rate of discharge, cutoff voltage, temperature); usually the manufacturer's rating.

VITA

Marjorie Anne Nicholson was born at ██████████████████, ███████, ██████████████ the fifth of seven children born to Samuel and Priscilla Kresge Nicholson. She graduated from Killeen High School, Killeen, Texas, in May of 1976, and was a National Merit Scholarship Finalist. She continued her education at Texas A&M University, where she was a member of the Corps of Cadets. While a cadet in ROTC, she completed Army Airborne School and Missile Launch Officer's Training School. Upon graduating in December 1980 with a Bachelor's degree in Chemistry, she worked at Dow Chemical Company, Freeport, Texas, first as a chemist at Chlor-alkali Research where she worked on methods of on-line analysis and then at Chlorine Plant #6. There she managed the analysis laboratory and installed multi-sample equipment to monitor the anolyte and catholyte of twelve series of chlorine/caustic cells. She returned to College Station in 1982 to obtain a teaching certificate in secondary science and math, and then to pursue a Master of Science degree in Chemistry. She is married to Dr. Ralph E. White and has four children: ███████████████████ ████████.

Permanent Mailing Address for Ms. Nicholson is 2912 Arroyo Court South, College Station, Texas 77845.

APPENDIX B